6-18-2015

Coupling Nuclear Induced Phonon Propagation with Conversion Electron Mössbauer Spectroscopy

Michael J. Parker

COUPLING NUCLEAR INDUCED PHONON PROPAGATION WITH CONVERSION ELECTRON MÖSSBAUER SPECTROSCOPY

THESIS

Michael J. Parker, Capt, USAF

AFIT-ENP-MS-15-J-054

DEPARTMENT OF THE AIR FORCE
AIR UNIVERSITY

AIR FORCE INSTITUTE OF TECHNOLOGY

Wright-Patterson Air Force Base, Ohio

The views expressed in this thesis are those of the author and do not reflect the official policy or position of the United States Air Force, Department of Defense, or the United States Government. This material is declared a work of the United States Government and is not subject to copyright protection in the United States.

AFIT-ENP-MS-15-J-054

COUPLING NUCLEAR INDUCED PHONON PROPAGATION WITH CONVERSION ELECTRON MÖSSBAUER SPECTROSCOPY

THESIS

Presented to the Faculty

Department of Engineering Physics

Graduate School of Engineering and Management

Air Force Institute of Technology

Air University

Air Education and Training Command

In Partial Fulfillment of the Requirements for the

Degree of Master of Science in Nuclear Engineering

Michael J. Parker, BS

Capt, USAF

April 2015

DISTRIBUTION STATEMENT A
APPROVED FOR PUBLIC RELEASE; DISTRIBUTION UNLIMITED

AFIT-ENP-MS-15-J-054

COUPLING NUCLEAR INDUCED PHONON PROPAGATION WITH CONVERSION ELECTRON MÖSSBAUER SPECTROSCOPY

Michael J. Parker, BS
Captain, USAF

Committee Membership:

Dr, Larry W. Burggraf
Chair

Maj Benjamin R. Kowash
Member

Dr. William Bailey
Member

Abstract

Mössbauer spectroscopy is a very sensitive measurement technique (~10^{-8} eV) which prompted motivation for the experiment described in this thesis. Namely, can a sensitive detection system be developed to detect nuclear recoils on the order of 10 to 100 of eVs? The hypothesis that this thesis tests is: Nuclear induced phonon bursts caused by Rutherford scattered alphas, decayed from ^{241}Am, in a type-310 stainless steel material can couple with 7.3keV conversion electron Mössbauer events at the other end of the material which will have a statistically significant effect on a Mössbauer spectrum. The phonon bursts produced by the alpha collisions are expected to be very low energy at the other end of length of material. Since Mössbauer spectroscopy is sensitive and can detect the very low energy phonons, the spectrum is expected to change in at least one of the five areas after coupling occurs: broadening in the spectrum peaks, increased/decreased background counting rate, Mössbauer peak asymmetry, increased/decreased counting rate under the peak, and/or a peak centroid shift. This research aims to determine the significance of changes between spectra with phonon bursts and with no phonon bursts through hypothesis testing, where the null hypothesis is where phonons do not affect Mössbauer spectra in one of the five areas mentioned previously. After the spectra and results were analyze using an f-test and t-test comparisons, this experiment failed to reject the null result. Leading to the conclusion that additional research must be conducted.

Acknowledgments

First and foremost, I'd like to thank Dr. George John, a very intelligent and good natured man. I'd also like to thank my family, Major Kowash, and Dr. Burggraf for not giving up on me in my time of need and their support through this long, long process.

Michael J. Parker

Table of Contents

List of Figures

List of Tables

COUPLING NUCLEAR INDUCED PHONON PROPAGATION WITH CONVERSION ELECTRON MÖSSBAUER SPECTROSCOPY

I. Introduction

1.1 Motivation

The Mössbauer effect has many different applications in a variety of areas; such as, the demonstration of the gravitational red-shift, nuclear physics with the study gamma decay, and solid-state physics with the study of lattice dynamics and hyperfine interactions. Currently, the main area of focus is in the study of chemical and physical environments of a nucleus. Due to the extreme precision and sensitivity of the effect, it has been used as a way determining the change in energy as a photon falls in a gravitational field. In 1964, the shift in frequency of electromagnetic radiation as it passed through a difference in gravitational potential was measured to be 0.859 ± 0.085 times the value predicted by Einstein's Theory of Relativity's Principle of Equivalence [3]. This measurement made by Cranshaw (1964), following Pound and Rebka's 1960 $\Delta E/E$ measurements of 4.902×10^{-15} for a 45m round trip, gave increase fidelity to their measurement. These were the most precise tests of the General Theory of Relativity, and it would not have been possible without the great sensitivity provided by the Mössbauer effect [12]. It is this sensitivity that gives motivation to the experiment performed and described herein. Depending on the speed of the Mössbauer velocity drive and radiation source, the sensitivity can be tuned to energy regimes of interest down to Γ/E_γ per channel.

Solids can absorb energy in many ways other than by removing atoms from their lattice sites. At low energies and temperatures, the primary way is through lattice vibrations, called phonons [12]. Propagation of these phonons through a lattice is responsible for the familiar properties such as mechanical and acoustical waves. One of the proposals of this experiment is to detect extremely small nuclear recoils made by radiation scattering from individual nuclei. During a scattering event the nucleus is displaced sending phonons into the material lattice. These phonons can then constructively and destructively interact with nuclei in the region where the resonance measurements are being made. The result would then be a Mössbauer spectrum that is perturbed from one where no scattering source is present.

1.2 Background

There are two broad types of Mössbauer spectroscopy that have been applied over the past six decades: transmission Mössbauer spectroscopy (TMS) and emission Mössbauer spectroscopy. TMS requires a thin foil of material to allow transmission of γ-photons to a detector behind the absorber. Photons that are resonant with the absorber and captured then fluoresce in 4π space producing *dip(s)* in the Mössbauer spectrum. Conversion electron Mössbauer spectroscopy (CEMS) is a type of emission Mössbauer spectroscopy that allows for the surface of materials to be studied. In CEMS, the conversion electrons emitted by the resonantly excited nuclei on the surface of the absorber are detected producing *peak(s)* in the Mössbauer spectrum. In both cases, the *dip(s)* and *peak(s)* in each respective spectrum are analyzed to determine the chemical and nuclear environment at of the material in question. CEMS is the technique that was selected for this research over TMS because the thickness of the absorber can be considered irrelevant.

CEMS only penetrates about 50 Å to 4000Å into the material and does not consider the chemical environment beyond this local area [9, 21]. However, energy can be transmitted through the material into the surface regime through phonons. Phonons are quasi-particles that transfer energy through solids in a vibrational wave motion. In essence, the nuclei vibrate and transfer energy down the line to the next nuclei. This propagation of this vibrational energy can extend meters in distance depending on the material structure and the initial cause of the phonon generation. These phonons can be generated through radiation induced nuclear recoils. In this experiment, alpha particles are used to induce these recoils and therefore generate a phonon wave that will travel down an absorber to localized Mössbauer events at the other end of the absorber on the surface. It is in this localized area on the surface where the sensitivity of Mössbauer spectroscopy (down to ~10^{-15} eV/eV) can possibly exploit subtle perturbations in the spectra from the phonon interactions.

1.3 Problem Statement

Nuclear induced phonons can couple with conversion electron Mössbauer events to have a statistically significant effect changes on a Mössbauer spectrum. The spectrum is expected to change in at least one of the four areas: broadening in the peaks, increased/decreased background counting rate, Mössbauer peak asymmetry, and increase/decreased counting rate under the peak. This research aims to determine significance of changes between spectra with phonons and no phonons through hypothesis testing, where the null hypothesis is where phonons do not affect Mössbauer spectra.

1.4 Objectives and Approach

The primary objective of this thesis is to compare Mössbauer spectra that are created in the presence of a scattering source to spectra created without a scattering source to determine if there is a statistical difference between the two sets of spectra. This is accomplished through the use of CEMS, an absorber of sufficient length to allow for phonon propagation, and a radiation source that will induce the phonons through nuclear recoils.

II. Theory

The theory section will cover Mössbauer spectroscopy, description of phonons, and phonon coupling with Mössbauer events. This section is meant to create a basis for the overall experiment, but if more detail is desired, please use the references in the back.

2.1 Mössbauer Spectroscopy

2.1.1 Overview

Just as atoms have quantized energy states, so do nuclei. Transitions between nuclear energy levels, like atoms, can be accomplished through the emission or absorption of photons in a resonant process. When a radioactive isotope decays by the emission of an alpha or beta particle, the resulting nucleus is often left in an excited state, which subsequently decays to its ground state by the emission of one or more γ-rays. These energy levels (ground and excited) are influenced by the environment that surrounds the nucleus; chemical, electronic and magnetic, which can shift or split these energy levels. This 'hyperfine splitting' will be discussed further in section 2.1.8. These changes in the energy levels can provide information about the atom's local environment within a system and ought to be observed using resonance-fluorescence [12]. There are two major obstacles in obtaining information on the atoms' local environment: the hyperfine interactions between the nucleus and its environment are extremely small, and the recoil of the nucleus as the γ-ray is emitted or absorbed prevents resonance. [12] In an example of a γ-ray emitted by an isolated isotope, the nucleus recoils, and results in a decrease of the γ-ray's energy, which was the difference between the excited and ground states of the nucleus. Due to this recoil energy loss, the emitted γ-ray will not be absorbed by another nucleus disallowing resonant absorption.

In 1958, Rudolf Mössbauer discovered that, in some cases, if the nucleus is tightly bound in a crystal lattice, the whole crystal recoils rather than the individual nucleus [19]. Due to the much greater mass involved in recoil, the energy loss of the emitted γ-ray is reduced so that the energy becomes very close to that of the difference in energy between the nuclear energy levels; thus, making resonant absorption possible. For the discovery of this effect, now known as the Mössbauer Effect, Mössbauer received the Nobel Prize in 1961. This discovery is the basis of Mössbauer spectroscopy, which has been used to investigate material properties by looking at the hyperfine structure of nuclear energy levels. The technique was also used to verify the prediction of General Relativity that the energy of a photon is affected by a gravitational field [12].

The most widely studied Mössbauer isotope is ^{57}Fe. The decay scheme of this nucleus is shown in Figure 1. Radioactive decay of ^{57}Co by electron capture leaves the resulting ^{57}Fe nucleus in an excited state. As shown in Figure 1, 9% of the excited nuclei decay to the ground state by emitting a 137 keV γ -ray, while the remaining 91% decay in two stages: the transition from first excited state to the second excited state emitting 123 keV γ -rays, then the transition from the second excited state to the ground state emitting 14.4 keV γ –rays. This second emission occurs with a mean lifetime of 141 ns (half life of 97.7 ns). It is this 14.4 keV γ-ray that is frequently used in Mössbauer spectroscopy.

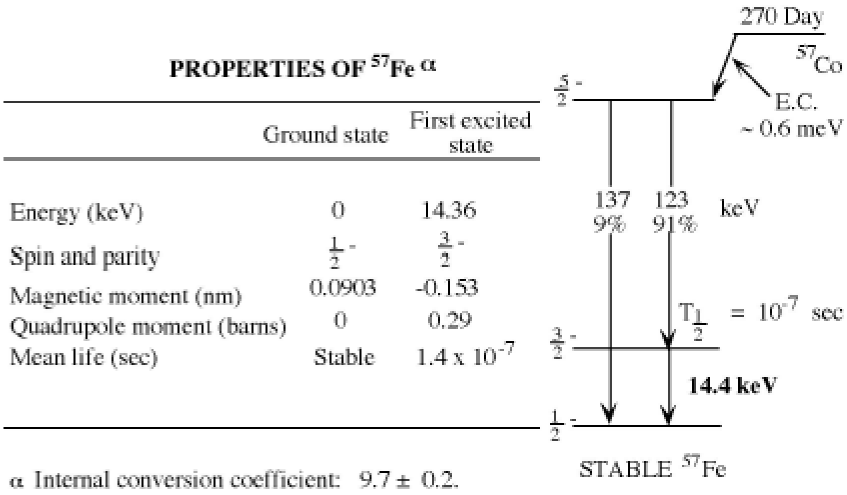

PROPERTIES OF ^{57}Fe α

	Ground state	First excited state
Energy (keV)	0	14.36
Spin and parity	$\frac{1}{2}$ -	$\frac{3}{2}$ -
Magnetic moment (nm)	0.0903	-0.153
Quadrupole moment (barns)	0	0.29
Mean life (sec)	Stable	1.4 x 10^{-7}

α Internal conversion coefficient: 9.7 ± 0.2.

Figure 1: Energy level structure of the 57Fe nucleus. Modified from [14]

Not all resonant absorption events will be recoil free (i.e. the individual nucleus recoils instead of the lattice). If the recoil energy is not sufficient to generate a phonon, recoil of the individual nucleus is not possible, and the recoil momentum is taken up by the crystal as a whole, as shown in Figure 2. The top shows the recoil of free nuclei in emission or absorption of a γ-ray. The bottom shows recoil-free emission or absorption of a γ-ray when the nuclei are in a solid matrix such as a crystal lattice. As a result, the Mössbauer Effect is typically observed only for γ-rays of sufficiently low energy (5 to 50 keV), since high energy gamma rays will create larger recoils which results in a very low recoil free fraction.

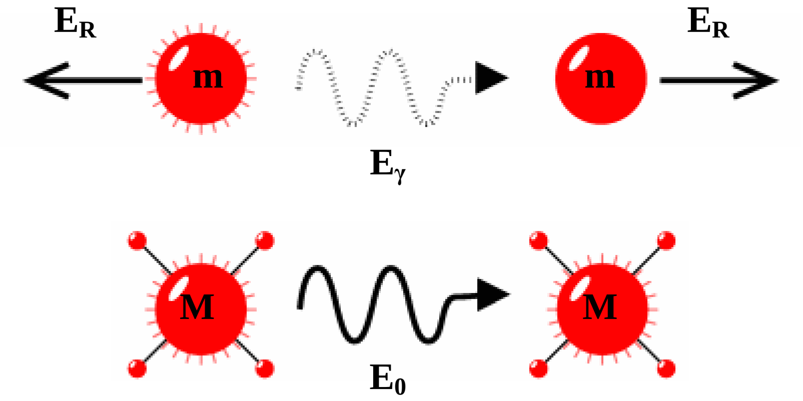

Figure 2: Diagram of Free and Bound Nuclei.

The Mössbauer effect, as generally applied to the study of minerals, relies on the fact that ^{57}Fe, which is a decay product of ^{57}Co, is unstable. ^{57}Fe decays by emitting a gamma ray (γ-ray), along with other types of radiation. Figure 3 shows the nuclear decay scheme for $^{57}\text{Co} \rightarrow {}^{57}\text{Fe}$ and various backscattering processes for ^{57}Fe that can follow resonant absorption of an incident gamma photon [6]. If a nucleus gives off radiation or any other form of energy (in this case, in the form of a γ-ray), the nucleus must recoil (or move) with an equal and opposite momentum to preserve its energy (E_γ), just like a gun (by analogy, the nucleus) recoils with a recoil energy E_R when firing a bullet (the γ-ray). A more in-depth discussion of the recoil energy loss can be found in Section 2.1.4.

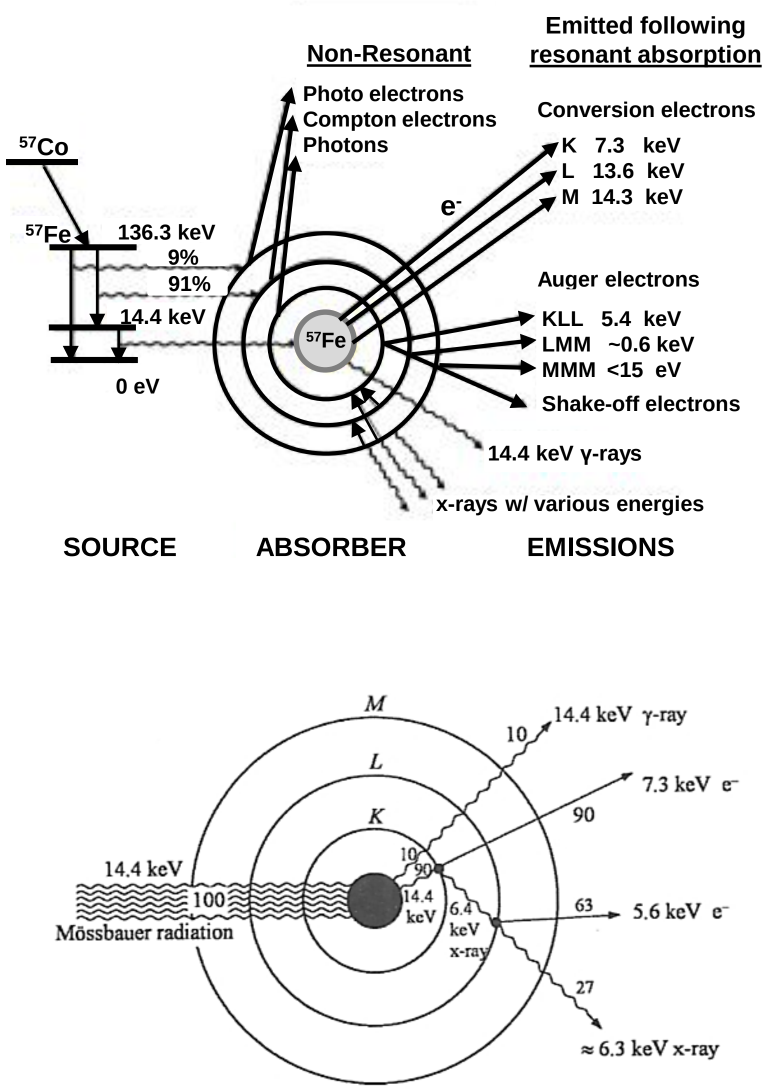

Figure 3: Top: The nuclear decay scheme for ^{57}Co → ^{57}Fe. Modified from [4, 21] Bottom: Probabilities of gamma and conversion electron emission following resonant absorption. [21, 23]

2.1.2 Nuclear Resonance Fluorescence

Nuclear resonance fluorescence, the main principle of the Mössbauer effect, is a process in which a nucleus absorbs and emits γ-rays. Figure 4 shows the idealized representation, where an excited source emits a gamma, the gamma is then incident on another identical atom, which is subsequently absorbed and re-emitted by an absorber through resonant capture. The simplistic figure assumes that the gamma carries away the entire energy of the nuclear transition. E_e represents the excited energy state. As the case for atomic electrons, resonance absorption requires the phonon have the exact quantized transition energy. Nuclear resonance fluorescence was observed before Mössbauer's discovery, but the experiments suffered from several difficulties. Primary among these is that the energy of the emitted photon is reduced below the natural line width of the absorber due to the recoil of the emitting nucleus that is required to conserve momentum. Thus the emitted photons have insufficient energy required for resonant absorption to occur, and thus some other mechanism (typically thermal or mechanical excitation) is required to give the photon a boost in energy so that resonance absorption can occur [8].

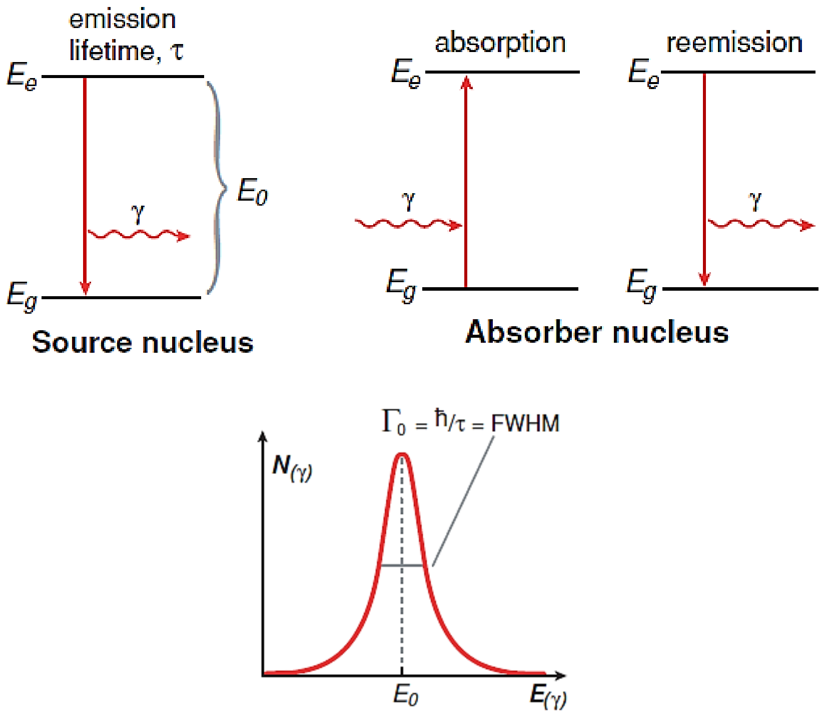

Figure 4: Idealized representation of nuclear resonance fluorescence and natural line width. Modified from [6]

2.1.3 Natural Line Width

Due to the Heisenberg uncertainty principle, the line width of the γ-ray transition is determined by the lifetime of the first excited state which causes the energy of the gamma to not be precisely defined. This is shown in the bottom image of Figure 4. The profile obeys a Lorentzian (or Breit-Wigner) distribution centered on E_0:

$$f(E) \propto \frac{\Gamma^2}{\Gamma^2+4(E-E_0)^2} \tag{2.1}$$

where $\Gamma = \hbar/\tau$, τ is the mean lifetime of the first excited state, and E_0 is the energy difference between the two levels. Emission and absorption profiles are the same.

For the 14.4 keV ^{57}Fe γ-ray, the mean lifetime of the first excited state is 97.7 ns [6], corresponding to a line width Γ = 4.65x10^{-9} eV. Because the energy of the excited state is not *sharp*, the absorption will occur even when the energies of the γ-rays differ slightly from the resonant value. This very narrow line width makes possible Mössbauer spectroscopy which allows the hyperfine structure of nuclear energy levels to be investigated.

2.1.4 Recoil Energy Loss

Consider a nucleus of mass m, at rest, in an excited state of energy E_0 which decays to the ground state by emission of a γ-ray of energy E_γ, Figure 2. From conservation of momentum and energy we find that the energy of the photon and the energy of recoil E_R are given by

$$E_\gamma = E_0 - E_R \tag{2.2}$$

$$E_R = \frac{1}{2}mv^2 = \frac{p^2}{2m} = \frac{p^2c^2}{2mc^2} = \frac{E_\gamma^2}{2mc^2} \qquad (2.3)$$

For the 14.4 keV γ-ray emitted from ^{57}Fe, the recoil energy is 0.002 eV, which greatly exceeds the width of the natural line width of ^{57}Fe (i.e. resonant absorption is not possible without an additional mechanism). If the nucleus is in a crystal lattice and the whole lattice recoils, m is replaced by the mass of the crystal, M, (M >> m), so that $E_R \rightarrow 0$ and $E_\gamma \approx E_0$. Resonant absorption is now possible. .

2.1.5 Doppler Broadening

So far in the discussion, an important factor that limits resonant absorption has been neglected: Doppler broadening. In practice, the natural line width would not be observed; instead the added contribution from Doppler broadening would be the primary contributor to increased line width [12]. This broadening occurs because the nuclei of the source and absorber are not at rest, but in fact have thermal motion at any temperature, T. The higher the temperature, the broader the line widths become represented by E_D. This profile is presented in Figure 5.

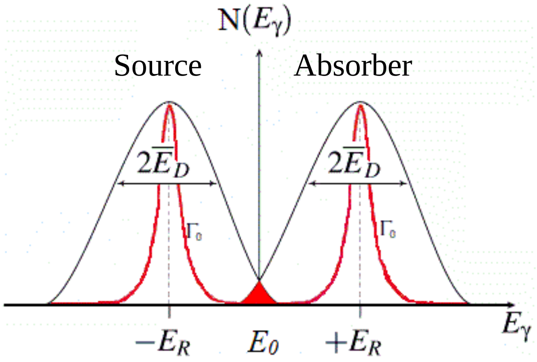

Figure 5: Resonance Overlap. Note: Overlap extremely exaggerated.

In the lab frame, the emitted and absorbed photons appear Doppler shifted with energies shown in Equation 2.4.

$$E'_\gamma = E_\gamma(1 \pm \frac{v_x}{c}) \tag{2.4}$$

where, v_x is the velocity component along the photon direction. The motion of the nuclei is typically represented by the Maxwell velocity distribution with the Doppler shifted energies. This produces a Gaussian distribution of width E_D, shown in equation 2.5 and Figure 5:

$$E_D = \sqrt{\ln 2}\, E_\gamma \sqrt{\frac{2kT}{Mc^2}} \tag{2.5}$$

where, kT is the thermal motion using k, Boltzmann's constant and the temperature, T. At room temperature kT ≈ 0.025 eV; this is on the order of magnitude of ^{57}Fe's recoil energy, $E_{R,}$ and produces a slight resonant overlap shown in Figure 5. It is therefore possible (albeit with low probability) to observe some resonant absorption at room temperature due to the Doppler broadening of the peaks. If you follow common sense, it would be safe to assume that as the temperature of the source and absorber are lowered;

the Doppler broadening effect would vanish, reducing the overlap to zero and making resonant absorption impossible.

2.1.6 The Mössbauer Effect

For more in depth information, Fraunfelder [7] summarizes important early developments and provides reprints of early works. For a more thorough description of the theory behind Mössbauer spectroscopy, Wegener [29] is another good source. In Mössbauer spectroscopy, an absorber material contains nuclei that are resonant with energy emitted from a photon source. These sources and absorber nuclei are closely coupled and are typically a parent and daughter nuclei in Mössbauer spectroscopy. The source emits a photon at a given energy, assuming no energy loss, the absorber nuclei is resonant with the photon and absorbs the energy of the photon. The nuclei excite and reemit the photon's energy in either another photon of the same energy or conversion electrons. This process of emission, absorption and remission is called nuclear resonance fluorescence. Unfortunately, the photon emitted by the source does lose energy through recoil and the absorber nuclei recoils when it absorbs the photon. To overcome this energy loss, energy is imparted to the emitted photon to allow for resonant absorption in the absorber nuclei. This method of adding energy to the parent nuclei photon, so that the photon carries the full transition energy is the basis of the Mössbauer effect. This method has been used since 1958 to study hyperfine structures caused by chemical environments of materials. Typically, the absorber materials used in the study are thin, but due to the nature of the CEMS method, thicker materials can be used. This does not change the spectrum generated, if the absorber is kept at room temperature ($T \approx 300K$).

In conversation electron emission spectroscopy (CEMS), the recoil-free nuclear resonance is the fundamental principle of Mössbauer spectroscopy where 7.3 keV conversion electrons together with 5.4 and 6.2 keV Augur electrons are detected for ^{57}Fe nuclei [21]. The CEMS technique can only occur at the surface of the absorber, as shown in the bottom image of Figure 6. If the resonance occurs in the bulk of the absorber the conversion electrons and Auger electrons will not be able to make it to the detector shown in the top of Figure 6; however, if the resonance occurs on the surface layer (400nm), which is determined by the penetration depth of the 7.3 keV conversion elections [21]. Just as described earlier for photons, the conversion electrons that are resonantly emitted from the ^{57}Fe nuclei, have the same line width as the 14.4 keV gammas, $\Gamma = 4.65x10^{-9}$ eV. In the spectrum shown in Figure 6, the velocity of the motor correlates to the energy imparted on the 14.4 keV gamma, where 1 mm/s = 4.81×10^{-8} eV. So far to date, the most sensitive measurement made with Mössbauer spectroscopy was ~10^{-15} eV when the gravitation shift on a photon was measured [3]. Because of the resolution that will be used in this experiment (~10^{-8} eV), the setup discussed on Chapter 3 should be sensitive to shifts in energy on the same order of magnitude. The resolution or sensitivity of the Mössbauer spectrum is dependent on the motor velocity. Increasing motor velocity will, decrease the resolution of the spectrum, while decreasing motor velocity will increase the resolution. The generation of the spectrum as it is dependent on motor velocity can be seen in Figure 7.

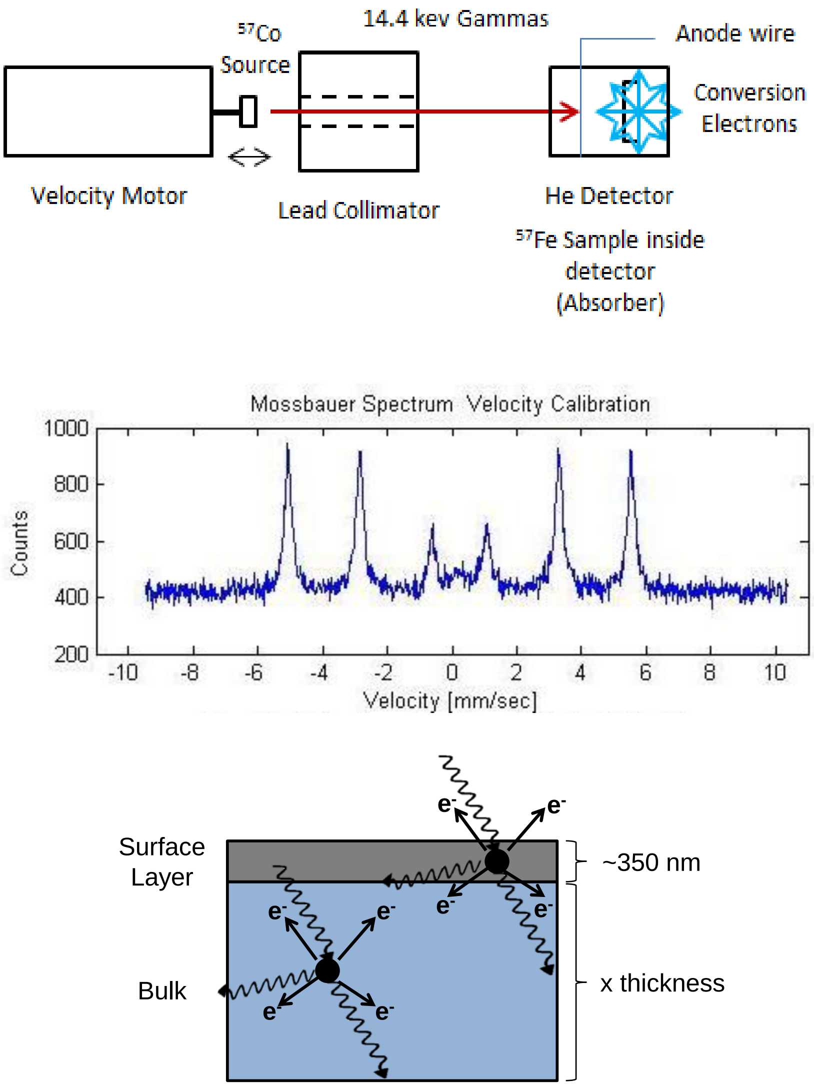

Figure 6: Top: Example of conversion electron Mössbauer spectrometer setup with a corresponding spectrum. Bottom: Depiction of CEMS resonance locations in the absorber near the surface and in the bulk.

In Figure 7, the source (black line) is oscillated back and forth imparting energy to the 14.4keV photon. The absorber resonant wave function (red line) is fixed at quantized transition energy (dotted line) due to the properties of the environment surrounding the absorber nuclei. The Mössbauer spectrum (blue) is generated as the source spectrum overlaps the absorber wave function. The overlap is the resonant absorption, while everything below the formation of the peak is from the non-resonant absorption. Depending on the environment surrounding the absorbing nuclei, the Mössbauer spectrum will change. For instance, increased temperature in the absorber will broaden the absorption wave function to the point where, regardless of the location of the source wave function a peak will not be able to be defined in the Mössbauer spectrum. Please note, the source wave function is considered a recoil-free emission, which allows a *scanning* of the abruption wave function.

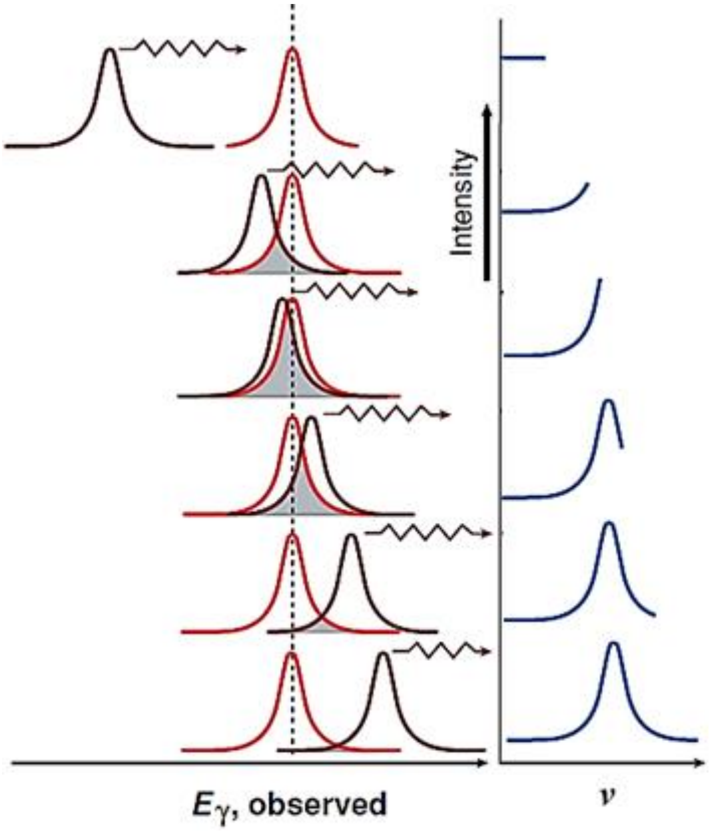

Figure 7: Formation of a Mössbauer Spectrum using CEMS, the source is moved to Doppler shift the center. Modified from [4].

2.1.7 Recoil-Free Emission of Gamma Rays

To help understand recoil-free emission of gamma rays, a representational schematic of the vibrational energy levels in a solid is shown in Figure 8. This figure assumes an Einstein solid with a frequency, ω. Please note $\hbar$ is Planck's constant divided by 2π. On the left, the recoil energy E_R of an emitted γ-ray is less than what is needed to reach the next higher energy level, so that excitation of a vibrational mode has low probability. The probability that no excitation will occur is given the symbol *f*, which represents the fraction of recoil-free events, shown in equation 2.6.

$$f = 1 - \frac{E_R}{\hbar\omega} \qquad (2.6)$$

A γ-ray would be emitted without losing energy to the solid, in what is called a zero-phonon transition [6]. In other words, sometimes the nucleus absorbs the energy of the γ-ray and it doesn't recoil (instead, the entire structure, rather than just the nucleus, absorbs the energy). The variable *f* indicates the probability of this happening and should be sufficiently large, $E_R \gg \hbar\omega$. This process of recoil-less emission forms the basis for Mössbauer spectroscopy. On the right, E_R is significantly greater in energy than the lowest excitation energy of the solid, which is E_{n+1}- E_n. Absorption of the recoil energy, E_R, by the solid thus becomes probable, and the photon emerges with energy reduced by E_R and with Doppler broadening [6].

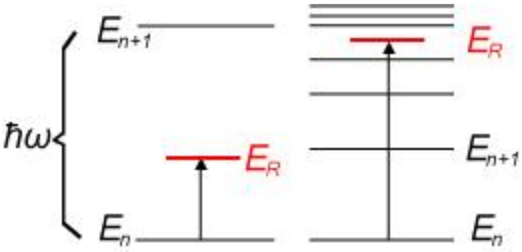

Figure 8: Schematic of the vibrational energy levels in a solid. [17]

The crystal lattice does not always produce a gamma with zero recoil, if the emitting and absorbing nuclei are in different crystal structures, the different chemical environment is sufficient to perturb the nuclear energy levels differently so that resonant absorption is precluded. Only a small Doppler shift in frequency, however, obtained by moving the source, is sufficient to allow absorption by canceling out the effects of the natural Doppler shift with the induce Doppler shift by moving the motor. The *scanning velocity* of the Mössbauer photons source is the basis of Mössbauer spectroscopy, which allows nuclear absorption spectra to be recorded. In other words, a Mössbauer spectrum is a recoil-free resonance curve.

2.2 Phonon Sources

In this experiment, alpha particles, $^4He^{2+}$, from an Americium-241 (^{241}Am) source were used to bombard the absorber and imparting energy to the absorber through Rutherford scattering. As ^{241}Am decays, 5.49 MeV (85%) and 5.44 MeV (13%) alphas are emitted. Ideally, there is no attenuation through the ^{241}Am source casing and microns of air before the absorber material. A 5.49 MeV alpha has a range of about 4.05cm in dry air at 1 atm [11]. For the theoretical section, the ideal situation is assumed. Since alpha particles are positively charged, Rutherford scattering is the mechanism in which the alpha will impart energy to the absorber nuclei. Assuming that the absorber was solely comprised of ^{57}Fe, the Rutherford scattering cross section can be calculated using equation 2.7:

$$\sigma = \pi Z^2 \left(\frac{ke^2}{KE}\right)^2 \left(\frac{1+cos\theta}{1-cos\theta}\right) \tag{2.7}$$

Where Z is the atomic number of the scattering nuclei (26 for ^{57}Fe), k is Coulomb's constant, e is the electric charge KE is the kinetic energy of the alpha (~5 MeV), and $\left(\frac{1+cos\theta}{1-cos\theta}\right)$ is the scattered fraction for angles greater than θ. If the scattering angle was 0°, then the cross section would be infinite. Scatters greater than 90° will impart the most energy and have a cross section of 1.76 barns at a rate of 1.41x10^7 collisions/s assuming the activity of the ^{241}Am is 3.5x10^9 decays per second as shown in Figure 9. Using conservation of energy and momentum, the energy transferred ranges from 0.025 to 1.45 MeV at scattering angles of 90° and 180°, respectively. Each transfer of energy, will produce phonons in the absorber.

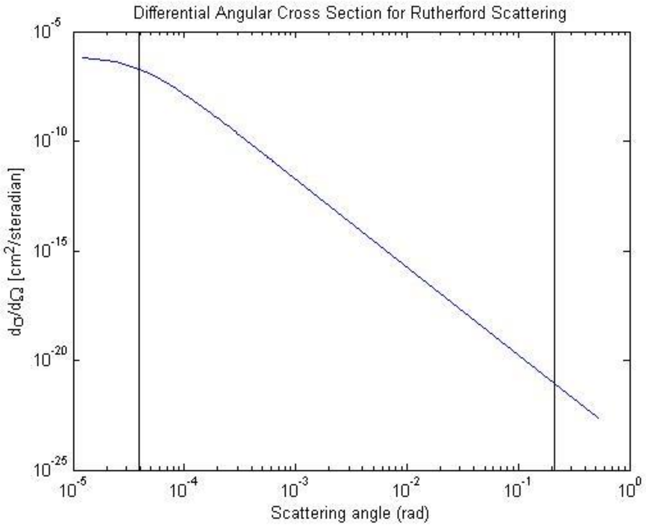

Figure 9: Differential angular cross section for Rutherford scattering in stainless steel type 310 with an alpha particle with 5.5 MeV energy.

2.3 Phonon Propagation

It is known that thermal spikes associated with the energy deposition events can produce acoustic waves in the source and surrounding materials. Since more than 95% of the energies released from radioactive decays are dissipated through atomic lattice vibrations, acoustic waves generated by the fission products and fragments can potentially be used as acoustic signatures for the radiation detection. The energies required to displace an atom in solids are normally on the order of tens of electron volts, which are significantly lower than kinetic energies of most energetic particles (e.g., about 5 MeV for an alpha particle). Therefore, cascades of atomic displacements up to tens of micrometers are observed for fission products and alpha decays in most solids. The highly localized deposition of energy, which causes fast melting along the particle track, followed by recrystallization or amorphization after the impact, can be described by the thermal spike model proposed by Seitz and Koehler [9, 22]. They suggested that the main result of the passage of the heavy atom through the solid is the development of highly concentrated lattice vibrations along the trajectory, phonons.

2.3.1 Phonons and Interactions

Phonons are quantized atomic vibrations in a lattice structures. These phonons transferred energy from one nucleus to another through sinusoidal displacement, which can be seen in Figure 10. Since this experiment does not go in to phonon transport modeling, a simple explanation of the mechanisms that phonons scatter as they propagate in a material. These mechanisms are phonon-phonon scattering, phonon-impurity scattering, phonon-electron scattering, and phonon-boundary scattering. Each scattering mechanism affects the normal phonon wave vector dissipating the phonon energy as propagation occurs. As phonons scatter, their energy dissipates. Ideally, the scattering of the phonons would be reduced with a pure crystal lattice allowing for a propagation vector to be preserved with minimal scattering. Unfortunately, a pure crystal was not practical for this current experiment and a material with ^{57}Fe was required.

2.3.2 Material Properties

The energy deposition from the Rutherford scattered alpha particles in localized areas produce acoustic waves, which can also be described as phonons. As the distance from the energy deposition location is increased, the energy of the phonons decay. The properties of a material paly a large part in phonon propagation as discussed above. One property of a material is the stiffness, which is a property of a metal, which gives it the ability to resist being permanently, deformed. As the stiffness of a material increases, large Young's modulus (Y) and low density (ρ), the speed of sound will increase, as shown in equation 2.8.

$$a_1 = \sqrt{Y/\rho} \qquad (2.8)$$

This allows for a faster acoustic wave in the material which can transfer the phonon energy to the Mössbauer event sites. The absorber used in this experiment is stainless steel Type-310, austenitic steel with 2% ^{57}Fe and a predicted average counting rate of 0.604 Mössbauer events/s. Austenitic steels have austenite as their primary phase (face centered cubic crystal). These alloys are annealed to produce a recrystallized microstructure with a uniform grain size. The grain boundaries cannot be eliminated from the material and will be a cause of the decay of the phonon propagation in the experiment.

2.4 Coupling – Mössbauer Events and Phonons - Expectations

In austenite stainless steel, atoms are firmly bound in a face centered cubic structure at specific lattice points. The atoms vibrate around their equilibrium position and as a consequence, the displacement from one atom will cause movement in the surrounding atoms. This motion propagates through the entire solid producing wave motion [18]. Figure 10 shows two different acoustic wave motions generated by the atomic vibrations in solids generated by the addition of phonon energy. The more phonons that are coupled in the wave motion, the larger the amplitude. Therefore, the more phonons that are produced, the more energy that can be coupled and theoretically traverse the entire length of the stainless steel bar to Mössbauer event surface.

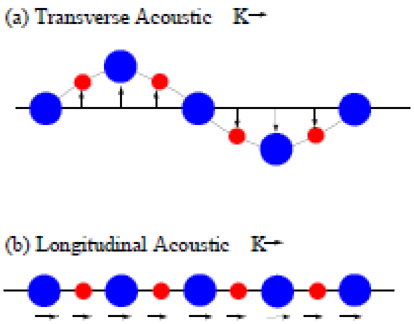

Figure 10: Acoustic (a) transverse, (b) longitudinal motion: the atoms move together. [26]

The emitting nucleus of a Mössbauer event can also interact with the atoms of a solid and participate in lattice vibrations, shown in the Doppler broadening of the Mössbauer spectrum (see Figure 5). In the thesis by E.A. Tanis, the concept of phonon density of states was studied in ^{57}Fe. It was established that resonant excitation takes place with the assistance of phonon annihilation or phonon creation as shown in Figure 11. In Figure 11.a, a phonon is annihilated to boost the incoming energy of the resonant energy. In Figure 11.b, a phonon is created to subtract from the incoming energy to achieve the resonant energy. The annihilation and the creation create what the author calls side wings, shown in Figure 11.c and translates to the excitation probability density S(E) [26]. The term S(E) correlates to the off resonance area in the Mössbauer spectrum, which is this experiment is the background.

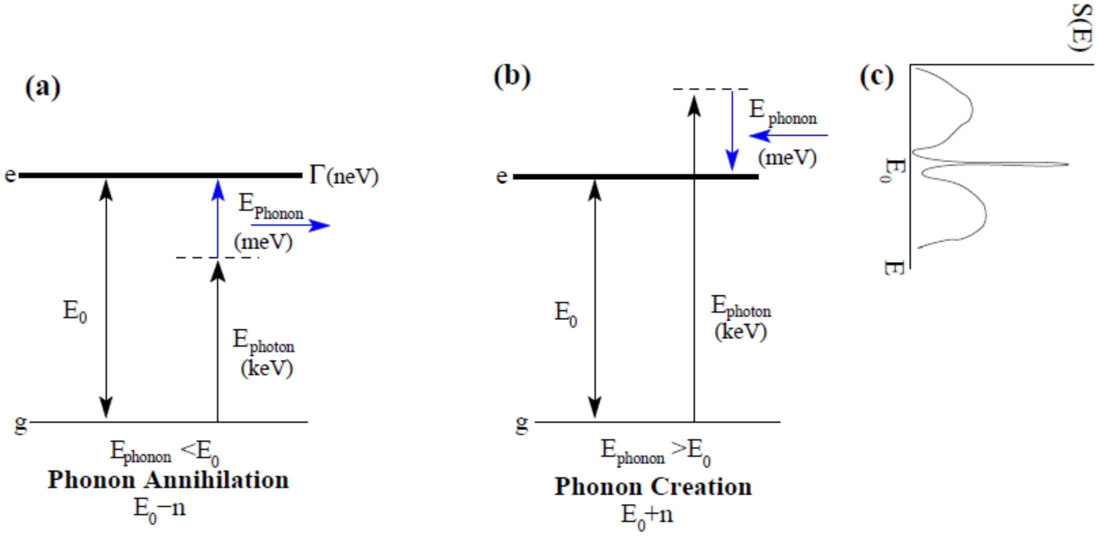

Figure 11: Phonon Annihilation and Creation. [26]

Based on these phenomena we expect to observe certain behaviors in our results to show that nuclear induce phonons that are coincident with Mössbauer events can couple. In order to verify that nuclear induced phonons will couple, this experiment will compare spectra with only one variable: presence of phonons. Mössbauer spectra will be with or without the ^{241}Am phonon source. All other parameters mentioned in the sections of Chapter 3 were held constant. Spectra without the phonon source will be used as a control and compared with spectra with the phonon source. There are several expected behaviors in the Mössbauer spectra with phonons. One is a broadening in the full width half max (FWHM) and a broadening in the wings due to high momentum phonon collisions with the Mössbauer event sites. A second possibility is that the counting rate of the background should increase while the area under the resonant peak should decrease due to phonon disruption of resonance sites. This is reflected physically by a change in the recoil free fraction of the material. A reduction in in recoil free fractions, as discussed in section 2.1.7, should reduce the peak of the spectrum, i.e. change the counting rate of the peak and increase the counting rate of the non-resonant background. Various statistical tests will be used to determine if there are any differences between the two spectra in Section 3.4.

III. Methodology and Experimental Setup

This section is intended to give insight into the development of the experimental set up, i.e. the reasoning behind choosing Mössbauer materials, the absorber, the detector design, and the phonon source. It will also go into detail behind each run accomplished.

3.1 Detector Design

3.1.1 Mössbauer Technique

In order to harness the sensitivity of Mössbauer spectroscopy, while allowing for phonons to couple with the Mössbauer events, a new detection system was designed. The detection system used the Conversion Electron Mössbauer Spectroscopy (CEMS) technique over traditional transmission Mössbauer spectroscopy (TMS) technique. In CEMS, the conversion electrons are emitted at the surface of the material and detected. Unlike TMS, CEMS does not have a dependence on the thickness of the Mössbauer absorber. This means more material can be used to mount the alpha source at the other end of the bar which can be seen in Figure 12. In our setup, it will be shown the large amounts of material (thicknesses >1mm) are not required due to the relatively large Rutherford scattering cross section for alpha particles in iron.

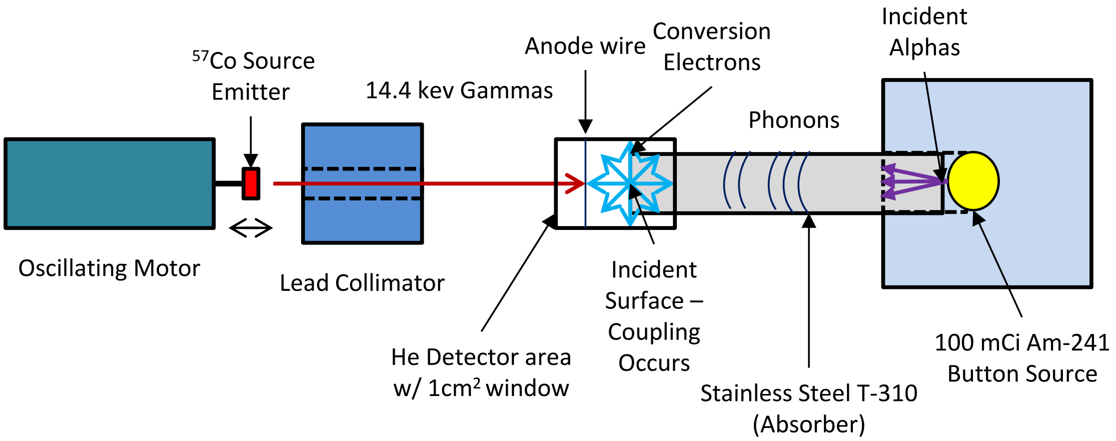
57Co Source Emitter
14.4 kev Gammas
Anode wire
Conversion Electrons
Incident Alphas
Phonons
Oscillating Motor
Lead Collimator
Incident Surface – Coupling Occurs
He Detector area w/ 1cm2 window
Stainless Steel T-310 (Absorber)
100 mCi Am-241 Button Source

Figure 12: Conversion Electron Mössbauer Spectroscopy (CEMS) Experimental Setup. Starting from the left: ^{57}Co source emitter attached to the oscillating motor, a lead collimator for the 14.4 keV gammas, CE proportional gas detector attached to left side of 1" diameter stainless steel type-310 bar, phonon source encased in a mounting device attached to the right side of the same bar.

3.1.2 Mössbauer Emitter

With the CEMS technique chosen, the next step is to choose the radiation source and subsequently an absorber isotope. The quality of a Mössbauer source depends upon the properties of the isotope and the host (matrix) material. The Mössbauer source should satisfy the following criteria [1]:

1. The photon energy, E_γ, should be of low energy, preferably between 5 to 50 keV. As E_γ increases, the resonance cross section, σ_0, decreases. Due to this behavior, energies above 50 keV will result a in little or no output. Energies below 5 keV would be lost compared to too much self-absorption.

2. The desired half-life of the source excited state should lie between 1 to 100 ns to have a desirable natural line width of first excited state, Γ_n. Too short and

Γ_n would not allow for any hyperfine structures to be resolved. Conversely, too long and Γ_n would be too narrow allowing small mechanical vibrations to destroy the resonance condition.

3. The internal conversion coefficient, α, should be small to ensure a large γ-ray emission from the source compared to the electron emission.

4. The source should balance high activity with a long half-life.

5. The Mössbauer isotope should not have high spin, which would produce complicated spectra, i.e. hyperfine splitting.

6. The Mössbauer isotope should have a relatively high natural abundance that enrichment would not be required and allow for an increased counting rate of Mössbauer events.

Among the isotopes in which the Mössbauer effect has been observed, the ^{57}Co parent in a Rhodium (Rh) matrix and ^{57}Fe daughter satisfies all the above requirements. The ^{57}Co source produces a high recoilless fraction, has a convenient line width, and an intense 14.4 keV γ-ray. Additionally, with a 271 day half-life and relatively low energy gamma rays (highest energy is 136 keV), ^{57}Co is a convenient source to use in the laboratory. The activity of the ^{57}Co source used in this experiment is shown in Figure 13.

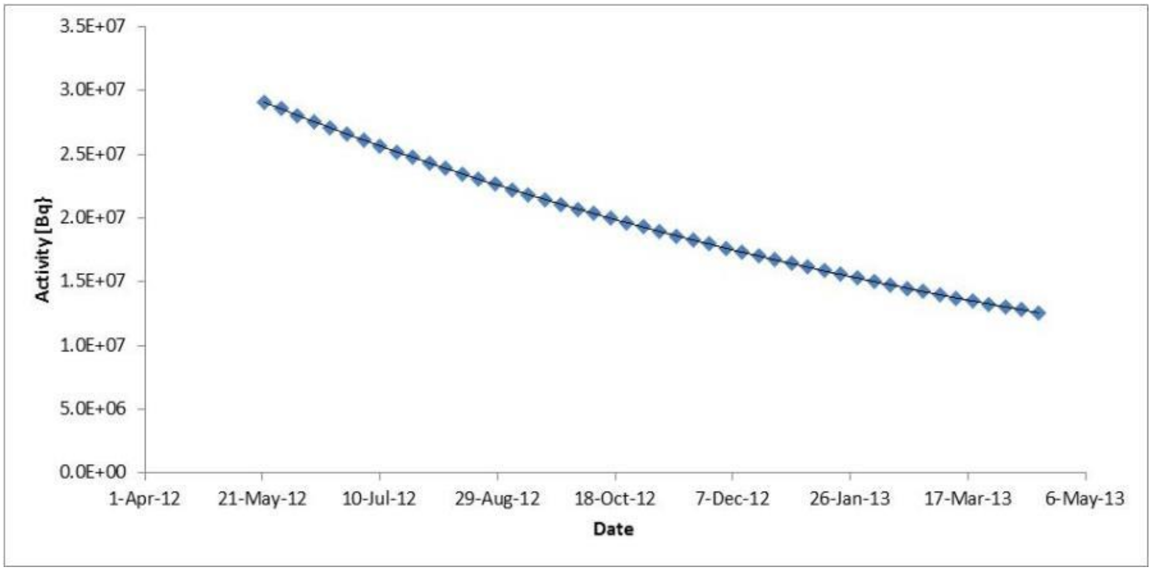

Figure 13: ^{57}CoMössbauer Source in a Rhodium matrix, T-137. Source assay: 2 Oct 2009. Activity at assay: 100 mCi.

3.1.3 Conversion Electron Detector

Upon absorption of a resonant photon, the first excited state of ^{57}Fe will decay via internal conversion 90% of the time and gamma emission 10% of the time (Ref. Figure 3). Remitted gammas cannot be differentiated in a detector from incident gammas from the source, and do not provide information in CEMS. Thus, we rely on the 7.3 keV conversion electron to produce a signal for the Mössbauer events. Since conversions electrons emitted in the ^{57}Fe resonance are 90% more likely to occur than 14.4 keV phonons, phonon coupling is more likely to occur more often with the conversion electrons, if coupling does occur (Ref. Figure 3). However, this does not mean that the counting rate is expected to increase, since the maximum penetration depth of the 7.3 keV CE is only 400nm. A majority of the resonances will have occurred in the bulk of the material.

In order to detect these conversion electrons, while ignoring the gammas a suitable detector must be chosen. Since electrons are charged, they quickly dissipate their energy in matter, thus most detectors will be sufficient for detection. However, gammas are significantly more penetrating and a small detector with low density will be insensitive to the gammas. Thus, a small gas proportional counter is ideal for this application.

Much of the background radiation in Mössbauer spectroscopy can be suppressed by using a resonant detector. In this experiment, a Ranger Instrument SD-200 conversion electron detector was used. These detectors count the 7.3, 6.2, and 5.4 keV electrons generated by the internal conversion process and Auger electrons after the Mössbauer gamma ray is absorbed. Since this process is very efficient, an extremely good signal-to-noise ratio is achieved. Table 1 shows a list of key parameters for the SD-200 proportional detector. Discounting electronic noise, the primary source of unwanted counts would be photoelectrons and Compton electrons created inside the detector by incoming radiation, which can be kept to a small fraction with detector optimization.

Table 1: Ranger Instrument SD-200 Detector Specifications [24]

Anode Voltage	1200 Volts
Gas Flow	1cc/minute of 96% He – 3% CH$_4$
Detector Capacitance	8.6 pF
Electron Energy Resolution	0.6 keV
Solid Angle of Detection	2π Stearadians
Detector Efficiency	97%
Mössbauer Effect	10% for single line source and absorber
Mössbauer Line Width	Natural line width, due to absence of thickness broadening
Detection Limit	60μfm/cm^2 of sample containing at least 10% of iron
Counting Rate	50 kHz maximum
Size	1” x 2” x 0.4”
Connectors	UG – 931/U

For Compton and photoelectric effects, Helium filled proportional counters have a low background, are insensitive to x-ray radiation and are very efficient in detecting low energy electrons. The SD-200 an aluminum rectangular box with two wires spaced 0.166 inches apart, as notionally shown in Figure 14. During the operation of the dual wire detector, the anodes are kept at 1200V to remain in the proportional region for the SD-200 configuration. As shown in the right side of Figure 15, there is an inlet and outlet tub to allow the air to be purged of air and a constant flow of Helium gas quenched with 3% Methane at approximately 1 cm^3/s. The counter has two ½ inch windows. The front window is covered with aluminum foil and yellow Mylar tape to allow incident gammas from the Mössbauer source. A lead-aluminum shield was place in front of the window with a 1/16 inch diameter hole to restrict the incident radiation to the desired area of the window, shown in the left side of Figure 15. The other window, opposite the front and on the other side of the anode wires has a removable cover to allow for the absorber material. A seal is created when putting the absorber into place.

In order to characterize the SD200 proportional detector, an electron spectrum of the ^{57}Fe taken, using a bare ^{57}Co source inside the detector without a sample, as shown in Figure 16. Since the detector us virtually invisible to the 14.4 keV gamma, spectrum gives the SD200 response to the 7.3 keV conversion electrons emitted from the bare source. The spectrum to the left of the peak is the Compton continuum along with Auger electrons. Along with the bare source electron spectrum, Figure 17 shows the pulse height spectrum of photoelectrons and conversion electrons with the source scanning at high velocities (a) and the source at rest (b). The source at rest corresponds to the sum of the background and resonantly generated electrons. The energy degrades continuously in both spectra as the electrons escape from varying depth of the absorber. Pleae note that the lower discriminator at 2 keV and upper discriminator at 8 keV in the TSCA.

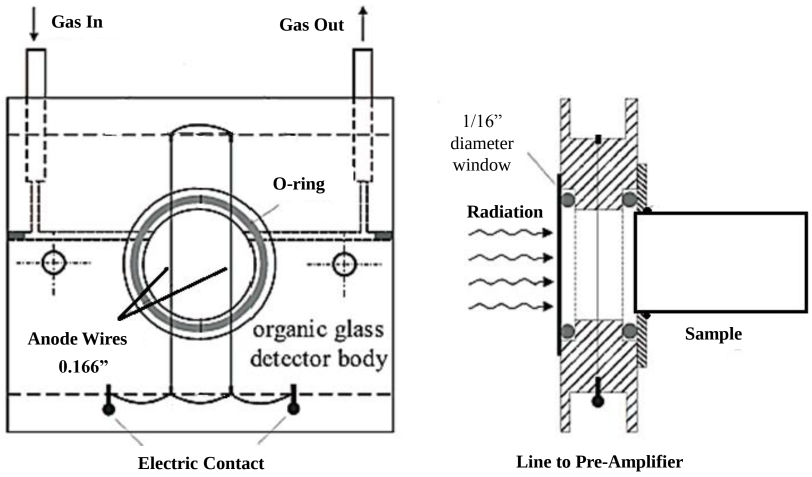

Figure 14: Simple diagram of the SD200: a gas-flow proportional detector for CEMS.

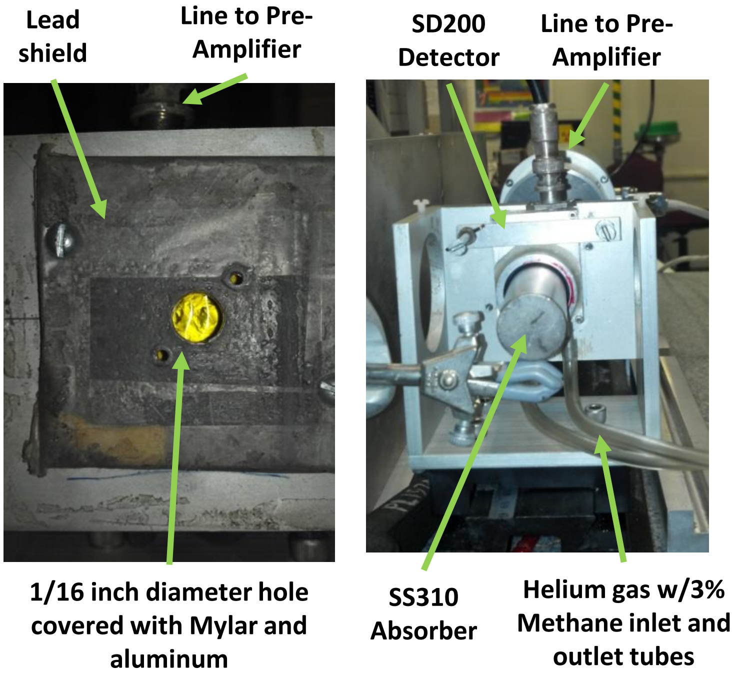

Figure 15: Left: Lead-Aluminum radiation shield with 1/16” diameter hole in front of the detector. Right: SD200 detector with inlet and outlet tubes for He w/3% CH_4 gas.

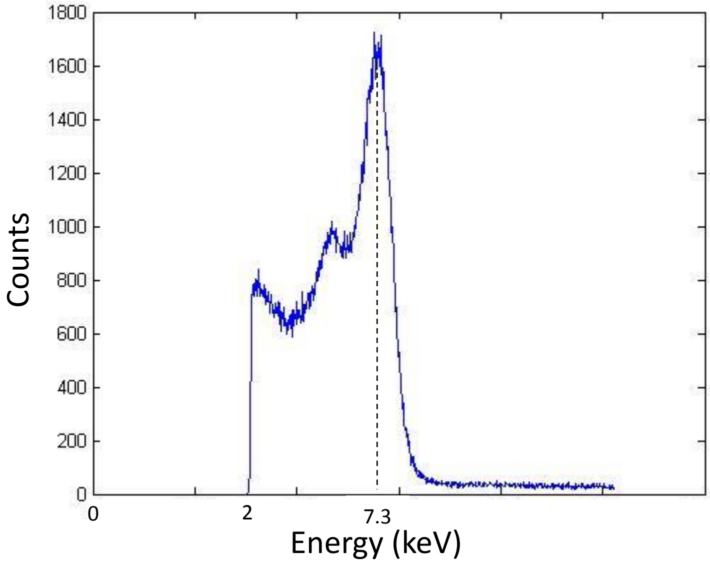

Figure 16: Conversion Electron Spectra for the T123 Co^{57} bare source. Shows the SD200 detector running with only the bare source inside the sample chamber. Note the 7.3 keV conversion electron peak.

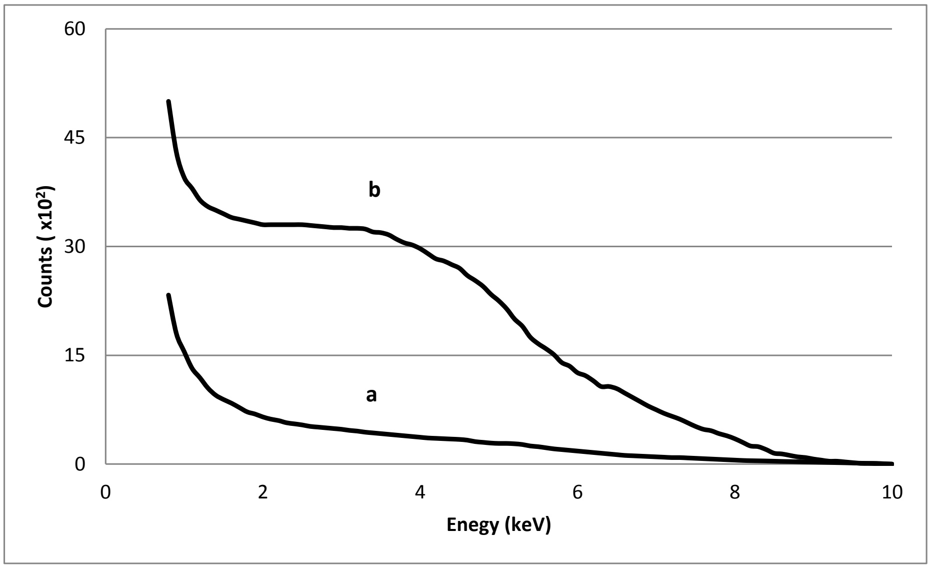

Figure 17: Pulse height Spectrum. Energy distribution of photoelectrons and conversion electrons obtained by source-detector off resonance (a) and in resonance (b). Lower discriminator at 2 keV and upper discriminator at 8 keV. [23]

3.1.4 Mössbauer Spectrometer

The MS-1200 Mössbauer Spectrometer is a computer based system built by Ranger Scientific. The spectrometer combines a multichannel analyzer and Mössbauer control circuits in a single unit, with data transfer to a PC. The Ranger Mössbauer Spectrometer is made up of two basic systems: A Doppler Modulator and a Gamma Ray Analyzer. The gamma ray analysis aspect of the spectrometer was not used during this experiment. Instead, the signal from the detector goes through a pre-amplifier with the 14.4 keV peak from ^{57}Co source isolated using a timing single channel analyzer (TSCA) with the upper limit at 6.8, the lower limit at 4.0 and the delay at 1.0 micro-second (see Figure 18).

The Doppler Modulator, VT-1200 mechanically oscillates the source and is controlled by the MS-1200. This velocity drive system is not only the most important component, but also a feature unique to Mössbauer spectroscopy. The motor is an electromagnetic drive system composed of a waveform generator, a drive circuit, a feedback circuit, and a velocity transducer. The electromagnetic velocity transducer works the same way as a loudspeaker [10, 29]. The transducer converts an applied current to the velocity of the source through a drive coil and provides a signal proportional to the actual velocity through the pickup coil. This produces a virtually frictionless movement of the shaft in the center of the motor. The radiation source is placed on the end of the shaft and a photodiode is installed at the other end to measure velocity. The system exhibits excellent stability, linearity, and reliability.

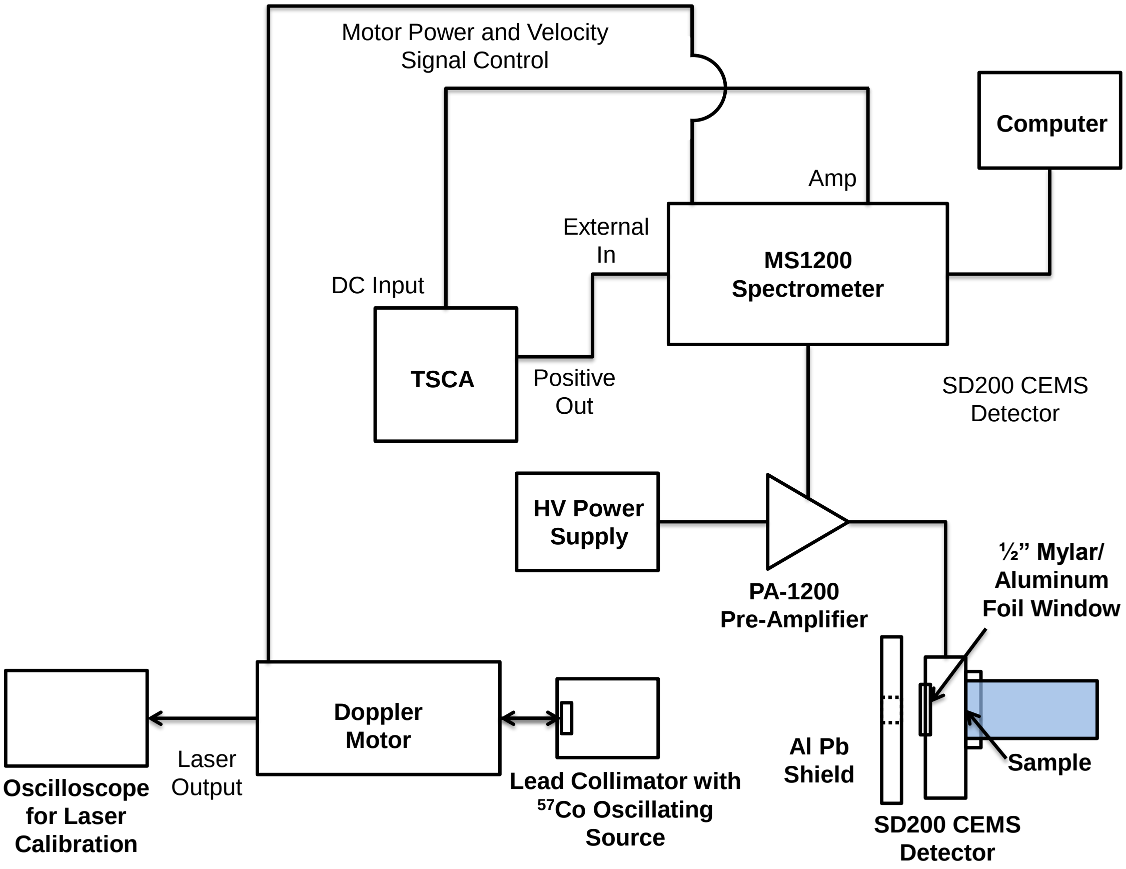

Figure 18: Block Diagram of Mössbauer Spectrometer Electrical System

The waveform generator is used to provide the drive system with a reference signal which determines the waveform and the source motion. The VT-1200 can operate in the symmetric or flyback mode. The symmetric sinusoidal mode gives a two mirror image spectrum, while the flyback (saw tooth, ramp up) produces only one spectrum. Since the symmetric sinusoidal mode produce some nonlinearity in the spectrum, a linear saw tooth waveform was applied. In this waveform, the source has a constant acceleration as shown in Figure 19a. The velocity starts at $-v_{max}$, goes through zero, and increases linearly to $+v_{max}$. It then decreases uniformly back down to $-v_{max}$. The velocity of the motor is in the units of mm/s and is equivalent to $\Delta E = 4.80766x10^{-8}$ eV. The velocity parameter on the spectrometer was set to both ±11 mm/s and ±22 mm/s.

The system uses a laser calibration to determine the speed of the motor velocity and velocity turn around. Since the Doppler Module is the most important part of a Mössbauer spectrometer by adding and subtracting energy from the radiation source, it is imperative that the motor is calibrated. This calibration assigns a velocity / energy to the channel numbers. This is done by using laser interference fringes and Michelson patterns to measure the absolute values of the source velocity. An oscilloscope was used to determine the laser focus on the photodiode. These fringes are transformed by the photodiode into pulse, which are counted by the multiscaler in the spectrometer which produces a V-shape spectrum as seen in Figure 19b. One issue with this method is that the fringe counts at low speeds are not as accurate, especially at zero velocity. The maximum noise introduced into velocity spectrum is $2x10^{-3}$ mm/s. The system also has a non-linearity less than 0.05% for the 11 mm/s velocity range [24].

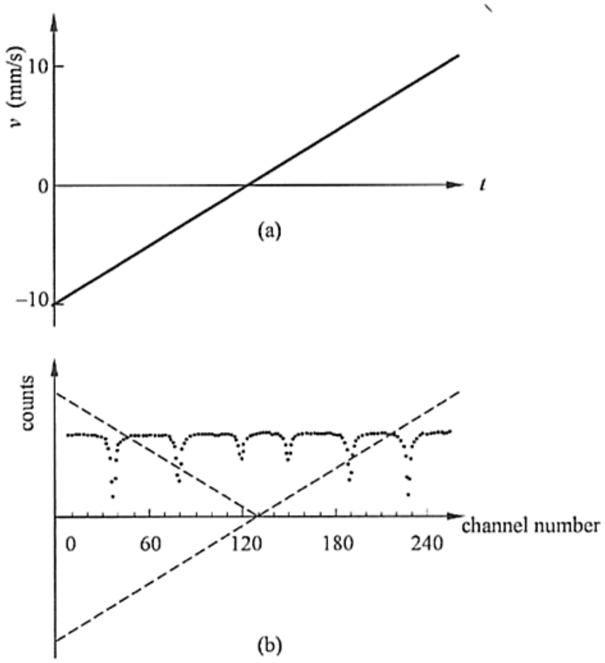

Figure 19: (a) Triangular drive voltage. (b) A V-shaped interference fringe spectrum, superimposed on a sextet spectrum. [1]

The last components of the system are the shielding, collimator, dampers and railings. The shielding confines the system to block out and reduce background radiation. The collimator is used to confine the gammas towards the detector window and helps eliminate indirectly scattered gamma rays which contribute to measurement noise. The Doppler module, collimator, shielding, and detector are placed on a railing system to lock the components into place and keep motor and source alignment with the detector window. As shown in Figure 20, the source and the surface of the detector window are separated by 50cm distance. The entire detection system is placed on a heavy table to damp out any random vibrations and isolate it from the ambient environment.

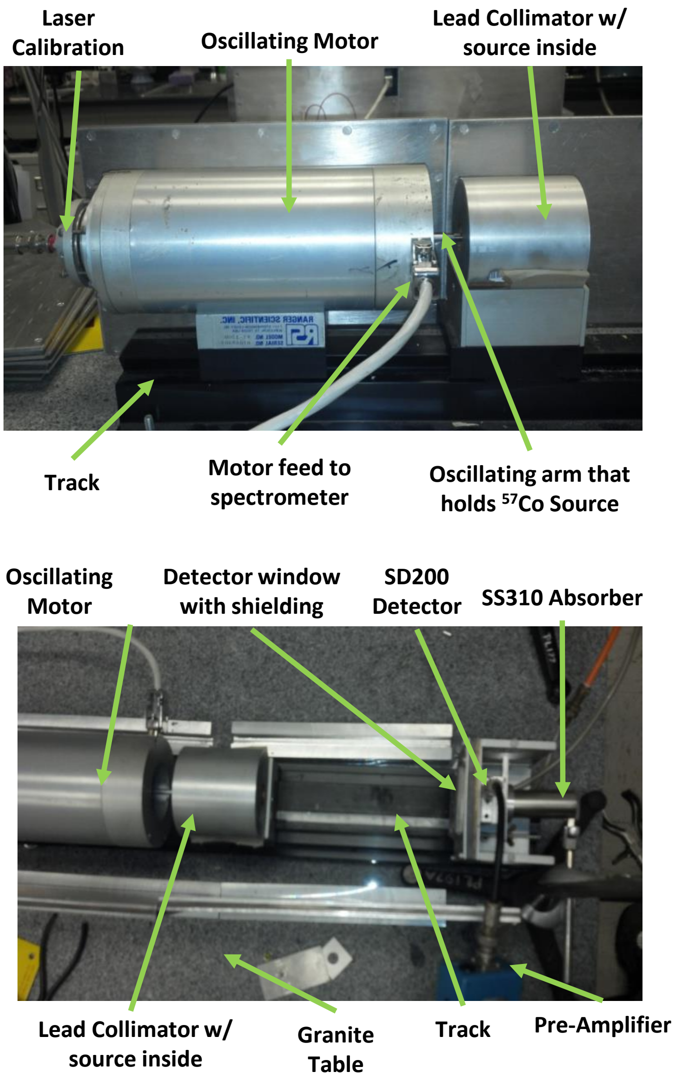
Laser Calibration
Oscillating Motor
Lead Collimator w/ source inside
Track
Motor feed to spectrometer
Oscillating arm that holds ^{57}Co Source
Oscillating Motor
Detector window with shielding
SD200 Detector
SS310 Absorber
Lead Collimator w/ source inside
Granite Table
Track
Pre-Amplifier

Figure 20: Top: Image of the oscillating motor, laser calibration, ^{57}Co source location and lead collimator. Bottom: Source orientation from detector window, SD200 detector and SS310 absorber rod.

3.1.5 Material/Absorber

Because this experiment uses a ^{57}Co emitter, an absorber containing ^{57}Fe must be used to capture the resonant photons and create conversion electrons. One question of interest related to the absorber is: what configuration should the iron isotope be in the material to achieve the goals of the experiment? A few of the considerations in the material selection process that will be discussed are isotope abundance, form of the Mössbauer spectrum created, geometry, and available materials.

The first question to be answered is how the abundance of the ^{57}Fe isotope in the absorber affects acquisition times. In the laboratory, we had slightly oxidized foil samples of 95% enriched ^{57}Fe, 90% enriched ^{57}Fe (feeler gauge) and natural iron (α-Fe ~2% ^{57}Fe) that were 12.5µm, 25µm and 25µm thick, respectively. The 95% enriched foil was used as a calibration standard for the experiment. The feeler gauge had a stainless steel backing with an ^{57}Fe enriched surface and was used for the preliminary studies. The feeler gauge and the natural iron samples were used to conduct a study of counting rates for acquisition times. It was expected that the enriched sample would produce a more pronounced spectrum in a shorter time, while the natural iron would take longer, with the time difference directly proportional to the amount of ^{57}Fe in the foil. The foil samples were kept in a low oxygen environment with desiccant and only exposed to the laboratory air while inserting them into the detector. Figure 21 shows several Mössbauer spectra for different forms of iron. Note that oxidation does not change the counting rate of the spectra, but can affect the location and number of peaks measured.

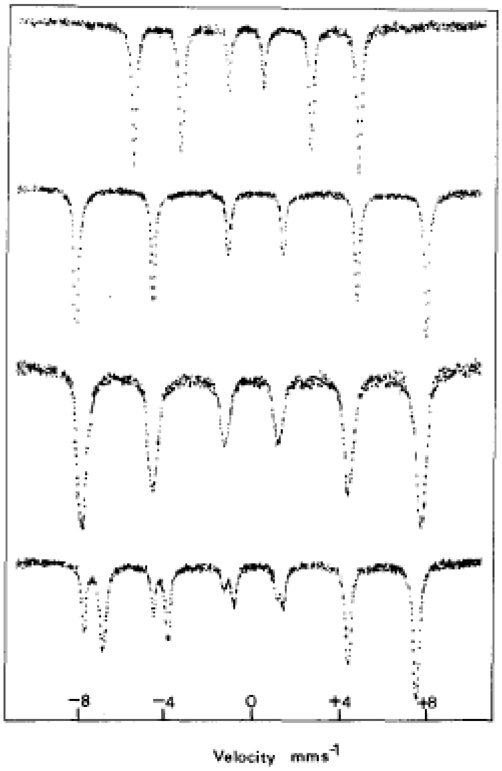

Figure 21: Iron-57 Mössbauer transmission spectra of (from top to bottom) α-Fe, α-Fe_2O_3, γ- Fe_2O_3, Fe_3O_4 [9]. Oxidation does not change the counting rate, but does shift and create new peaks. The iron isotope only changes the oxidation state, but not it's resonance cross section.

Figure 22 shows the Mössbauer spectra of the enriched iron feeler gauge and the natural iron foil were taken for 2 hours and 6 days, respectively. The baselines for both spectra were moved to the zero by removing the background counts. The six peaks in the spectra were located using the enriched standard and fitted with a Lorentzian at those peak locations. The area under the Lorenzian peaks were summed up and divided by the exact acquisition time. The data show that the enriched iron sample had an average Mössbauer event counting rate of 4.85 counts per second with an error of 5.37% in the peak fitting for the 2 hour spectrum. The natural iron sample had an average Mössbauer event counting rate of 0.344 counts per second with an error of 10.45% in the peak fitting for the 6 day spectrum. Please note that the 10.45% error associated with the natural iron sample is inconsequential to determining future acquisition times. It was evident that using an absorber with enriched ^{57}Fe is preferred. Other than using the foil samples already available in the lab, ^{57}Fe enrichment of an absorber was not possible due to time and budget constraints.

Knowing that we were required to use materials with natural iron, we needed to consider materials that would produce spectra that would be simpler to analyze. If an α-Fe material was used, there would be six peaks to analyzed from the hyperfine structures due to the material properties, see (a) and (b) of Figure 22. Note that in (a) the two middle peaks were virtually useless because the peaks barely rose above the noise. This would create a challenge to analyze. Secondly, the spectrum was acquired for 6-days and the outside four peaks, even though they were above the noise, the signal-to-noise ratio was only 3:2. This was after 144 hours of acquisition time. Not only are the six peaks close enough together where they overlap slightly, there was not a large signal to noise ratio. Considering this, a simpler spectrum needed to be analyzed.

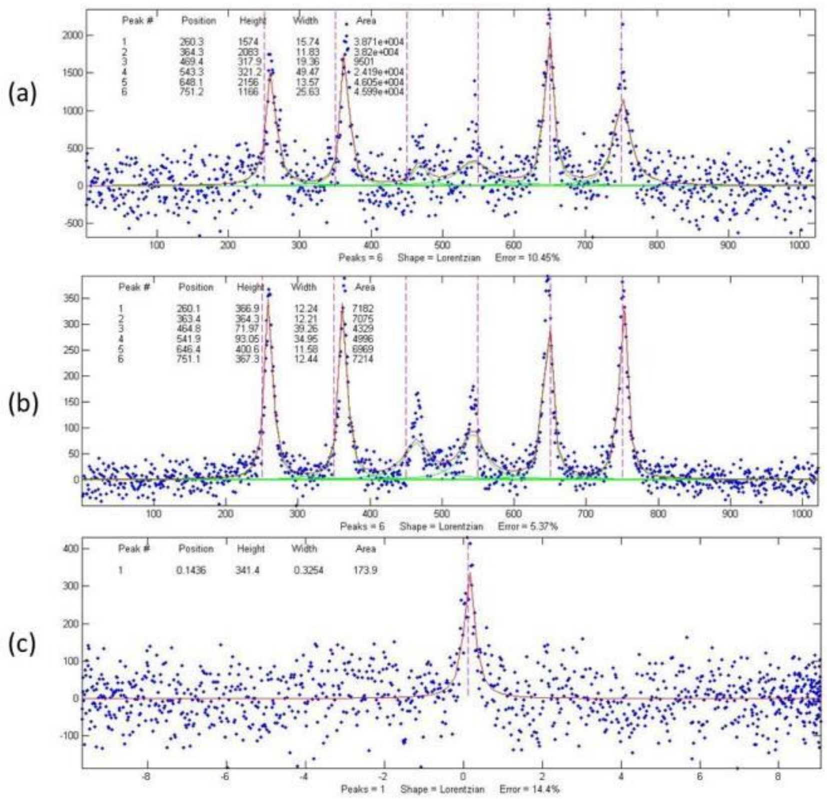

Figure 22: Absorber spectrum comparison. (a) Natural iron foil with a 6-day acquisition time. (b) Enriched iron-57 feeler guage with a 2-hr acquisition time. (c) Stainless Steel Type 310 foil with a 40-hr acquisition time. The vertical is relative counts verse channel number/velocity.

Fortunately, literature directed the experiment to a material that would produce a simpler spectrum, stainless steel type 310 which was available to test in the lab [Stewart, 1986]. A 25μm SS Type 310 foil sample was placed in the detector and the spectra was acquired for 40 hours. The stainless steel sample produced only one peak that was right of center, as seen in (c) of Figure 22. This material produced the same signal to noise ratio for under a third of the time. Also, the sample had an average Mössbauer event counting rate of 0.18 count/s with an error of 14.45% in the peak fitting. Even though the counting rate was lower, it was only for one peak. Changes in the spectrum would be easier to detect and interpret. The stainless steel type 310 properties can be seen in Table

2. To calibrate the stainless steel peak location, the six peaks of the enriched ^{57}Fe standard was used to convert the channel numbers to velocity and energy. Section 4.1 will discuss the code that was used for the calibration.

Table 2: Stainless Steel Type 310 Properties

Composition	Fe	48.18% (1.02% Fe^{57})
	C	0.25%
	Cr	26%
	Ni	22%
	Mn	2%
	Si	1.5%
	P	0.05%
	S	0.03%
Density	8.03	g/cm^3
Elastic Modulus	200	GPa
Hardness – Rockwell B (HR B) max	95	
Hardness – Brinell (HR) max	217	
Number of Mössbauer Peaks	1	

The next consideration was the geometry of the absorber. The absorber not only had to fit in the CEMS detector opening, but had to allow a phonon inducing radiation source to be attached at the opposite end. A 1 inch diameter cylindrical rod with two SP12 size 118 O-rings was inserted into the CEMS detector, and the seals kept the Helium gas from leaking. This can be seen in the right side of Figure 15. A radiation source holder was then attached to the other side of the steel rod. The holder could accommodate a small unsealed button source of ^{241}Am, and would hold it directly against the end of the steel rod. A schematic of the rod and source holder are shown in Figure 21. The required length of the rod was unknown. To help facilitate phonon propagation through less material, a 3 inch long rod was used and switched to a 2 inch rod later in the experiment to help decrease distance traveled by the phonons.

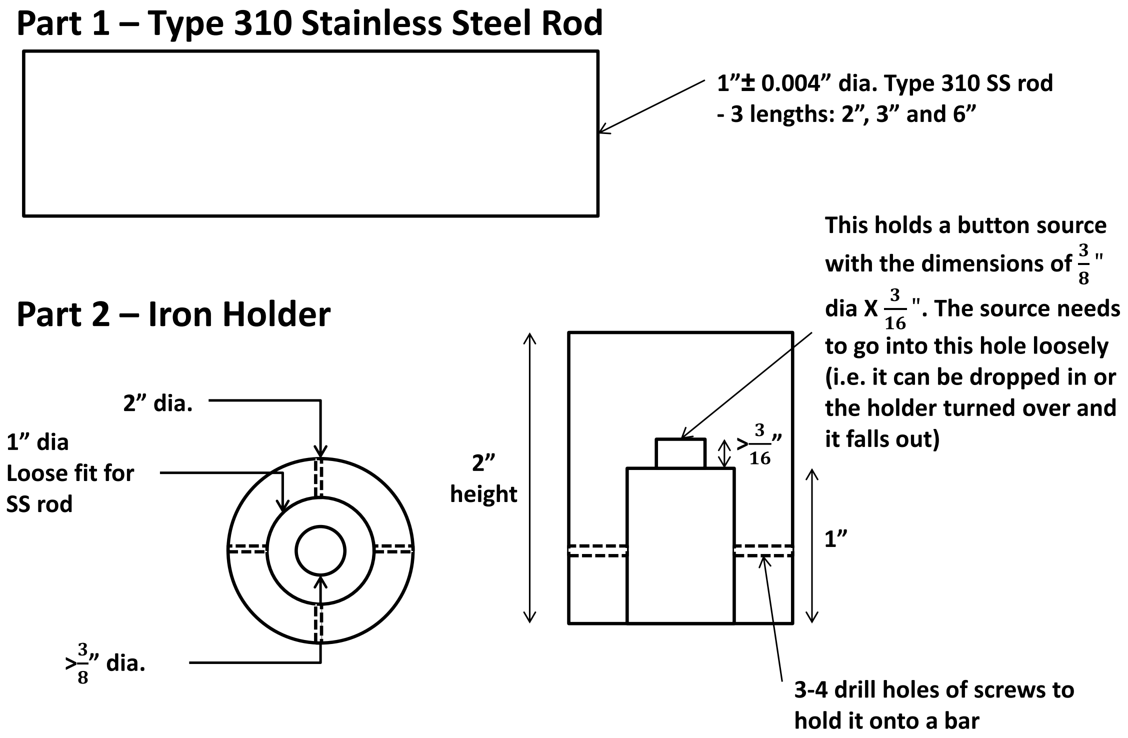
Part 1 – Type 310 Stainless Steel Rod
1"± 0.004" dia. Type 310 SS rod
- 3 lengths: 2", 3" and 6"
Part 2 – Iron Holder
2" dia.
1" dia
Loose fit for
SS rod
>3/8" dia.
2"
height
>3/16"
1"
This holds a button source with the dimensions of 3/8" dia X 3/16". The source needs to go into this hole loosely (i.e. it can be dropped in or the holder turned over and it falls out)
3-4 drill holes of screws to hold it onto a bar

Figure 23: Specifications for the absorber and the iron phonon source holder

3.1.6 Phonon Source

The alpha decays from ^{241}Am were used to produce an acoustic signal, i.e. phonons, in the stainless steel (SS) absorber, via Rutherford scattering. The Am^{241} source used for the experiment was assayed 12 Nov 1972 with a 100 mCi initial activity. Since Am^{241} has a half-life of 432.6 years, the source isotropically emits 3.6x10^{9}alphas/s. The button Am^{241} source was placed against the back surface of the SS rod reducing air attenuation to virtually zero and generating a 2π Steradian solid angle. Therefore, 1.8x10^{9} alphas/s with decay energies of 5.49 MeV (85%) and 5.44 MeV (13%) will leave the source and be incident on the bar, after slight attenuation.

3.2 Experimental Runs and Descriptions

The overarching goal to design of the experiments is to attempt to detect a change in the Mössbauer spectrum for the stainless steel type 310 (SS310) bar between phonons present and absent. If this spectrum change is detected, then the change can only be due to one condition, the coupling of phonons. In order to show this, a characterization of the detection system and procedures is required. The first part of this procedure is to confirm the reproducibility of the measurements. To show this, the enriched iron standard was placed in the detector and a spectrum was acquired for 2 hours. This was repeated 3 times to show stability of the spectra. Table 3 shows the results from the 3 trials. Due to the oxidation of the enriched iron standard, the 3rd and 4th peak information was omitted in the reproducibility analysis since the oxidation generates irregular peaks in the center of ^{57}Fe spectrum. Overall, the differences in the numbers are within the combined curve fitting errors of the Lorentzian fits.

Table 3: Reproducibility HV = 1250V, Doppler Motor Laser Calibration Green

Trial	Sample	Acquisition Time	Peak Position	FWHM (# of Channels)	Counting Rate (counts/s)	Error in Curve Fitting
1	95% Enriched ^{57}Fe Standard	2.0 hours	(1) 260 (2) 363 (5) 646.7 (6) 751.1	(1)13.16 (2) 12.15 (5) 12.32 (6) 12.66	(1) 0.99 (2) 0.94 (5) 0.91 (6) 0.93	5.65%
2	95% Enriched ^{57}Fe Standard	2.25 hours	(1) 260.1 (2) 363.4 (5) 646.4 (6) 751.1	(1) 12.24 (2) 12.21 (5) 11.58 (6) 12.44	(1) 0.89 (2) 0.87 (5) 0.86 (6) 0.89	5.37%
3	95% Enriched ^{57}Fe Standard	2.75 hours	(1) 260.4 (2) 363.3 (5) 646.6 (6) 751	(1) 12.10 (2) 11.72 (5) 11.68 (6) 12.89	(1) 0.96 (2) 0.92 (5) 0.87 (6) 0.94	4.9%

During early phases of material selection for the absorber, a neodymium ($Nd_2Fe_{14}B$) bar was considered before the SS310 bar due to the magnetic properties of the material. The idea behind the consideration was the magnetic field would give directionality to the phonons generated by the phonon source. At this time neutrons were still being considered as a phonon inducing source and the boron in the material would allow for the B(n,α)Li + 2.31 MeV reaction to produce the phonons. The bar would not have been enriched and would contain 1.8% ^{57}Fe atoms (more than the SS310), but there would have been 6 peaks for the counts to be distributed from the magnet instead of one from the SS310 bar. When the magnet arrived in the lab, the bar has a 20µm thick nickel coating to protect the magnet from corrosion. Instead of cutting off coating at the surface to expose the iron in the material due to the 6 peaks, an enriched film could be attached to the surface to help speed up acquisition times. Because of this consideration, two additional experiments were conducted.

Since the enriched ^{57}Fe feeler gauge was available and only the magnetic field was to be characterized, the feeler gauge was inserted into the detector without the magnet first to characterize the detector. The Mössbauer spectrum was acquired for an hour. Then, the magnetic Neodymium bar was placed with the feeler gauge sample into the detector to characterize the effects of a magnetic field on the Mössbauer spectrum. The sample with the bar was acquired for 1.78 hrs. After the experiment, different foils in the lab were attached to the bar magnet. The foils bent and crumpled in the magnetic field. It was determined that artificially enriching the surface of the bar magnet would create discontinuity in the media and was not the best method to observe the presence of phonons. Because of this and other reasons previously mentioned, the experiment used

SS310 as the material. Figure 24 shows the rest of the experiments used the SS310 absorber.

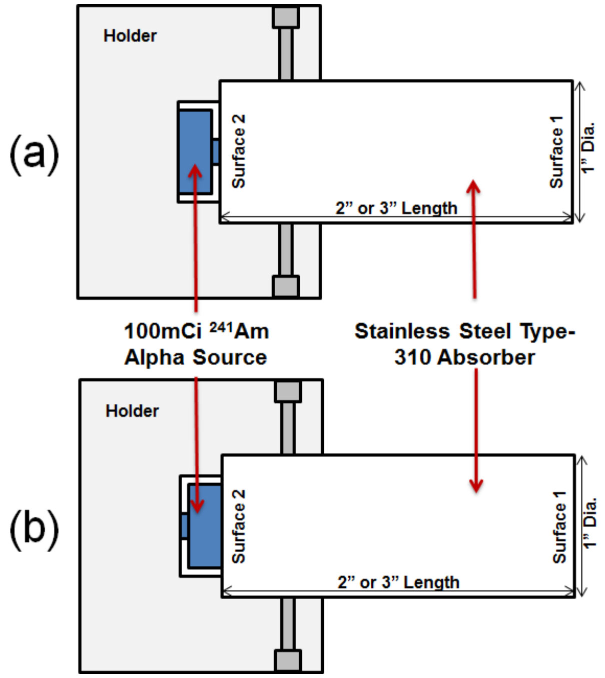

Figure 24: ^{241}Am alpha source configuration with holder and SS310 absorber rod. Surface 1 was used for the Mössbauer event sites and surface 2 was used for the incident alphas. (a) Button directed towards absorber surface, alphas incident. (b) Button directed away absorber surface, alphas shielded, only gammas.

For the remainder of the section, the experiments that were performed will be described in full detail. Table 4 shows a complete summary for these experiments. Generally speaking, data acquisition alternated between using the alpha source and not using the alpha source. This was to make sure that runs were independent from each other. Also, it helps reducing a the amount of correction for the Mössbauer ^{57}Co source decay when comparing the alphas/no alphas measurement by having have the measurements taken one after the other. In the first set of experiments (Runs #19-21), premixed helium gas with 3%Methane was not available. Instead, He-gas was run through a flask filled with 125ml inert oil on top of 25ml of methyl alcohol at a flow rate of 2.4 bubbles per sec and a flow meter reading of 3.5. This set up produced He gas quenched with 3% methane. The high voltage (HV) power supply on the detector was set to 1250V. From Run22 and on, the fill gas was replaced with premixed He-3%CH_4 gas and gas flow registered at 4cfm. The HV power supply was set to 1200V at Run27, where the SD200 detector still operated in the proportional region. This was to help prevent a possible reason the HV power supply from tripping by not putting too much strain the power supply. To help address possible future trips, the equipment and data was monitored and saved more frequently.

Table 4: Summary of Experimental Runs Performed

Run #	Sample	Phonon Source	Acquisition Time (hrs)	Motor Velocity [mm/s]	Detector Fill Gas	HV Power Supply
19	3" SS310 Rod with NO source holder	None	23.98	11	Flask Pre-mix He-3%CH_4	1250V
20	3" SS310 Rod with source holder	None	1.92	11	Flask Pre-mix He-3%CH_4	1250V
21	3" SS310 Rod	^{241}Am alpha Source	24.23	11	Flask Pre-mix He-3%CH_4	1250V
22	Enriched ^{57}Fe Standard Calibration	None	10.45	11	Pre-mix He-3%CH_4	1250V
23	6" SS310 Rod with source holder	None	24.00	11	Pre-mix He-3%CH_4	1250V
24	3" SS310 Rod	^{241}Am alpha Source	24.45	11	Pre-mix He-3%CH_4	1250V
25	3" SS310 Rod with source holder	None	(A) 15.13 (B) 17.97 (C) 28.20 (D) 40.63 (E) 48.00	11	Pre-mix He-3%CH_4	1250V
26	3" SS310 Rod	^{241}Am alpha Source	(A) 24.00 (B) 28.20 (C) 40.63	11	Pre-mix He-3%CH_4	1250V
27	3" SS310 Rod	^{241}Am alpha	(A) 27.00	11	Pre-mix	1200V

		Source	(B) 48.00		He-3%CH_4	
28	3” SS310 Rod with source holder	None	(A) 24.00 (B) 48.00	11	Pre-mix He-3%CH_4	1200V
29	3” SS310 Rod with source holder	None	(A) 26.35 (B) 96.32	11	Pre-mix He-3%CH_4	1200V
30	3” SS310 Rod	^{241}Am alpha Source	(A) 26.35 (B) 96.00	11	Pre-mix He-3%CH_4	1200V
31	3” SS310 Rod	^{241}Am alpha Source	(A) 48.08 (B) 136.1	11	Pre-mix He-3%CH_4	1200V
32	2” SS310 Rod with source holder	None	182.47	11	Pre-mix He-3%CH_4	1200V
33	2” SS310 Rod	^{241}Am alpha Source	182.5	11	Pre-mix He-3%CH_4	1200V
34	2” SS310 Rod	^{241}Am alpha Source	217.42	11	Pre-mix He-3%CH_4	1200V
35	2” SS310 Rod with NO source holder	None	167.53	11	Pre-mix He-3%CH_4	1200V
36	6” SS310 Rod with NO source holder	35°C Heat Tape	165.52	11	Pre-mix He-3%CH_4	1200V
37	6” SS310 Rod with NO source holder	46°C Heat Tape	167.17	11	Pre-mix He-3%CH_4	1200V
38	6” SS310 Rod with NO source holder	None	91.08	11	Pre-mix He-3%CH_4	1200V
39	2” SS310 Rod with source holder	None	164.2	22	Pre-mix He-3%CH_4	1200V
40	2” SS310 Rod	^{241}Am alpha Source	(A) 122.2 (B) 239.6 (C) 293.3 (D) 410.8 (E) 433.6 (F) 510.9	22	Pre-mix He-3%CH_4	1200V
41	2” SS310 Rod with source holder		(A) 116.6 (B) 167.5 (C) 237.5 (D) 283.2 (E) 332.8 (F) 497.8	22	Pre-mix He-3%CH_4	1200V
42	2” SS310 Rod	^{241}Am alpha Source	(A) 73.93 (C) 173 (D) 240.4 (E) 266.8 (F) 335.8 (G) 1331	22	Pre-mix He-3%CH_4	1200V
43	2” SS310 Rod	^{241}Am alpha Source	168.3	22	Pre-mix He-3%CH_4	1200V
44	2” SS310 Rod	^{241}Am Source flipped – Figure 24 (b)	(A) 218.1 (B) 383.4 (C) 459.9 (D) 552.9	22	Pre-mix He-3%CH_4	1200V

			(E) 675.8 (F) 893.3 (G) 1151 (H) 1320 (I) 1804			
45	2” SS310 Rod	^{241}Am alpha Source	(A) 188.1 (B) 384.9 (C) 547.3	22	Pre-mix He-3%CH_4	1200V

The absorber sample in Run19 was a 3” SS310 rod with the phonon source holder attached, but not the phonon source. This was a background run for the SS310 rod and holder and to characterize the Mössbauer spectrometer. The spectrometer was run for 24 hours. Then in Run20, the holder was removed to verify that the holder did not have an effect on the spectrum. Data was acquitted for roughly half the time of Run19, 10.45 hours. Then the ^{241}Am alpha source was placed in the holder and on the SS310 absorber in configuration (a)(see Figure 24). Since alphas are now incident on the bar, an external source of phonons was introduced. The spectrum was acquired for 24.23 hours and will be used for comparison with Run19.

Since the gas mixture was changed, the SD200 detector was recalibrated using the enriched iron standard. The HV turned off at some point during Run22’s 10.45 hour run. The power supply was checked and a 6” long SS310 rod was placed in the detector with the holder attached and no alpha source. Data was acquired for 24 hrs. This was to check to see if absorber length mattered, characterize the spectrometer and to check the HV power supply.

Following Run23, Run24 used a 3” long SS310 rod with the alpha’s incident on surface 2 of the absorber. Data was collected for 24.25 hours. Run25 was configured with the 3” long absorber and holder attached. The data was saved periodically to see how the spectra changed and gather more data sets for future analysis. During this run, the HV power supply tripped at some point between Run25A and Run25B. The alpha source was placed back into the holder for Run26. At some point during Run26B and Run26C the power supply turned off again. To help mitigate the problem, the HV power supply was changed from 1250V to 1200V.

The alpha source remained in the holder for Run27 and data was acquired for 27 and 48 hrs. Then the alpha source was removed for Run28 and Run29. Then the alpha source was replaced again for Run 30 and 31. For Runs 29, 30, and 31 the acquisition times were extended for the second save to increase the peak to background ratio. As the data was being acquired, there did not appear to be any visual difference in the spectra. This prompted a change in the length of the absorber from 3 inches to 2 inches. A 2 inch absorber was used for the remainder of the runs starting with Run32, except for Runs 36, 37, and 38, which will be discussed later.

Since this was the first time the 2” long rod was used, the purpose of Run32 was a no alpha source baseline for the other 2” long rod experiments. Data was acquired for 182.47 hours. Runs 33 and 34 had the alpha source placed back into to the holder and data was acquired for 182.5 and 217.42 hours, respectively. But Run34 flipped the bar around from surface 1 to surface 2 to see if there was an inhomogeneity in the material from one surface to the other. Run35 was configured without the alpha source and holder; the bar orientation was not switched back (same surface as in Run34) and ran for 167.53 hours. Again, this was to allow for spectra comparison between Run34 and Run35.

In the experiment that consisted of Runs 36, 37, 38 and 39, we wanted to check if another source of phonons could be used other than the alpha source that has been used. To do this, we used the 6” long rod and wrapped it in a heat tape. For Run36, the temperature of the heat tape was held at 35.2°C, the ambient temperature registered at 22.4°C, and data was collected for 165.52 hours. For Run37, the temperature of the heat tape was held at 46.7°C, the ambient temperature registered at 22.4°C, and data was collected for 165.52 hours. The heat tape was removed for Run38, the temperature returned to room temperature and data was collected for 91.08 hours.

To check to see if there was any phonon interaction in higher energy ranges of the spectra, the Doppler velocity was increased from 11mm/s to 22mm/s to increase the window size of the remaining spectra. The laser was recalibrated to the new speed. Run39 was configured with the 2” bar, holder and no source. Data was acquired for 164.2 hours. Then the alpha source was placed back against the absorber for Run40. Data was saved 6 times in the 510.9 hour run. A slight shoulder appeared on the right side of the peak. The alpha source and holder was removed in Run41 to use the data as a background comparison against Run40. Data was saved 6 times for the 497.8 hour run. To check if the shoulder on the peak was real, Run40 was repeated for Run42. This time, the Data was acquired for 1331 hours and saved 6 times. Run43 was configured the same as Runs 40 and 42, but the system died after the first save point at 168.3 hours. This forced another Doppler motor laser calibration.

The last two experiments; Run44 and Run45 check the orientation of the alpha source button. The alpha source was flipped to configuration (b) shown in Figure 24 to block shield the absorber from alphas. The peak appeared symmetric; assuming the only thing the bar sees is gammas and x-rays from the ^{241}Am source. Data was collected for 1804 hours and saved 9 times. The alpha source was flipped back to configuration (a) shown in Figure 24 for Run45. A shoulder appeared on the left side of the peak and disappeared as the data acquisition ran longer. Section 4.2.2-3 will discuss the details found. Also, the HV power supply tripped between (A) and (B). Data was acquired for 547.3 hours and saved 3 times.

3.3 Statistical Tests

3.3.1 Curve Fitting

Due to the natural line width of the excited state, the Mössbauer spectra will have Lorentzian profile. Any variations to the Lorentzian are assumed to be Gaussian broadening due to Doppler shifts in the oscillating resonance sites. Performing a convolution of the two functions will result in a line shape that has a Voigt profile [Vandenberghe]. A non-linear optimization algorithm in MATLAB can be used to decompose a complex, overlapping-peak signal into its component parts, such as: peak location, peak height, area under the peak and the FWHM. The objective is to determine whether spectra can be represented as the sum of fundamental underlying peaks shapes. After a few iterations from starting values, the spectrum with the lowest root mean square fit error is used. The area under the peak, along with acquisition time gives the counting rate of Mössbauer events. This can also be done for the background of the spectra.

3.3.2 Statistical Hypothesis Tests

As a metric to determine the significance of our results, hypothesis tests can be used to quantify the differences between measured spectra and help determine if the observed differences can be attributed to chance. There are 4 parts to hypothesis testing. First, the quantitative objective of the research needs to be converted into null and alternative hypotheses. For this research, the null hypothesis (H_0) is that the presence of phonons ***does not*** change the Mössbauer spectra. This hypothesis claims that there will not be a difference. Opposing H_0 is the alternative hypothesis (H_1), which is that the presence of phonons ***does*** change the Mössbauer spectra. The H_1 is the goal of this research.

The second part of hypothesis testing is to a test statistic, in our case: the FWHM, full width10th max, counting rate under peak and counting rate in the background. The test statistic is required to be something that is measured in the experiment. For the third part, the test statistic is used to determine a conditional probability called a p-value. The p-value provides evidence against the null hypothesis. For instance if the p-value is high, greater than 0.10, the observed difference is *not significant*. If the p-value is low, less than or equal to 0.01, the observed difference is *highly significant*. To calculate a confidence to reject the null from the p-value we use,

$$Confidence\ Interval = (1 - pvalue) * 100\%. \tag{3.1}$$

This leads into the final part of hypothesis testing, making a decision on whether to reject or fail to reject the null hypothesis. The p-value tells you next to nothing about the size of the effect, only that there is a statistically significant difference between the two data sets. Failing to reject the null hypothesis does not mean that the null hypothesis is true and phonons do not contribute to the spectra. Instead, failing to reject the null hypothesis simply means that experiment was not adequate enough to show significant differences in the spectra. More evidence would be needed. To reject the null hypothesis, means that the experiment has shown that the presence of phonons made a significant difference in the Mössbauer spectra. The statistical test used to test the null hypothesis in this research is the f-test.

The f-test is used to determine if two variances are statistically different base on their standard deviations. Equation 3.2 gives the relationship between F and the variance of the two methods (phonons/no phonons). By convention, the variance of the first method, s_1^2 , is greater than the variance of the second method, s_2^2. A list of f-values at the 95% confidence level is given in Table 5. If the f-value calculated exceeds the value in the table, then there is a significant difference between the two methods, i.e. the p-value is small. Actual p-values were calculated using the Microsoft Excel statistics analysis tool.

$$F = \frac{s_1^2}{s_2^2} \qquad (3.2)$$

To give an example on how to calculate the f-value and subsequently the p-value, let's assume the following parameters for Run 1 and Run 2, each with run containing 31 measurements:

Run 1:			Run 2:		
Number of observations	=	240	Number of observations	=	240
Mean	=	688.9987	Mean	=	611.1559
Standard deviation	=	65.54909	Standard deviation	=	61.85425

In this example, the null hypothesis is tested to see if the variances of the two Runs are equal. With these parameters, the f = 1.123 each with a degrees of freedom (v_1 and v_2) equal to 30. If a 95% confidence was desired. The 1.123 would be compared to the 1.84 in Table 5. Since 1.123 < 1.84, there is not enough evidence to reject the null that the two variances are equal at the 95% confidence level. The calculated p-value for this example is 0.376 which corresponds to 62.4% confidence that the results are the same. Since the confidence level is so low, the null cannot be rejected with this statistical test.

Table 5: f values at the 95% Confidence Level where v_1 and v_2 are the degrees of freedom (# of runs minus 1). Table used as reference point, while actual confidence intervals calculated using Microsoft Excel.

	v_1 = 2	3	4	5	6	7	8	9	10	15	20	30
v_2 = 2	19	19.2	19.2	19.3	19.3	19.4	19.4	19.4	19.1	19.4	19.4	19.5
3	9.55	9.28	9.12	9.01	8.94	8.89	8.85	8.81	8.79	8.7	8.66	8.62
4	6.94	6.59	6.39	6.26	6.16	6.09	6.05	6	5.96	5.86	5.8	5.75
5	5.79	5.41	5.19	5.05	4.95	4.88	4.82	4.77	4.74	4.62	4.56	4.5
6	4.14	4.76	4.53	4.39	4.28	4.21	4.15	4.1	4.06	3.94	3.87	3.81
7	4.74	4.35	4.12	3.97	3.87	3.79	3.73	3.68	3.64	3.51	3.44	3.38
8	4.46	4.07	3.84	3.69	3.58	3.5	3.44	3.39	3.35	3.22	3.15	3.08
9	4.26	3.86	3.63	3.48	3.37	3.29	3.23	3.18	3.14	3.01	2.94	2.86
10	4.1	3.71	3.58	3.33	3.22	3.14	3.07	3.02	2.98	2.85	2.77	2.7
15	3.68	3.29	3.06	2.9	2.79	2.71	2.64	2.59	2.54	2.4	2.33	2.25
20	3.49	3.1	2.87	2.71	2.6	2.51	2.45	2.39	2.35	2.2	2.12	2.04
30	3.32	2.92	2.69	2.53	2.42	2.33	2.27	2.21	2.16	2.01	1.93	1.84

IV. Analysis and Results

This chapter is intended to describe the analysis performed on the data collected as described in chapter 3. Since the basis of the analysis revolves around the curve fitting routines, the data fitting will be discussed in section 4.1. Afterwards, the statistical analysis described in the chapter 3 will be performed on 4 different aspects of the data acquired. This will lead to the conclusions drawn in chapter 5.

4.1 Data Fitting

After the each run finished, the raw data was saved to a text file and loaded in MATLAB. The data in the file was restructured into an array for analysis. In order to extract useful information from the raw data, the data needed to be fit to a model using code in MATLAB called ‘peakfit.m’. The model required is non-linear and would not work well with linear least squares curve fitting method that is considered simple and fast. Instead the set of data was fit using the iterative method, which is a general fitting routine that uses trial and error. The parameters are adjusted systematically until the equation for the model chosen fits the data. There are 4 main steps that the code uses to fit a model to the data [O’Haver]. First, a model for the data is selected. Second, an initial guess for the non-linear parameters are chosen. Third, the ‘peakfit.m’ code computes the model and compares it to the data set, calculating a fitting error. Lastly, if the fitting error is greater than the required fitting accuracy, the code systematically changes one or more of the parameters and loops back to step 3. The method that the code uses is the Nelder-

Mead method, which is a standard non-linear optimization technique that uses an educated guess search method that can converge on non-stationary points.

As discussed previously, Mössbauer spectra are best fit with a Voigt function. If the wrong model was chose, then the results would not be expected to be accurate. For instance, a Lorentzian and a Gaussian model was fit to the same data that the Voigt was fit. The Voigt model also has a peak shape parameter called 'extra,' which is a ratio of the Lorentzian width to the Doppler width. Run19 and Run44I data were used as the confirming the Voigt over the Lorentzian and the Gaussian. This can be seen in Figure 25. Both the short and long runs (Runs 19 and 44I respectively) had a lower fitting error for the Voigt compared to the Gaussian and the Lorentzian. The larger the fitting errors the larger the parameter errors, but the parameter errors are not equal to the fitting error. Parameter errors are not given because the true peak values are not known before the experiments were run. Also notice the residual plots for Run44I, the Voigt residuals are much more random compared to the Gaussian and Lorentizian. Artifacts near the peaks can be seen in the other two models. Due to the short acquisition time for Run19, artifacts in the residuals near the peaks have not developed and appear random for all three.

For the type-310 stainless steel absorber, only one peak is identified in theory and one peak was used for the analysis. During the analysis, an asymmetry was observed as the peaks developed. We considered fitting two peaks to the data. The fitting error decreased as expected, but the second peak was unstable in position, width, and height. The second peak instability was observed in the in-experiment runs where the data was saved multiple times to watch the peaks develop. This instability was due to the code fitting to random noise and not an actual peak. Therefore, another method was used to

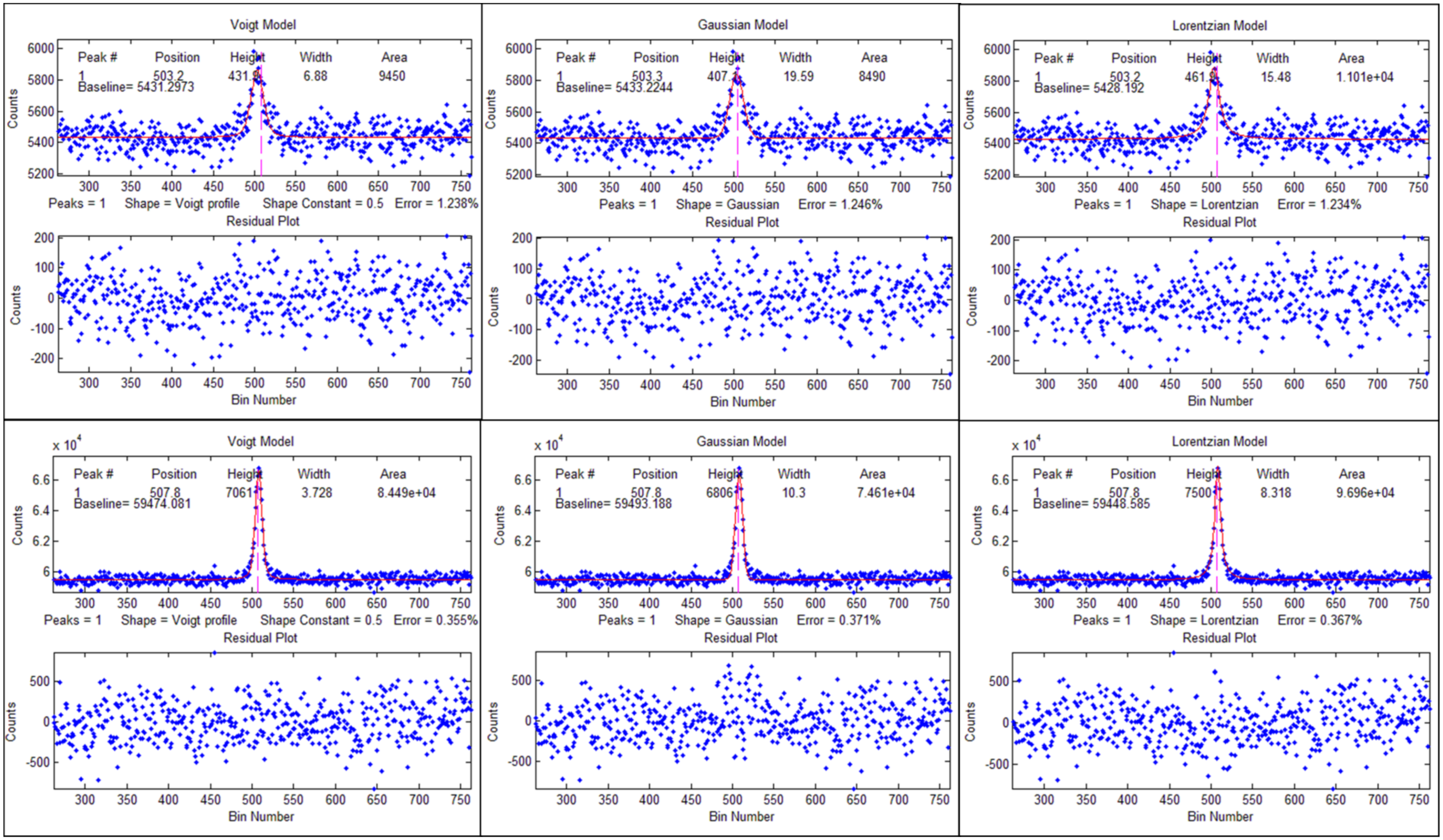

Figure 25: Voigt, Gaussian, Lorentzian Model Fit Comparison. Top row: Run19 with fitting errors: V-1.238%, G-1.246%, L-.234%. Bottom row: Run44I with fitting errors: V-0.355%, G-0.371% and L-0.367%. Note the pink like is an initial estimate of the peak location and not the actual location.

analyze the peak asymmetry and is discussed in section 4.2.3. This method makes better use of the codes ability to fit a peak with noise and will be discussed next.

The fitting error that is calculated by the ‘peakfit.m’ code is a root-mean-square difference between the model and the data. This error is minimized through the iterative process discussed previously. The parameter errors are directly proportional to the noise in the data and to the fitting error. Figure 26, taken from Thomas O’Haver, shows the variability of the fitting error, which is caused by random small variations in the initial guesses rather than the noise in the signal. Notice in the figure that the errors are the smaller for peak position and worse for the peak height and width. The fitting error, as well as the parameter errors, is dependent of the number of data points in the width of the peak. The more points the code has to draw from the more accurate the fit. When the experiment switched from 11mm/s to 22mm/s, the number of points to fit decreased. This is because the number of energy bins (channels) that were utilized decreased and the number of channels for the background increase due to the increase in motor velocity. The data was run for a longer period of time to compensate for the fewer data points in the narrower peak by increasing the signal to noise ratio.

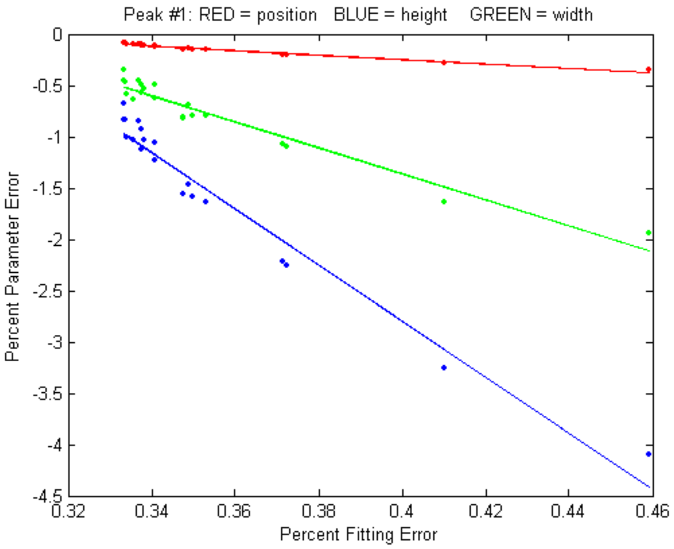

Figure 26: Iterative Fitting Errors. Typical percent parameters errors as a function of fitting error for a simulated noisy Gaussian signal. [20]

In practice, the best way to evaluate a proposed fitting model is to fit several repeat measurements of the same signal. Then compute the standard deviation of the peak parameter values. This was attempted in this experiment, but was not practical since the acquisition times were incredibly long. Also, other variables that might affect the Mössbauer spectrum were tested alongside the repeat measurements as mentioned in the experimental runs and description section. This caused a conundrum for the experiment, as only a single Mössbauer spectrum was available to compare what needed to be repeated experiments. Fortunately, the effect of the noise on the peak parameters' standard deviation can be predicted approximately by the bootstrap method. This method is a procedure that involves choosing random sub-samples with replacement from a single data set and analyzing each sample the same using the iterative method [20]. The bootstrap method uses the actual noise in the data set. This means that the greater the actual noise in the data set, the greater the range of results. This enables uncertainty estimates of the parameters. This multivariate method allows for a statistical inference for the peak FWHM, height, and position which will be used in this experiment's hypothesis testing [27].

Table 6: Bootstrap Data for Run34 using the Voigt model. Appendix B.2 contains bootstrap data for other runs

Run	Parameters	Peak Position	FWHM	Area	Counting Rate
34	Mean	522.79	6.67	69058.68	0.1008
	STD, s	0.083	0.093	890.189	0.001299
	Variance, s^2	0.007	0.009	792436	1.69E-06

The Voigt model is fitted using a flat linear baseline which is superimposed with the background. The presence of the background has little effect on the peak positions. However, the background must be brought to a zero baseline to accurately measure the peak heights, FWHM and areas using the Voigt model fitting routine. The background as mentioned previously is the signal from the non-resonant absorption processes and cannot be entirely eliminated experimentally. According to the thesis by Tanis, the background contains information on the phonon density of states. In his work, Tanis looked over a much broader energy range (~50 meV), while this experiment focused in a narrower energy range, (~10 neV). Much higher motor velocities than used in this experiment are required to for a phonon density of states analysis on the background.

With this information, Run34 is shown in Figure 27 as an example. The channels are abscissa and the counts on the ordinate. Each channel represents the motor velocity with channel 512 representing 0mm/s. The baseline was calculated to be 22867 counts.

This value is derived from a flat linear line fit to the background data points with the peak removed. To get a true understanding of the background area, the baseline should be multiplied by 1024 for each channel. Since the channel number is a constant in every run, the baseline is treated as the background.

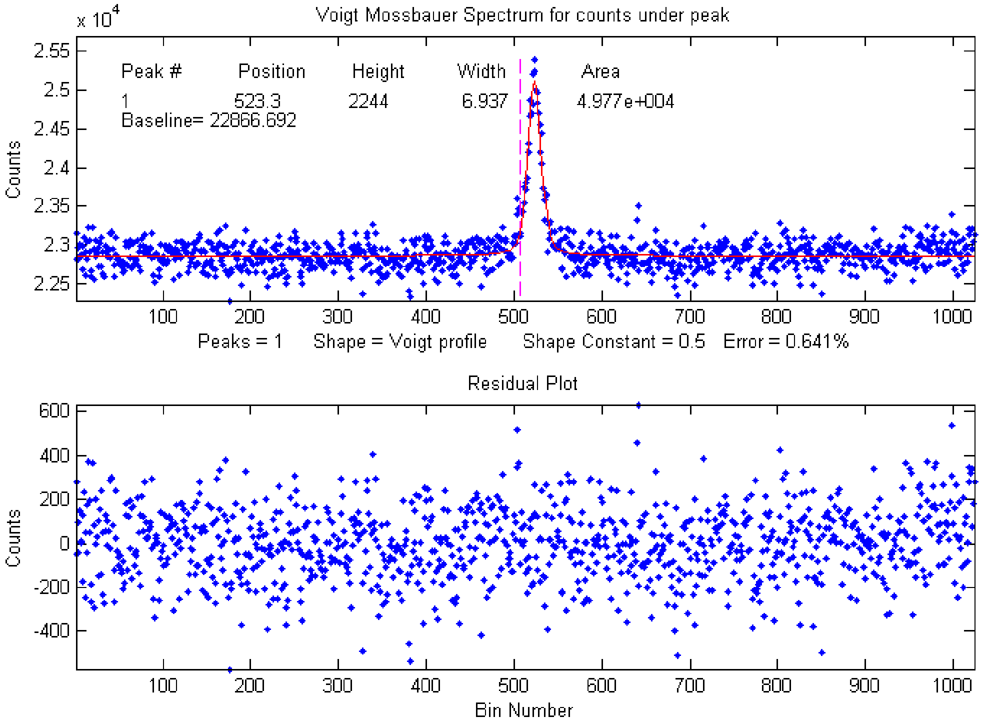

Figure 27: Voigt Model Fit to Run34 data. Blue dots are the measured data points, the red line is the Voigt model fit to the data. Fit parameters are displayed in the top subplot. The pink dotted line was the initial peak center estimate before the fit iteration. The lower subplot below displays the residuals from the model fit. In all cases, the mean of the residuals trended towards zero.

The blue points are the raw data with the red line representing the fitted Voigt model. The Voigt model was iterated 100 times and the best fit was chosen to give the parameters displayed in the figure. The fitting error was calculated to be 0.641%. The lower the fitting error the more accurate the fit, since the parameters are proportional to the fitting error. The subplot represents the residuals left over from the fit. The residuals should be uniform and random, where-as not to produce artifacts near the fitted peak. The mean of the residuals is 6.1E-13, essentially zero (as is the case with all runs where the residual means were calculated). This indicates a good and unbiased fit. The peak parameters were measured using the bootstrap method with N =100, where N is the number of trials for each bootstrap iteration and can be seen in Table 6. The sample standard deviation, s, is given for each parameter. The sample variance is: s^2. Since the bootstrap method randomly samples the data, greater noise will lead to greater variability in the parameters.

4.2 Statistical Analysis

There are three parameters that the following statistical analyses focus on: FWHM, peak counting rate and background counting rate. The FWHM is pulled directly from the peak fitting routine, while the peak counting rate and the background counting rate are normalized by dividing the peak area and the baseline from the fitting routine by the acquisition time. The counting rates were then corrected for the source decay shown in Figure 13 by assuming the ^{57}Co source had a normalized activity of 1 on the date the data acquisition started, 10 May 2012. The normalized activity for the last run was 0.467. To correct for source decay, each counting rate was divided by the normalized activity. This allows for an equitable comparison of counting rates between experiments. There are, however, various variable changes from Run set to Run set shown in Table 4.

One example to note is the motor velocity changing from 11mm/s to 22mm/s. This increases the energy range of the incident 14.4 keV gamma, which means that there is a narrower channel band allocated to the resonant absorptions. This decreases the FWHM, but keeps the peak height the same; therefore, decreasing the area under the peak. This might sound counter intuitive, but less time is spent in resonance (the motor sweeps faster) and gammas from the Mössbauer source have less of a chance to arrive at the absorber with the correct energy. The same effect is seen in the background baseline, which decreases the background counting rate of the 22mm/s compared to the 11mm/s run. Because of these reasons, the 11mm/s data cannot be compared to the 22mm/s data and have to be treated separately. One parameter that does not change is the peak location. But due to the age of the motor, the equipment did not remain in perfect calibration which caused slight shifts the peak locations. Occasional recalibration of the motor was required. Since the calibration of the motor required visually minimizing the interface pattern from Michelson interferometer in the laser diode of the motor, there were slight adjustments in the peak location. Fortunately, this does not affect the statistical analyses since peak location was not taken into consideration and the peak location did not affect the shape of the Mössbauer spectrum peak. The peak did slightly oscillate during the runs, but did not continuously drift in a preferential direction, which would have skewed the results of the peak asymmetry analysis. The level and period of the oscillation would need to be investigated further.

4.2.1 Experimental Run Analysis

The ideal statistical analysis would compare many spectra with a phonon source to many spectra without a phonon source. While all other variables like absorber material length, motor velocity, phonon source, detector gain, and detector gas would remain constant. Unfortunately, due to the time limit and refinement of the experimental process as time progressed, some of these variables did change. Fortunately, at least one spectrum with a phonon source and no phonon source were taken before a variable change. Due to limited sample sizes, the resulting statistics would be very poor if one just compared one spectrum to another. A percent difference would not give any insight to whether or not the null hypothesis can be rejected. To add meaning to a spectrum to spectrum comparison, the bootstrap method mentioned previously was implemented. In essence, the method produces a hundred independent trial runs for each spectrum by replacing a percentage of the data points randomly with other random data points in the spectrum. There is substantial evidence that this method can be effectively used to give a standard deviation of the FWHM and peak counting rate parameter [20, 27]. All the bootstrap data can be seen summarized in Appendix B.2. The background was not included in the bootstrap data. To get an overall perspective of the data (given in Appendix B.1) variability, comparisons were made as a whole shown in Figure 28, Figure 29, and Figure 30.

The first comparison, Figure 28, was to see the how the peak and background compared to each other for the 11mm/s motor velocity. As shown in the figure, the counting rate for both the peak and background counts decreased over time even with the Mössbauer source decay correction. Also, both the phonon source and no source run groupings held the same trend. The runs with a phonon source showed more variability in the peak counting rate, while the opposite was true for the source run background counting rate. Note it was observed that the detector bias shut off at some point between Runs 25A & B and 26B & C. Since the bias shut off for these, Runs 25B-E and 26C were excluded from the statistical comparison. For the counting rate comparisons, there is a 70% confidence that the null result can be rejected for the peak and a 57% confidence to reject the null result for the background. Statistically, the null result cannot be rejected from this test.

The next comparison is for the 22mm/s motor velocity regime and can be found in Figure 29. For row (a), the counting rates are uniform barring the Run39 outlier. The most likely reason Run39 was off is the electronics. The motor was velocity was changed to 22mm/s and recalibrated from Run38. After Run39, the motor started acting up and had to be fixed and recalibrated for Run40. To make sure the motor remained in working order for each run afterwards; it was recalibrated and monitored after each run. Unfortunately, this did not help the data acquisition for Runs 42G, 43A, and 45B-C.

The detector bias tripped for those runs, which would explain the large oscillations in those runs. These runs and Run39 were not included in the statistical analysis shown in Table 7. The F test was applied with these exclusions and for the peak counting rate there is a 92.3% confidence that the null result can be rejected. For the background counting rate there is an 87.6% confidence that the null result can be rejected. Unfortunately, more test should be ran for the data to have more confidence in the test performed. The runs with no source and a source were one long data run for each and saved at various intervals. Technically, there were 2 runs without a source and 3 runs with a source. The evolution of each run was analyzed in the next section.

The last comparison made on the data as a whole was between the FWHM with and without the phonon source for the 11mm/s and 22mm/s motor velocity, shown in Figure 30. For the FWHM statistical analysis, the same runs were excluded that were excluded in the peak and background counting rate comparisons. In Table 7, the confidences for the FWHM were calculated. For the 11mm/s motor velocity, there is only a 12% confidence that the null result can be rejected. Curiously, for the 22mm/s motor velocity, there is a 92.8% confidence that the null result can be rejected. The disparity between the 11mm/s and the 22mm/s confidence levels sends a mixed message on whether the null result can be accepted or rejected. A possible reason for the disparity is the number of 'independent' runs for the 11mm/s compared to the 22mm/s. Further data collection would be required to truly understand the disparity.

Table 7: Statistical comparisons for phonon source and no phonon source in Figure 28, Figure 29, and Figure 30. The f-test was the primary method used to calculate a p-value and a confidence interval for the FWHM, the peak and background counting rates.

No Phonon Source vs Phonon Source							
Motor Velocity	**Statistic**	**Peak Counting Rate**		**Background Counting Rate**		**FWHM**	
		No Source	**Source**	**No Source**	**Source**	**No Source**	**Source**
11mm/s	Mean	0.1185	0.1237	58.36	59.15	7.285	7.576
	s	0.0185	0.0130	7.09	5.43	0.758	0.813
	Variance, s^2	0.0003	0.0002	50.31	29.46	0.575	0.661
	F test p-value	*0.3003*		*0.4271*		*0.8793*	
	Confidence %	*70%*		*57.3%*		*12.1%*	
22mm/s	Mean	0.0236	0.0231	17.74	16.43	3.576	3.804
	s	0.0012	0.0020	2.20	3.42	0.121	0.0695
	Variance, s^2	1.51E-6	4.17E-6	4.56	11.70	0.015	0.005
	F test p-value	*0.0770*		*0.1242*		*0.0717*	
	Confidence %	*92.3%*		*87.6%*		*92.8%*	

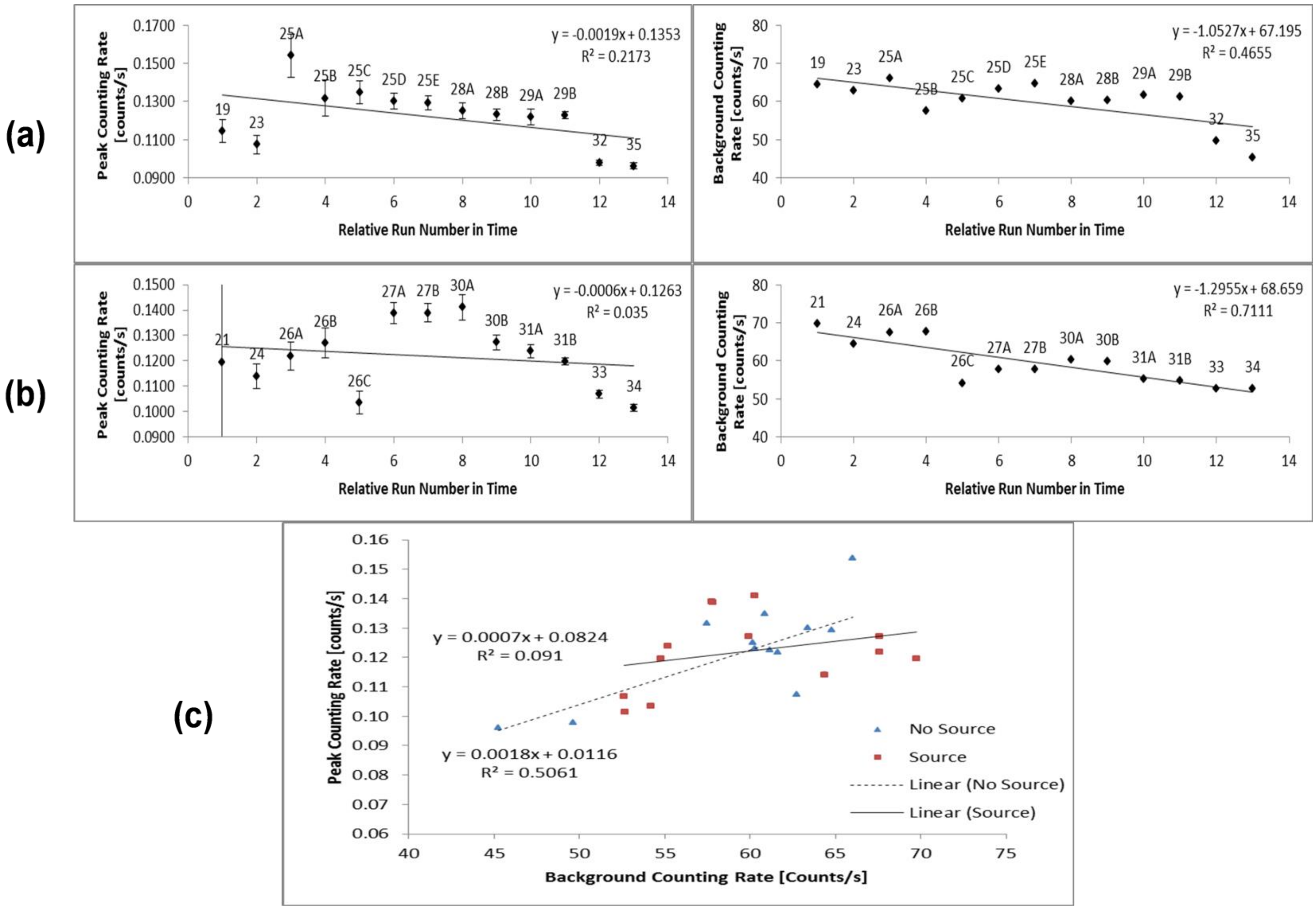

Figure 28: **Peak and background counting rate graphical comparison for 11mm/s motor velocity. Source runs: (a) No Phonon (b) Phonon and (c) Peak vs Background trends**

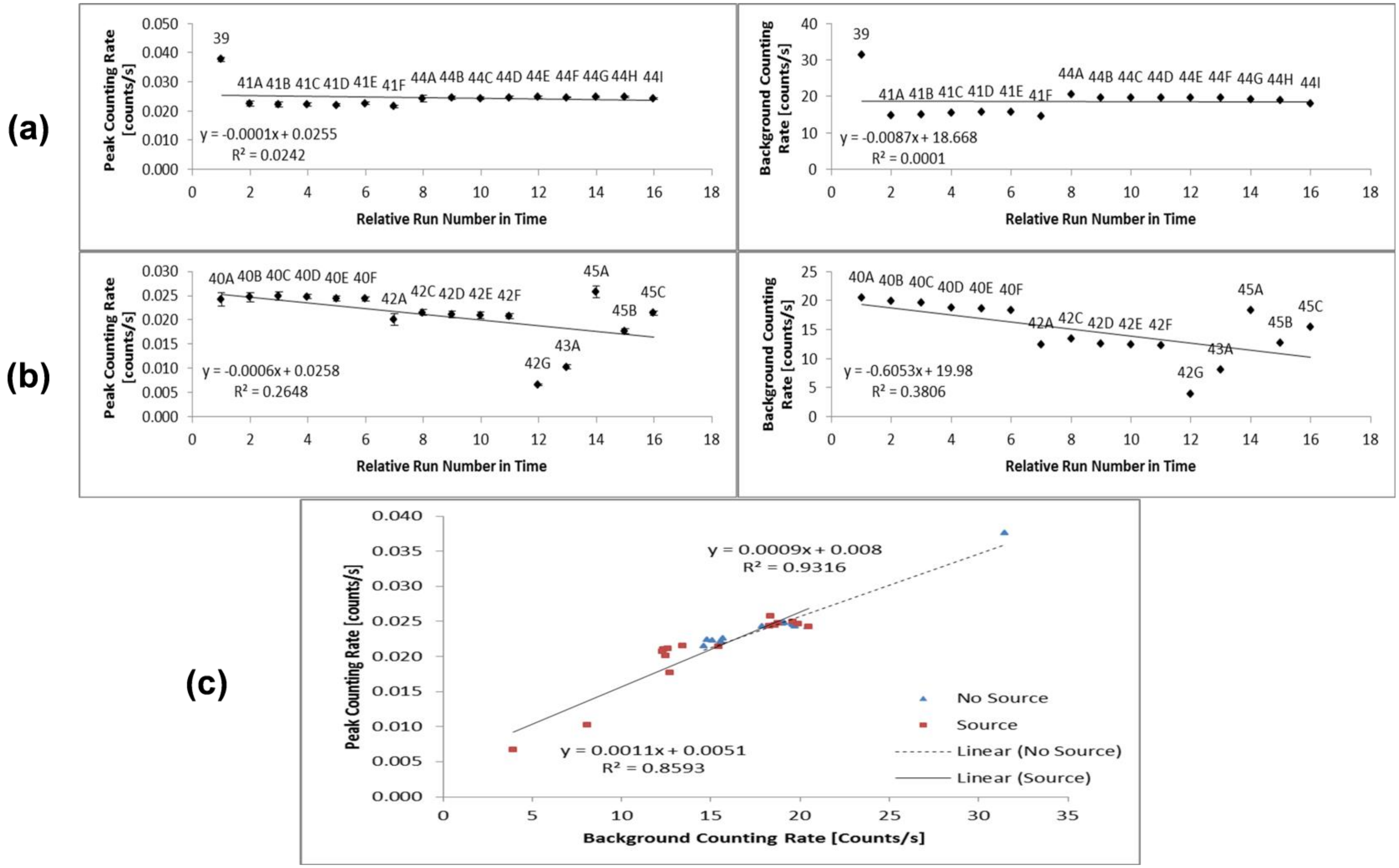

Figure 29: Peak and background counting rate graphical comparison for 22mm/s motor velocity. Source Runs: (a) No Phonon (b) Phonon and (c) Peak vs Background Trends

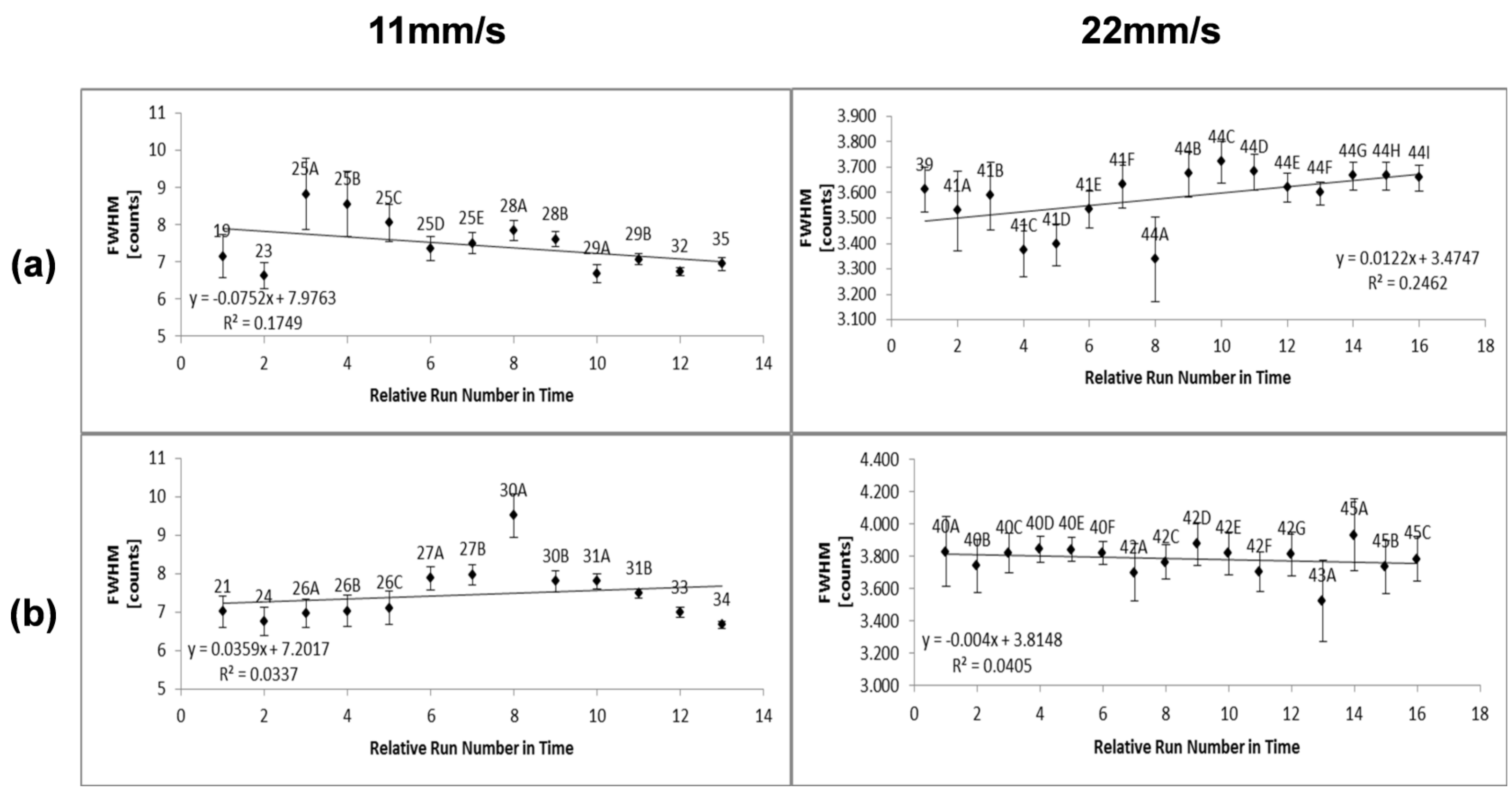

Figure 30: FWHM graphical comparison for 11mm/s and 22mm/s motor velocities. Source Runs: (a) No Phonon (b) Phonon

Now that a perspective has been established for the data as a whole, similar source/no source runs were compared using the F test. There had to be at least 1 degree of freedom with each comparison for a confidence interval. The runs that were compared are shown in Table 8 along with the p-value results and confidence percentages.

Table 8: 11mm/s motor velocity run f-test p-value and confidence interval comparisons for the FWHM, the peak and background counting rates. The two columns on the left represents the runs that were associated with a phonon source or no phonon source.

	No Source	**Source**	**Peak Counting Rate**		**Background Counting Rate**		**FWHM**	
			p-value	**Confidence**	**p-value**	**Confidence**	**p-value**	**Confidence**
A	23 25A	24 26A/B	*0.0758*	*92.4%*	*0.6675*	*33.3%*	*0.0186*	*98.1%*
B	28A/B 29A/B	27A/B 30A/B 31A/B	*0.0100*	*99%*	*0.0829*	*91.7%*	*0.6275*	*37.3%*
C	32 35	33 34	*0.4188*	*58.1%*	*0.0307*	*96.9%*	*0.7244*	*27.6%*

The p-value results were curious for the 3 different comparisons. In all the comparisons, the confidence was drastically below the 60% confidence to reject the null in at least one compared parameter. On the other hand, many of the results have above a 90% confidence with one being 99% to reject the null hypothesis. There is another disparity in the statistics. More like runs need to be made to increase significance that the null result can be rejected. The FWHM only had one p-value < 0.05, while the others are much higher. This is most likely due to the extra parameter in the Voigt model fitting remaining constant. The FWHM was the most susceptible parameter to this peak shaping factor. To decrease errors in the future, the ‘peakfit.m’ code can be modified to allow for a third iterative parameter, which will cause the code to run slower, but could prove to give lower fitting errors for the FWHM and area under the peak.

4.2.2 In-experiment Development and Variances

Even though it may look like there are 30 different experiments for Runs 40A-F, 41A-F, 42A-G, 44A-I, and Run 45A-C, they are technically only 5 long running experiments with the data saved periodically during the run. Because of this, the development of the signal can be studied, allowing a check to see if the peak development proceeds as expected by comparing the standard deviations and variances. Figure 31 gives a visual representation on the peak development. All the bootstrap fitting routine results can be seen in Appendix B.2. All the Voigt fitting data can be seen in Appendix B.1. All peak locations remained stable within the individual runs (ex. 40A-F), as expected, but slightly shifted (max shift 1.34 channels) between these run sets. Runs 42G and 45A-C will be excluded due to the voltage bias shutting off during the run. What will be looked at in this section will be the normalized peak height, peak counting rate and FWHM. The normalized peak height was determined by dividing the height by the hourly counting rate. The value would describe how the peak height grows per hour.

Table 9: In-experiment peak development statistics for the 22mm/s motor velocity runs. Parameters: mean, standard deviation (STD) and variance of each all the runs in a set. Example: Run set 40, runs in the set A-F.

	Parameter	Normalized Peak Height	FWHM	Peak Counting Rate
Run 40A-F	*Mean*	7.169	3.813	0.0246
	STD	0.110	0.035	0.000254
	Variance	0.0122	0.0012	6.47E-08
Run 41A-F	*Mean*	7.047	3.507	0.0222
	STD	0.231	0.095	0.000342
	Variance	0.0532	0.0090	1.17E-07
Run 42A-F	*Mean*	6.121	3.769	0.0209
	STD	0.104	0.068	0.000475
	Variance	0.0109	0.0047	2.25E-07
Run 44A-I	*Mean*	7.591	3.623	0.0246
	STD	0.227	0.107	0.000194
	Variance	0.0513	0.0114	3.76E-08

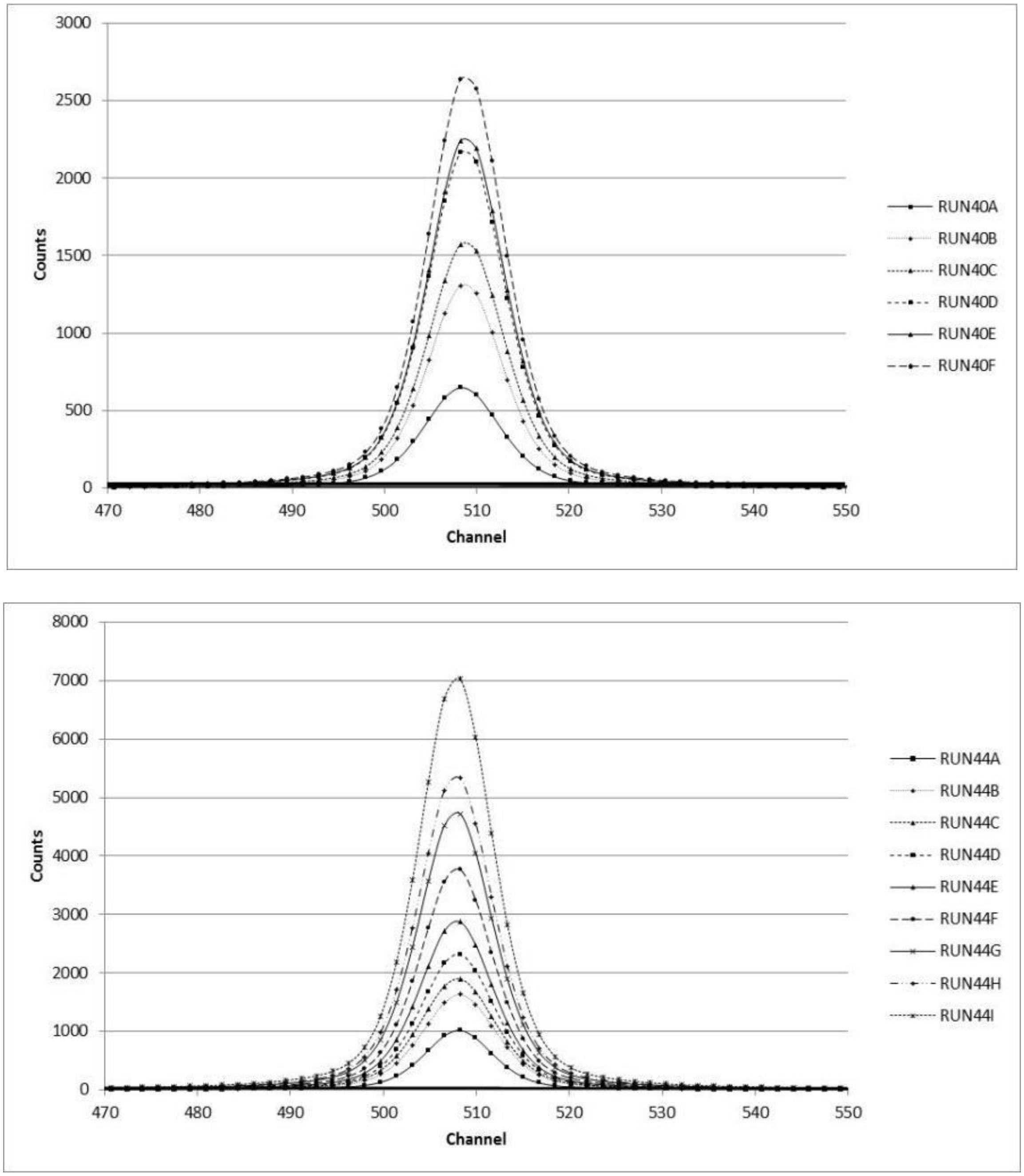

Figure 31: Peak Development for In-Experiment Runs. Peaks are the Voigt fit to the data. Top: Run40A-F. Bottom: Run44A-I.

As the peaks developed, the fitting error decreased along with the variances on the normalized peak height, the peak counting rate and the FWHM. This is as expected due to the stabilization of the peak with an increased counting time. The number of counts remained consistent and the FWHM generally remained constant for each run. There was a general trend in the normalized peak height data for each save in a particular run: it decreased. The value in initial save was always higher than the value in the final save. There were slight variations, but the trend was to decrease. As peak develops, the probability of a count entering that peak 'bin' will remain equal throughout the run time, unless something changes that probability (i.e. phonons disrupting the resonance peak). Unfortunately, both phonon source and no phonon source exhibited this trend and the most likely answer is the Mössbauer source decay was not accounted for properly. In this experiment, a correction factor for the MS source decay was applied at each save. The saves earlier in the run had a smaller correction factor applied than later saves. For example, a correction factor of 1.34 was applied to Run40A, while a correction factor of 1.37 was applied to Run40F. The more decay, the larger the correction factor. It should be noted however, that the peak did not vary as much for the runs with the phonon source present compared to the runs without the phonon source, see Table 9.

4.2.3 Peak Asymmetry Analysis

In order to analyze peak asymmetry, two methods were considered: an exponential Gaussian fit and peak splitting. The first method was to fit an exponential Gaussian to the whole data set. A timing parameter in the fitting routine, called *extra*, allows for an asymmetry towards the left or the right side of the peak with either a positive (right) or negative (left) parameter. When running the analysis, this method produced an order of magnitude higher errors verse the second method. The second routine, which was the one that was used for the analysis, found the peak center and compared the left and right side of the peak. This was accomplished by splitting the data at the peak center where the left and right data points were mirrored with themselves to produce two new symmetric spectra to analyze. One spectra was the left mirrored and the other was the right mirrored. The spectra were fitted with the Voigt fitting routine described in the previous section. The MATLAB code for this process can be seen in Appendix A.2. The two spectra were compared and the differences were compared with each other as well as the other left and right spectra generated from the other runs.

There characteristics of the spectra were compared: the peak area counting rate, the background counting rate, and the FWHM. Data can be seen in Appendix B.3. An F test was done on all the spectra characteristics. It was discussed to use a t-test for an additional analysis, but the parameters being tested were the mean of the distributions. To be significantly different the probability (p-value) of the test need to be <0.05 to have a 95% confidence that the null result can be rejected, anything >0.10 the null result cannot be rejected. Before the left and right side of the peaks were compared, the left side runs with a source were compared to the runs without a source for the 11mm/s and the 22mm/s data sets. Then same was done for the right side peaks. This was to give another check to see if differences in the spectra are statistically significant. After this, the left side runs without a source were compared to the right side runs with a source. The data runs that were compared and analyzed can be seen in Table 6.

Table 10: A list of the runs that were analyzed and compared in the peak asymmetry analysis

11mm/s motor velocity		22mm/s motor velocity	
No Source	Source	No Source	Source
23	24	39	40A
25A	26A	41A	40B
25B	26B	41B	40C
25C	26C	41C	40D
25D	27A	41D	40E
25E	27B	41E	40F
28A	30A	41F	42A
28B	30B	44A	42C
29A	31A	44B	42D
29B	31B	44C	42E
32	33	44D	42F
35	34	44E	45A
		44F	45B
		44G	45C
		44H	
		44I	

The results of the F test calculations are summarized in Table 11. Looking at the calculated probabilities, the null result (phonons do not cause an asymmetry in the peak) cannot be rejected with certainty. There are a few cases where there is statistical variance to have a basis to reject the null result. The F-test probabilities of the right side peak indicate that there is a confidence of 90.4% and 93.7% that the FWHM of the source/no source peaks were different. Also, the peak counting rate for right side produced probabilities that indicate a confidence of 88.6% and 91.7% that the source/no source peaks were different. These two results show that the right sides of peaks were statistically different to be considered asymmetric. The asymmetry could be a result of the experiment or higher energy phonons coupled. More experiments would need to be run to determine which. As for the left side, the FWHM results were inconsistent to allow for any conclusive results. While, the peak and the background counting rate were consistent with low confidence levels. To use the 11mm/s velocity regime, the p-values would show a trend a trend that the peak counting rate remained the same and the FWHM could be different. A different conclusion would be drawn if the 22mm/s were only considered. The 22mm/s regime would indicate that the right sides of the peaks were different when considering the peak counting rate and the FWHM. At the same time there is low confidence that there was a change in the left side of the peak. This could indicate a peak asymmetry. The motor velocity would not have such an effect on the results, since it does not change the environment of the absorber. More data collection would be required.

Table 11: Calculated f-test p-values and confidence intervals for Peak Asymmetry. Top: Comparison of phonon source and no source for the left and right side of the peaks. Bottom: Comparison of the left and right side of the peaks for a phonon source and no source. For each comparison, the 11mm/s and 22mm/s motor velocity runs should not be compared with each other.

Motor Velocity		**No Source vs Source**					
		Left Side			**Right Side**		
		Peak Counting Rate	**Bkgd Counting Rate**	**FWHM**	**Peak Counting Rate**	**Bkgd Counting Rate**	**FWHM**
11mm/s	p-value	0.852	0.667	0.165	0.114	0.684	0.096
	Confidence	*14.8%*	*33.3%*	*83.5%*	*88.6%*	*31.6%*	*90.4%*
22mm/s	p-value	0.372	0.469	0.750	0.083	0.473	0.063
	Confidence	*62.8%*	*53.1%*	*25.0%*	*91.7%*	*52.7%*	*93.7%*

Left Side Peak verse Right Side peak							
Motor Velocity		**Peak Counting Rate**		**Background Counting Rate**		**FWHM**	
		No Source	**Source**	**No Source**	**Source**	**No Source**	**Source**
11mm/s	p-value	0.25	0.52	0.999	0.993	0.0041	0.96
	Confidence	*75.0%*	*48.0%*	*0.1%*	*0.7%*	*99.6%*	*4.0%*
22mm/s	p-value	0.20	0.73	0.997	0.998	0.918	0.165
	Confidence	*80.0%*	*27.0%*	*0.3%*	*0.2%*	*8.2%*	*83.5%*

Another analysis was done to compare the left side and right side of the peak for both the source and no source runs. Our statistical analysis of the data produced a curious result similar to the source/no source analysis of the left side of the peak. A high p-value for the F test would indicate no difference between two samples, while a low p-value would indicate a difference. We would expect that there would be no difference between the left and right side of the peak when phonons are not present or there is a natural phenomenon that causes an asymmetry in the peak. Additionally, when phonons are present we would expect that they would create an asymmetry where there is not one or vice versa. When analyzing the peak counting rate data for the left/right side peak comparisons, there is no confidence to determine whether there is or is not a difference in the peak, as shown in Table 11. For the FWHM, the 11mm/s motor velocity regime's p-values indicate the no source runs have a 99.6% confidence that the right and left side are asymmetric and the source runs have a 96% confidence that the right and left side peaks are symmetric. While the 22mm/s motor velocity produced p-values that were much less confident and would produce opposite conclusions.

4.2.4 Heat Tape

As explained in Chapter 3, another phonon source was used to see if there would be a better signal change. Heat tape was added to the bar in Runs 36, 37 and 38. The temperatures ranged from room temperature to 35°C and then 46°C. As the spectra developed, there did not seem to be differences in the peaks. The bootstrap method with the variances and the peaks increase in the FWHM (6.35, 6.76, and 6.91, respectively) would indicate that phonons would have an effect; especially since the standard deviation di not overlap between Run38 and the other two runs. More data would need to be taken to statistically confirm. Since time did not permit, a phone call was made to Dr.

Spikerman, the developer of the Mössbauer spectrometers Ranger Scientific Instruments, to see what temperature the bar needed to be heated. He said that the bar would need to be heated to about 1000°C to see a broadening in the peaks. This stopped the pursuit of this path. The data and Voigt fits can be seen in the appendices.

V. Conclusions and Recommendations

5.1 Summary

The experiment developed was set up to investigate whether nuclear induced phonons would have a visible effect on a Mössbauer spectrum. Stainless steel type-310 was used as the Mössbauer absorber material because it has three properties that would allow the investigation to occur. The first property is the ^{57}Fe in the material that allows for a resonant absorption with the ^{57}Co Mössbauer source. The second property is the single peak spectrum produced by the Mössbauer events. This property simplified the analysis to focus on the properties of a single peak and preclude any overlapping nature of other peaks. Lastly, the stainless steel has a stiffness that would allow for acoustic propagations and increased probability of a phonon coupling with a Mössbauer event. An alpha source, ^{241}Am, was used to induce phonons through the nuclear recoil produced from Rutherford scattering. To verify that that phonons induced by the alpha source had an effect, Mössbauer spectra with and without a phonon source were compared. Other experimental variables were to remain constant. Unfortunately, since the equipment was old, a few modifications to experiment were necessary to keep the experiment running and try to increase the likelihood that a phonon interaction with the Mössbauer events to occur.

Since there was not an obvious change in the 62 spectra acquired, hypothesis testing was used to see if there actually was a significant difference between the phonon and no phonon spectra. The null hypothesis tested was that phonons did not couple with the Mössbauer spectra. The statistical analysis used a two tailed F-distribution. This test is most common when comparing functions models fit to a data set by using analysis of variance. The comparisons that were looked at were changes in the a few parameters of the Voigt peak fit the data: FWHM, peak counting rate, and background counting rate. A shift in the peak centroid was not considered. The comparisons were done in the 11mm/s and the 22mm/s motor velocity regime. The data was compared as a whole between phonon source and no phonon source spectra. Then related runs were compared, as shown in Table 8 for the 11mm/s regime. It was determined that was not enough evidence to reject the null hypothesis for these tests. While some of the tests produced a 95% confidence interval, others produced less than 60% confidence. These results were conflicting.

The same conflict between confidence intervals came about when peak asymmetry was analyzed. In the analysis of the asymmetry, the peaks were mirrored about the centroid and the left and right sides were compared as if they were two separate symmetric Voigt peaks. The same parameters as before were compared, Table 11. The statistics in comparing one motor regime to another were conflicting and more tests would be required to confidently reject the null.

Another consideration to analyze was to check on how the peaks developed. This was accomplished with the 22mm/s motor regime. Five long runs, about 2 weeks each, were saved periodically. When the peak development was analyzed, the peaks developed as expected. It was noted that the peaks with no phonon source appeared to fluctuate more compared to the phonon source runs. It was not concluded that this is possible evidence to reject the null, but that further testing would be required to have confidence whether or not the null can be rejected. There is a possibility that changes in the side wings were outside the energy window established in this thesis. And the motor velocity should be increased and analyzed.

5.2 Significance of Research

As far as the author and his committee are aware, this research is the first to be done in this area of study. The coupling of phonons with Mössbauer events using a radiation source; in order, to detect the radiation source has not be attempted. The initial results, which this thesis provides, cannot say with certainty either way whether the phonon do substantially affect the Mössbauer spectra; there is indication either way to reject the null. The experiment would need to be refined to determine if this method can be used as a solid state detector for various radiation sources.

5.3 Future Work

There are a few methods that can be used to generate higher confidence whether the null result can be rejected.

- Cool the stainless steel bar to temperatures close to 77K using liquid nitrogen. This would decrease the inherent oscillations of the atoms in the stainless steel. It is predicted that this decrease in random vibrations would make any changes to the resonant peak more sensitive to the nuclear induced radiation.

- Create a solenoid to verify that induced phonons can couple with Mössbauer events. Copper wire would be wrapped around the stainless steel absorber and current would be passed through the wire to create the solenoid. Then the electric current would be oscillated to create pole flipping in the stainless steel that would induce phonons. The frequency of the oscillation would need to high enough to allow for and increased probability coincident phonon/Mössbauer events to occur. It would be best to perform simulations to verify the frequency of the electric current oscillations.

- Change the absorber and the phonon source used in the experiment. The recommended changes in the absorber would be a magnetic material to help directionalize the phonon propagation by aligning the grains and magnetic poles. One material to use would be Neodymium ($Nd_2Fe_{14}B$). This material contains a majority of iron for Mössbauer spectroscopy. Also, the material has boron which would be perfect for neutrons to be used as the phonon source. Natural boron contains 20% ^{10}B and ^{10}B is good thermal neutron absorber.

- Another material would be boron carbide with an enriched ^{57}Fe surface. The boron carbide is an extremely hard ceramic material that has a uniform crystalline structure. The material would be ideal for phonon propagation, since most of the literature recommends crystalline structures to reduce dispersion in phonon propagation. The enrichment of one surface with ^{57}Fe would increase the Mössbauer event counting rate and allow for a better signal to noise ratio.

APPENDIX A – MATLAB Code

A.1 Data Loading and Peak Fitting Parameters

```
%Data
%***************
% calibration data
% cal_fe_raw = load('E:\AFIT\Parker\Data\RUN18.TXT');
% acq_time = 20760; %[secs]
cal_fe_raw = load('E:\AFIT\Parker\Data\RUN22.TXT');
acq_time = 37620; %[secs]

%Data
% SS_raw = load('E:\AFIT\Parker\Data\SSFOIL3D.TXT');
% acquisition_time = 355740; %[secs]
% SS_raw = load('E:\AFIT\Parker\Data\RUN14.TXT');
% acquisition_time = 4620; %[secs]
% SS_raw = load('E:\AFIT\Parker\Data\RUN15.TXT');
% acquisition_time = 8040; %[secs]
% SS_raw = load('E:\AFIT\Parker\Data\RUN16.TXT');
% acquisition_time = 142980; %[secs]

% SS_raw = load('E:\AFIT\Parker\Data\RUN19.TXT');
% acquisition_time = 86340; %[secs]
% mid = 503;
% SS_raw = load('E:\AFIT\Parker\Data\RUN20.TXT');
% acquisition_time = 6900; %[secs]
% mid = 505;
% SS_raw = load('E:\AFIT\Parker\Data\RUN21.TXT');
% acquisition_time = 87240; %[secs]
% mid = 505;
% SS_raw = load('E:\AFIT\Parker\Data\RUN23.TXT');
% acquisition_time = 86400; %[secs]
% mid = 505;
% SS_raw = load('E:\AFIT\Parker\Data\RUN24.TXT');
% acquisition_time = 88020; %[secs]
% mid = 503;
% SS_raw = load('E:\AFIT\Parker\Data\RUN25A.TXT');
% acquisition_time = 54480; %[secs]
% mid = 506;
% SS_raw = load('E:\AFIT\Parker\Data\RUN25B.TXT');
% acquisition_time = 64680; %[secs]
% mid = 506;
% SS_raw = load('E:\AFIT\Parker\Data\RUN25C.TXT');
% acquisition_time = 101520; %[secs]
% mid = 505;
% SS_raw = load('E:\AFIT\Parker\Data\RUN25D.TXT');
% acquisition_time = 146280; %[secs]
% mid = 504;
% SS_raw = load('E:\AFIT\Parker\Data\RUN25E.TXT');
% acquisition_time = 172800; %[secs]
% mid = 505;
% SS_raw = load('E:\AFIT\Parker\Data\RUN26A.TXT');
% acquisition_time = 86400; %[secs]
% mid = 503;
% SS_raw = load('E:\AFIT\Parker\Data\RUN26B.TXT');
% acquisition_time = 101520; %[secs]
% mid = 503;
% SS_raw = load('E:\AFIT\Parker\Data\RUN26C.TXT');
% acquisition_time = 146280; %[secs]
% mid = 503;
% SS_raw = load('E:\AFIT\Parker\Data\RUN27A.TXT');
% acquisition_time = 97200; %[secs]
% mid = 504;
% SS_raw = load('E:\AFIT\Parker\Data\RUN27B.TXT');
% acquisition_time = 172800; %[secs]
% mid = 504;
% SS_raw = load('E:\AFIT\Parker\Data\RUN28A.TXT');
% acquisition_time = 86400; %[secs]
% mid = 502;
% SS_raw = load('E:\AFIT\Parker\Data\RUN28B.TXT');
% acquisition_time = 172800; %[secs]
% mid = 503;
% SS_raw = load('E:\AFIT\Parker\Data\RUN29A.TXT');
% acquisition_time = 94860; %[secs]
% mid = 504;
% SS_raw = load('E:\AFIT\Parker\Data\RUN29B.TXT');
% acquisition_time = 346740; %[secs]
% mid = 504;
SS_raw = load('E:\AFIT\Parker\Data\RUN30A.TXT');
acquisition_time = 94860; %[secs]
mid = 504;
% SS_raw = load('E:\AFIT\Parker\Data\RUN30B.TXT');
% acquisition_time = 345600; %[secs]
% mid = 504;
% SS_raw = load('E:\AFIT\Parker\Data\RUN31A.TXT');
% acquisition_time = 173100; %[secs]
% mid = 503;
% SS_raw = load('E:\AFIT\Parker\Data\RUN31B.TXT');
% acquisition_time = 489900; %[secs]
% mid = 504;
% SS_raw = load('E:\AFIT\Parker\Data\RUN32.TXT');
% acquisition_time = 656880; %[secs]
% mid = 523;
% SS_raw = load('E:\AFIT\Parker\Data\RUN33.TXT');
% acquisition_time = 657120; %[secs]
% mid = 523;
% SS_raw = load('E:\AFIT\Parker\Data\RUN34.TXT');
% acquisition_time = 782700; %[secs]
% mid = 523;
% SS_raw = load('E:\AFIT\Parker\Data\RUN35.TXT');
% acquisition_time = 603120; %[secs]
% mid = 523;
% SS_raw = load('E:\AFIT\Parker\Data\RUN36.TXT');
% acquisition_time = 595860; %[secs]
% mid = 522;
% SS_raw = load('E:\AFIT\Parker\Data\RUN37.TXT');
% acquisition_time = 601800; %[secs]
% mid = 522;
% SS_raw = load('E:\AFIT\Parker\Data\RUN38.TXT');
% acquisition_time = 327900; %[secs]
% mid = 523;
% SS_raw = load('E:\AFIT\Parker\Data\RUN39.TXT');
% acquisition_time = 591000; %[secs]
% mid = 508;
% SS_raw = load('E:\AFIT\Parker\Data\RUN40A.TXT');
% acquisition_time = 439800; %[secs]
% mid = 508;
% SS_raw = load('E:\AFIT\Parker\Data\RUN40B.TXT');
% acquisition_time = 862500; %[secs]
% mid = 509;
% SS_raw = load('E:\AFIT\Parker\Data\RUN40C.TXT');
% acquisition_time = 1056000; %[secs]
% mid = 509;
% SS_raw = load('E:\AFIT\Parker\Data\RUN40D.TXT');
% acquisition_time = 1479000; %[secs]
% mid = 509;
% SS_raw = load('E:\AFIT\Parker\Data\RUN40E.TXT');
% acquisition_time = 1560900; %[secs]
% mid = 509;
% SS_raw = load('E:\AFIT\Parker\Data\RUN40F.TXT');
% acquisition_time = 1839300; %[secs]
% mid = 509;
% SS_raw = load('E:\AFIT\Parker\Data\RUN41A.TXT');
% acquisition_time = 419700; %[secs]
% mid = 509;
% SS_raw = load('E:\AFIT\Parker\Data\RUN41B.TXT');
% acquisition_time = 603000; %[secs]
% mid = 509;
% SS_raw = load('E:\AFIT\Parker\Data\RUN41C.TXT');
% acquisition_time = 855000; %[secs]
% mid = 509;
% SS_raw = load('E:\AFIT\Parker\Data\RUN41D.TXT');
% acquisition_time = 1019400; %[secs]
% mid = 509;
% SS_raw = load('E:\AFIT\Parker\Data\RUN41E.TXT');
% acquisition_time = 1197900; %[secs]
% mid = 509;
% SS_raw = load('E:\AFIT\Parker\Data\RUN41F.TXT');
% acquisition_time = 1791900; %[secs]
% mid = 509;
% SS_raw = load('E:\AFIT\Parker\Data\RUN42A.TXT');
% acquisition_time = 266160; %[secs]
% mid = 509;

% SS_raw = load('E:\AFIT\Parker\Data\RUN42C.TXT');
% acquisition_time = 622620; %[secs]
% mid = 509;
% SS_raw = load('E:\AFIT\Parker\Data\RUN42D.TXT');
% acquisition_time = 865380; %[secs]
% mid = 509;
% SS_raw = load('E:\AFIT\Parker\Data\RUN42E.TXT');
% acquisition_time = 960300; %[secs]
% mid = 509;
% SS_raw = load('E:\AFIT\Parker\Data\RUN42F.TXT');
% acquisition_time = 1208880; %[secs]
% mid = 509;
% SS_raw = load('E:\AFIT\Parker\Data\RUN42G.TXT');
% acquisition_time = 4791780; %[secs]
% mid = 509;
% SS_raw = load('E:\AFIT\Parker\Data\RUN43A.TXT');
% acquisition_time = 606000; %[secs]
% mid = 509;
% SS_raw = load('E:\AFIT\Parker\Data\RUN44A.TXT');
% acquisition_time = 785100; %[secs]
% mid = 508;
% SS_raw = load('E:\AFIT\Parker\Data\RUN44B.TXT');
% acquisition_time = 1380300; %[secs]
% mid = 508;
% SS_raw = load('E:\AFIT\Parker\Data\RUN44C.TXT');
% acquisition_time = 1655700; %[secs]
% mid = 508;
% SS_raw = load('E:\AFIT\Parker\Data\RUN44D.TXT');
% acquisition_time = 1990500; %[secs]
% mid = 508;
% SS_raw = load('E:\AFIT\Parker\Data\RUN44E.TXT');
% acquisition_time = 2432700; %[secs]
% mid = 508;
% SS_raw = load('E:\AFIT\Parker\Data\RUN44F.TXT');
% acquisition_time = 3215700; %[secs]
% mid = 508;
% SS_raw = load('E:\AFIT\Parker\Data\RUN44G.TXT');
% acquisition_time = 4144500; %[secs]
% mid = 508;
% SS_raw = load('E:\AFIT\Parker\Data\RUN44H.TXT');
% acquisition_time = 4750500; %[secs]
% mid = 508;
% SS_raw = load('E:\AFIT\Parker\Data\RUN44I.TXT');
% acquisition_time = 6492900; %[secs]
% mid = 508;
% SS_raw = load('E:\AFIT\Parker\Data\RUN45A.TXT');
% acquisition_time = 677100; %[secs]
% mid = 508;
% SS_raw = load('E:\AFIT\Parker\Data\RUN45B.TXT');
% acquisition_time = 1385700; %[secs]
% mid = 508;
% SS_raw = load('E:\AFIT\Parker\Data\RUN45C.TXT');
% acquisition_time = 1970400; %[secs]
% mid = 508;

% %Delete the first column
cal_fe_raw(:,1) = [];       %Raw Energy Calibration Data
SS_raw(:,1) = [];           %Raw Stainless Steel (SS) Data
%Take the transpose
cal_fe = cal_fe_raw.';
[m,n] = size(cal_fe);
```

```
cal_SS = SS_raw.';
[mSS,nSS] = size(cal_SS);
%reshapes loaded data from a matrix to an array with the same number
%of elements (n x m)
counts = reshape(cal_fe, 1, m*n);
SScounts = reshape(cal_SS, 1, mSS*nSS);
Transpose_SScounts = SScounts';

%First 3 values are header and are deleted
%counts(:,1:3) = [];
array_length = length(counts);
bin = [1:1:array_length];
%SScounts(:,1:3) = [];
SSarray_length = length(SScounts);
SSbin = [1:1:SSarray_length];


%%*********************************************************************
Bootstrap

figure(2)
[FittedData, Error, Baseline, BestStart, XI, YI, BootResults] =  ...
    peakfit([SSbin' SScounts'],512, 1024, 1, 20,.5, 100,...
    [507.76 5.0591],3, 0, 2, 1)
subplot(2,1,1)
title('Voigt Mössbauer Spectrum for counts under peak')
ylabel('Counts')
subplot(2,1,2)
title('Residual Plot')
xlabel('Bin Number')
ylabel('Counts')
%%*********************************************************************
```

A.2 Peak Asymmetry

```
%%*********************************************************************
%Peak Asymmetry Analysis
%Left Side of Peak
leftLength = (mid-1)*2 +1;  %An array of odd length
leftMid = (leftLength - 1)/2 +1;
leftArray = zeros(1,leftLength);
for i = 1:mid,
    leftArray(1,i) = SScounts(1,i);
end
for i = (mid+1):leftLength,
    leftArray(1,i) = SScounts(1,leftLength - i +1);
```

```
end

figure(2)
[FittedData, Error] = peakfit(leftArray',leftMid, 1000, 1, 20,...
    .5, 100,[mid 5.0591],3, 0, 2, 1)
subplot(2,1,1)
title('Left Peak Spectrum Voigt Fit')
ylabel('Counts')
subplot(2,1,2)
title('Residual Plot')
xlabel('Bin Number')
ylabel('Counts')

%Right side of Peak
rightLength = (array_length - mid)*2 +1;  %An array of odd length
rightMid = (rightLength - 1)/2 +1;
rightArray = zeros(1,rightLength);
for i = rightMid:rightLength,
    rightArray(1,i) = SScounts(1,(i-rightMid + mid));
end
for i = 1:(rightMid-1),
    rightArray(1,i) = rightArray(1,(rightLength - i + 1));
end

figure(3)
[FittedData, Error] = peakfit(rightArray',rightMid, 1000, 1, 20,...
    .5, 100,[mid 5.0591],3, 0, 2, 1)
subplot(2,1,1)
title('Right Peak Spectrum Voigt Fit')
ylabel('Counts')
subplot(2,1,2)
title('Residual Plot')
xlabel('Bin Number')
ylabel('Counts')
%%**********************************************************************
```

A.3 MATLAB 'peakfit.m' Code

```
function
[FitResults,LowestError,baseline,BestStart,xi,yi,BootResults]=peakfit(s
ignal,center,window,NumPeaks,peakshape,extra,NumTrials,start,autozero,f
ixedparameters,plots,bipolar)
% A command-line peak fitting program for time-series signals, written
as a
% self-contained Matlab function in a single m-file. Uses a non-linear
% optimization algorithm to decompose a complex, overlapping-peak
signal
% into its component parts. The objective is to determine whether your
% signal can be represented as the sum of fundamental underlying peaks
% shapes. Accepts signals of any length, including those with non-
integer
```

```
% and non-uniform x-values. Fits any number of peaks of Gaussian,
% Lorentzian, equal-width Gaussian and Lorentzian, fixed-width Gaussian
and
% Lorentzian, biburfated Gaussian and Lorentzian, exponentially-
broadened
% Gaussian, Pearson, Logistic, exponential pulse, sigmoid,Gaussian/
% Lorentzian blend, Voigt, triangular or multiple combinations of those
% shapes. This is a command line version, version, usable from a remote
% terminal. It is capable of making multiple trial fits with sightly
% different starting values and taking the one with the lowest mean fit
% error (example 6), and it can estimate the standard deviation of peak
% parameters from a single signal using the bootstrap method (example
10).
%
% Version 5.2: Feb, 2014. Bug fixes. Adds baseline as output argument;
% multiple-shape models, designated by using a vector as the 5th input
% argument (see examples 17 and 18). Adds triangular peakshape=21.
%
% For more details, see
% http://terpconnect.umd.edu/~toh/spectrum/CurveFittingC.html and
% http://terpconnect.umd.edu/~toh/spectrum/InteractivePeakFitter.htm
%
% peakfit(signal);
% Performs an iterative least-squares fit of a single Gaussian
% peak to the data matrix "signal", which has x values
% in column 1 and Y values in column 2 (e.g. [x y])
%
% peakfit(signal,center,window);
% Fits a single Gaussian peak to a portion of the
% matrix "signal". The portion is centered on the
% x-value "center" and has width "window" (in x units).
%
% peakfit(signal,center,window,NumPeaks);
% "NumPeaks" = number of peaks in the model (default is 1 if not
% specified). No limit to maximum number of peaks in version 3.1
%
% peakfit(signal,center,window,NumPeaks,peakshape);
% Specifies the peak shape of the model: "peakshape" = 1-20.
(1=Gaussian
% (default), 2=Lorentzian, 3=logistic, 4=Pearson, 5=exponentionally
% broadened Gaussian; 6=equal-width Gaussians; 7=Equal-width
Lorentzians;
% 8=exponentionally broadened equal-width Gaussian, 9=exponential
pulse,
% 10=sigmoid, 11=Fixed-width Gaussian, 12=Fixed-width Lorentzian;
% 13=Gaussian/Lorentzian blend; 14=BiGaussian, 15=BiLorentzian,
% 16=Fixed-position Gaussians; 17=Fixed-position Lorentzians;
% 18=exponentionally broadened Lorentzian; 19=alpha function; 20=Voigt
% profile; 21=triangular; 22=multiple shapes.
%
% peakfit(signal,center,window,NumPeaks,peakshape,extra) Specifies the
% value of 'extra', used only in the Voigt, Pearson, exponentionally
% broadened Gaussian, Gaussian/Lorentzian blend, and bifurcated
Gaussian
% and Lorentzian shapes to fine-tune the peak shape.
%
% peakfit(signal,center,window,NumPeaks,peakshape,extra,NumTrials);
% Performs "NumTrials" trial fits and selects the best one (with lowest
% fitting error). NumTrials can be any positive integer (default is 1).
%
%
peakfit(signal,center,window,NumPeaks,peakshape,extra,NumTrials,start)
% Specifies the first guesses vector "firstguess" for the peak
positions
% and widths. Must be expressed as a vector , in square brackets, e.g.
% start=[position1 width1 position2 width2 ...]
%
%
peakfit(signal,center,window,NumPeaks,peakshape,extra,NumTrials,start,a
utozero)
% Sets autozero mode in the last argument: autozero=0 (default) does
not
% subtract baseline from data segment;. autozero=1 interpolates a
linear
% baseline from the edges of the data segment and subtracts it from the
% signal (assumes that the peak returns to the baseline at the edges of
the
% signal); autozero=2,  like mode 1 except that it computes a quadratic
% curved baseline; autozero=3 compensates for a flat baseline without
% reference to the signal itself (best if the peak does not return to
the
% baseline at the edges of the signal).
%
% [FitResults,FitError]=peakfit(signal,center,window...) Returns the
% FitResults vector in the order peak number, peak position, peak
height,
% peak width, and peak area), and the FitError (the percent RMS
% difference between the data and the model in the selected segment of
that
% data) of the best fit.
%
%
[FitResults,LowestError,BestStart,xi,yi,BootResults]=peakfit(signal,...
)
% Prints out parameter error estimates for each peak fit.
%
% Optional output parameters
% 1. FitResults: a table of model peak parameters, one row for each
peak,
%    listing Peak number, Peak position, Height, Width, and Peak area.
% 2. LowestError: The rms fitting error of the best trial fit.
% 3. BestStart: the starting guesses that gave the best fit.
% 4. xi: vector containing 600 interploated x-values for the model
peaks.
% 5. yi: matrix containing the y values of each model peak at each xi.
%    Type plot(xi,yi(1,:)) to plot peak 1 or plot(xi,yi) to plot all
peaks
% 6. BootResults: a table of bootstrap precision results for a each
peak
%    and peak parameter.
```

```
%
% Example 1:
% >> x=[0:.1:10]';y=exp(-(x-5).^2);peakfit([x y])
% Fits exp(-x)^2 with a single Gaussian peak model.
%
%        Peak number  Peak position   Height     Width      Peak area
%             1            5             1        1.665       1.7725
%
% >> y=[0 1 2 4 6 7 6 4 2 1 0 ];x=1:length(y);
% >> peakfit([x;y],length(y)/2,length(y),0,0,0,0,0,0)
% Fits small set of manually entered y data to a single Gaussian peak
model.
%
% Example 2:
% x=[0:.01:10];y=exp(-(x-5).^2)+randn(size(x));peakfit([x;y])
% Measurement of very noisy peak with signal-to-noise ratio = 1.
% ans =
%             1         5.0279       0.9272      1.7948      1.7716
%
% Example 3:
% x=[0:.1:10];y=exp(-(x-5).^2)+.5*exp(-(x-3).^2)+.1*randn(size(x));
% peakfit([x' y'],0,0,2)
% Fits a noisy two-peak signal with a double Gaussian model
(NumPeaks=2).
% ans =
%             1       3.0001      0.49489        1.642      0.86504
%             2       4.9927       1.0016       1.6597       1.7696
%
% Example 4:
% >> x=1:100;y=ones(size(x))./(1+(x-50).^2);peakfit(y,0,0,1,2)
% Fit Lorentzian (peakshape=2) located at x=50, height=1, width=2.
% ans =
%            1           50      0.99974       1.9971       3.1079
%
% Example 5:
% >> x=[0:.005:1];y=humps(x);peakfit([x' y'],.3,.7,1,4,3);
% Fits a portion of the humps function, 0.7 units wide and centered on
% x=0.3, with a single (NumPeaks=1) Pearson function (peakshape=4) with
% extra=3 (controls shape of Pearson function).
%
% Example 6:
% >> x=[0:.005:1];y=(humps(x)+humps(x-.13)).^3;smatrix=[x' y'];
% >> [FitResults,FitError]=peakfit(smatrix,.4,.7,2,1,0,10)
% Creates a data matrix 'smatrix', fits a portion to a two-peak
Gaussian
% model, takes the best of 10 trials.  Returns FitResults and FitError.
% FitResults =
%              1      0.31056  2.0125e+006      0.11057  2.3689e+005
%              2      0.41529  2.2403e+006      0.12033  2.8696e+005
% FitError =
%         1.1899
%
% Example 7:
% >> peakfit([x' y'],.4,.7,2,1,0,10,[.3 .1 .5 .1]);
% As above, but specifies the first-guess position and width of the two
% peaks, in the order [position1 width1 position2 width2]
%
% Example 8: (Version 4 only)
% Demonstration of the four autozero modes, for a single Gaussian on
flat
%  baseline, with position=10, height=1, and width=1.66. Autozero mode
%  is specified by the 9th input argument (0,1,2, or 3).
% >> x=8:.05:12;y=1+exp(-(x-10).^2);
% >> [FitResults,FitError]=peakfit([x;y],0,0,1,1,0,1,0,0)
% Autozero=0 means to ignore the baseline (default mode if not
specified)
% FitResults =
%             1           10       1.8561        3.612       5.7641
% FitError =
%         5.387
% >> [FitResults,FitError]=peakfit([x;y],0,0,1,1,0,1,0,1)
% Autozero=1 subtracts linear baseline from edge to edge.
% Does not work well because signal does not return to baseline at
edges.
% FitResults =
%             1       9.9984      0.96153        1.559       1.5916
% FitError =
%        1.9801
% >> [FitResults,FitError]=peakfit([x;y],0,0,1,1,0,1,0,2)
% Autozero=1 subtracts quadratic baseline from edge to edge.
% Does not work well because signal does not return to baseline at
edges.
% FitResults =
%             1       9.9996      0.81749       1.4384       1.2503
% FitError =
%        1.8204
% Autozero=3: Flat baseline mode, measures baseline by regression
% >> [FitResults,Baseline,FitError]=peakfit([x;y],0,0,1,1,0,1,0,3)
% FitResults =
%             1           10       1.0001       1.6653       1.7645
% Baseline =
%     0.0037056
% FitError =
%       0.99985
%
% Example 9:
% x=[0:.1:10];y=exp(-(x-5).^2)+.5*exp(-(x-3).^2)+.1*randn(size(x));
% [FitResults,FitError]=peakfit([x' y'],0,0,2,11,0,0,0,0,1.666)
% Same as example 3, fit with fixed-width Gaussian (shape 11),
width=1.666
%
% Example 10: (Version 3 or later; Prints out parameter error
estimates)
% x=0:.05:9;y=exp(-(x-5).^2)+.5*exp(-(x-3).^2)+.01*randn(1,length(x));
%
[FitResults,LowestError,BestStart,xi,yi,BootstrapErrors]=peakfit([x;y],
0,0,2,6,0,1,0,0,0);
%
% Example 11: (Version 3.2 or later)
% x=[0:.005:1];y=humps(x);[FitResults,FitError]=peakfit([x'
y'],0.54,0.93,2,13,15,10,0,0,0)
%
% FitResults =
%              1      0.30078       190.41      0.19131       23.064
%              2      0.89788       39.552      0.33448       6.1999
% FitError =
%       0.34502
% Fits both peaks of the Humps function with a Gaussian/Lorentzian
blend
% (shape 13) that is 15% Gaussian (Extra=15).
%
% Example 12:  (Version 3.2 or later)
% >> x=[0:.1:10];y=exp(-(x-4).^2)+.5*exp(-(x-5).^2)+.01*randn(size(x));
% >> [FitResults,FitError]=peakfit([x' y'],0,0,1,14,45,10,0,0,0)
% FitResults =
%              1       4.2028       1.2315        4.077       2.6723
% FitError =
%       0.84461
% Fit a slightly asymmetrical peak with a bifurcated Gaussian (shape
14)
%
% Example 13:  (Version 3.3 or later)
% >> x=[0:.1:10]';y=exp(-(x-5).^2);peakfit([x y],0,0,1,1,0,0,0,0,0,0)
% Example 1 without plotting (11th input argument = 0, default is 1)
%
% Example 14:  (Version 3.9 or later)
% Exponentially broadened Lorentzian with position=9, height=1.
% x=[0:.1:20];
% L=lorentzian(x,9,1);
% L1=ExpBroaden(L',-10)+0.02.*randn(size(x))';
% [FitResults,FitError]=peakfit([x;L1'],0,0,1,18,10)
%
% Example 15: Fitting the humps funciton with two Voigt profiles, flat
% baselinie mode
% [FitResults,FitError]=peakfit(humps(0:.01:2),71,140,2,20,1.7,1,[31
4.7 90 8.8],3)
%FitResults =
%              1       31.047       96.762       4.6785       2550.1
%              2        90.09       22.935       8.8253       1089.5
% FitError =
%       0.80501
%
% Example 16: (Version 4.3 or later) Set +/- mode to 1 (bipolar)
% >> x=[0:.1:10];y=exp(-(x-5).^2)-.5*exp(-(x-3).^2)+.1*randn(size(x));
% >> peakfit([x' y'],0,0,2,1,0,1,0,0,0,1,1)
% FitResults =
%              1       3.1636      -0.5433         1.62      -0.9369
%              2       4.9487      0.96859       1.8456       1.9029
% FitError =
%        8.2757
%
% Example 17: Version 5 or later. Fits humps function to a model
consisting
% of one Pearson (shape=4, extra=3) and one Gaussian (shape=1), flat
% baseline mode=3, NumTrials=10.
% [FitResults,Baseline,FitError]=peakfit([x;y],0.6,1,2,[4 1],[3
0],10,0,3)
% FitResults =
%             1      0.30154       84.671      0.27892       17.085
%             2      0.88522       11.545      0.20825       2.5399
% Baseline =
%         0.901
% FitError =
%        10.457
%
% Example 18: 5 peaks, 5 different shapes, all heights = 1, widths = 3.
% x=0:.1:60;
% y=modelpeaks2(x,[1 2 3 4 5],[1 1 1 1 1],[10 20 30 40 50],...
% [3 3 3 3 3],[0 0 0 2 -20])+.01*randn(size(x));
% peakfit([x' y'],0,0,5,[1 2 3 4 5],[0 0 0 2 -20])
%

% Copyright (c) 2013, Thomas C. O'Haver
%
% Permission is hereby granted, free of charge, to any person obtaining
a copy
% of this software and associated documentation files (the "Software"),
to deal
% in the Software without restriction, including without limitation the
rights
% to use, copy, modify, merge, publish, distribute, sublicense, and/or
sell
% copies of the Software, and to permit persons to whom the Software is
% furnished to do so, subject to the following conditions:
%
% The above copyright notice and this permission notice shall be
included in
% all copies or substantial portions of the Software.
%
% THE SOFTWARE IS PROVIDED "AS IS", WITHOUT WARRANTY OF ANY KIND,
EXPRESS OR
% IMPLIED, INCLUDING BUT NOT LIMITED TO THE WARRANTIES OF
MERCHANTABILITY,
% FITNESS FOR A PARTICULAR PURPOSE AND NONINFRINGEMENT. IN NO EVENT
SHALL THE
% AUTHORS OR COPYRIGHT HOLDERS BE LIABLE FOR ANY CLAIM, DAMAGES OR
OTHER
% LIABILITY, WHETHER IN AN ACTION OF CONTRACT, TORT OR OTHERWISE,
ARISING FROM,
% OUT OF OR IN CONNECTION WITH THE SOFTWARE OR THE USE OR OTHER
DEALINGS IN
% THE SOFTWARE.
%
global AA xxx PEAKHEIGHTS FIXEDPARAMETERS AUTOZERO delta BIPOLAR
% peakfit.m version 5, February 2014
format short g
format compact
warning off all
```

```
NumArgOut=nargout;
datasize=size(signal);
if datasize(1)<datasize(2),signal=signal';end
datasize=size(signal);
if datasize(2)==1, %  Must be isignal(Y-vector)
    X=1:length(signal); % Create an independent variable vector
    Y=signal;
else
    % Must be isignal(DataMatrix)
    X=signal(:,1); % Split matrix argument
    Y=signal(:,2);
end
X=reshape(X,1,length(X)); % Adjust X and Y vector shape to 1 x n
(rather than n x 1)
Y=reshape(Y,1,length(Y));
% If necessary, flip the data vectors so that X increases
if X(1)>X(length(X)),
    disp('X-axis flipped.')
    X=fliplr(X);
    Y=fliplr(Y);
end

% Isolate desired segment from data set for curve fitting
if nargin==1 || nargin==2,center=(max(X)-min(X))/2;window=max(X)-
min(X);end
% Y=Y-min(Y);
xoffset=0;
n1=val2ind(X,center-window/2);
n2=val2ind(X,center+window/2);
if window==0,n1=1;n2=length(X);end
xx=X(n1:n2)-xoffset;
yy=Y(n1:n2);
ShapeString='Gaussian';

% Define values of any missing arguments
switch nargin
    case 1
        NumPeaks=1;
        peakshape=1;
        extra=0;
        NumTrials=1;
        xx=X;yy=Y;
        start=calcstart(xx,NumPeaks,xoffset);
        AUTOZERO=0;
        plots=1;
        BIPOLAR=0;
    case 2
        NumPeaks=1;
        peakshape=1;
        extra=0;
        NumTrials=1;
        xx=signal;yy=center;
        start=calcstart(xx,NumPeaks,xoffset);
        AUTOZERO=0;
        plots=1;
        BIPOLAR=0;
    case 3
        NumPeaks=1;
        peakshape=1;
        extra=0;
        NumTrials=1;
        start=calcstart(xx,NumPeaks,xoffset);
        AUTOZERO=0;
        FIXEDPARAMETERS=0;
        plots=1;
        BIPOLAR=0;
    case 4
        peakshape=1;
        extra=0;
        NumTrials=1;
        start=calcstart(xx,NumPeaks,xoffset);
        AUTOZERO=0;
        FIXEDPARAMETERS=0;
        plots=1;
        BIPOLAR=0;
    case 5
        extra=zeros(1,NumPeaks);
        NumTrials=1;
        start=calcstart(xx,NumPeaks,xoffset);
        AUTOZERO=0;
        FIXEDPARAMETERS=0;
        plots=1;
        BIPOLAR=0;
    case 6
        NumTrials=1;
        start=calcstart(xx,NumPeaks,xoffset);
        AUTOZERO=0;
        FIXEDPARAMETERS=0;
        plots=1;
        BIPOLAR=0;
    case 7
        start=calcstart(xx,NumPeaks,xoffset);
        AUTOZERO=0;
        FIXEDPARAMETERS=0;
        plots=1;
        BIPOLAR=0;
    case 8
        AUTOZERO=0;
        FIXEDPARAMETERS=0;
        plots=1;
        BIPOLAR=0;
    case 9
        AUTOZERO=autozero;
        FIXEDPARAMETERS=0;
        plots=1;
        BIPOLAR=0;
    case 10
        AUTOZERO=autozero;
        FIXEDPARAMETERS=fixedparameters;
        plots=1;
        BIPOLAR=0;
    case 11
        AUTOZERO=autozero;
        FIXEDPARAMETERS=fixedparameters;
        BIPOLAR=0;
    case 12
        AUTOZERO=autozero;
        FIXEDPARAMETERS=fixedparameters;
        BIPOLAR=bipolar;
    otherwise
end % switch nargin

% Default values for placeholder zeros
if NumTrials==0;NumTrials=1;end
if isscalar(peakshape),
else
    % disp('peakshape is vector');
    shapesvector=peakshape;
    NumPeaks=length(peakshape);
    peakshape=22;
end
if peakshape==0;peakshape=1;end
if NumPeaks==0;NumPeaks=1;end
if start==0;start=calcstart(xx,NumPeaks,xoffset);end
if FIXEDPARAMETERS==0, FIXEDPARAMETERS=length(xx)/10;end
if peakshape==16;FIXEDPOSITIONS=fixedparameters;end
if AUTOZERO>3,AUTOZERO=3,end
if AUTOZERO<0,AUTOZERO=0,end
delta=1;

% % Remove linear baseline from data segment if AUTOZERO==1
bkgsize=round(length(xx)/10);
if bkgsize<2,bkgsize=2;end
lxx=length(xx);
if AUTOZERO==1, % linear autozero operation
    XX1=xx(1:round(lxx/bkgsize));
    XX2=xx((lxx-round(lxx/bkgsize)):lxx);
    Y1=yy(1:(round(length(xx)/bkgsize)));
    Y2=yy((lxx-round(lxx/bkgsize)):lxx);
    bkgcoef=polyfit([XX1,XX2],[Y1,Y2],1);  % Fit straight line to sub-
group of points
    bkg=polyval(bkgcoef,xx);
    yy=yy-bkg;
end % if
if AUTOZERO==2, % Quadratic autozero operation
    XX1=xx(1:round(lxx/bkgsize));
    XX2=xx((lxx-round(lxx/bkgsize)):lxx);
    Y1=yy(1:round(length(xx)/bkgsize));
    Y2=yy((lxx-round(lxx/bkgsize)):lxx);
    bkgcoef=polyfit([XX1,XX2],[Y1,Y2],2);  % Fit parabola to sub-group
of points
    bkg=polyval(bkgcoef,xx);
    yy=yy-bkg;
end % if autozero
```

```
PEAKHEIGHTS=zeros(1,NumPeaks);
n=length(xx);
newstart=start;
% Assign ShapStrings
switch peakshape(1)
    case 1
        ShapeString='Gaussian';
    case 2
        ShapeString='Lorentzian';
    case 3
        ShapeString='Logistic';
    case 4
        ShapeString='Pearson';
    case 5
        ShapeString='ExpGaussian';
    case 6
        ShapeString='Equal width Gaussians';
    case 7
        ShapeString='Equal width Lorentzians';
    case 8
        ShapeString='Exp. equal width Gaussians';
    case 9
        ShapeString='Exponential Pulse';
    case 10
        ShapeString='Sigmoid';
    case 11
        ShapeString='Fixed-width Gaussian';
    case 12
        ShapeString='Fixed-width Lorentzian';
    case 13
        ShapeString='Gaussian/Lorentzian blend';
    case 14
        ShapeString='BiGaussian';
    case 15
        ShapeString='BiLorentzian';
    case 16
        ShapeString='Fixed-position Gaussians';
    case 17
        ShapeString='Fixed-position Lorentzians';
    case 18
        ShapeString='Exp. Lorentzian';
    case 19
        ShapeString='Alpha function';
    case 20
        ShapeString='Voigt profile';
    case 21
        ShapeString='triangular';
    case 22
        ShapeString=num2str(shapesvector);
    otherwise
end % switch peakshape

% Perform peak fitting for selected peak shape using fminsearch
function
options = optimset('TolX',.001,'Display','off','MaxFunEvals',1000 );
```

```
LowestError=1000; % or any big number greater than largest error
expected
FitParameters=zeros(1,NumPeaks.*2);
BestStart=zeros(1,NumPeaks.*2);
height=zeros(1,NumPeaks);
bestmodel=zeros(size(yy));

for k=1:NumTrials,
    % StartVector=newstart
    % disp(['Trial number ' num2str(k) ] ) % optionally prints the
current trial number as progress indicator
  switch peakshape(1)
    case 1

TrialParameters=fminsearch(@(lambda)(fitgaussian(lambda,xx,yy)),newstar
t,options);
    case 2

TrialParameters=fminsearch(@(lambda)(fitlorentzian(lambda,xx,yy)),newst
art,options);
    case 3

TrialParameters=fminsearch(@(lambda)(fitlogistic(lambda,xx,yy)),newstar
t,options);
    case 4

TrialParameters=fminsearch(@(lambda)(fitpearson(lambda,xx,yy,extra)),ne
wstart,options);
    case 5
        zxx=[zeros(size(xx)) xx zeros(size(xx)) ];
        zyy=[zeros(size(yy)) yy zeros(size(yy)) ];

TrialParameters=fminsearch(@(lambda)(fitexpgaussian(lambda,zxx,zyy,-
extra)),newstart,options);
    case 6
        cwnewstart(1)=newstart(1);
        for pc=2:NumPeaks,
            cwnewstart(pc)=newstart(2.*pc-1);
        end
        cwnewstart(NumPeaks+1)=(max(xx)-min(xx))/5;

TrialParameters=fminsearch(@(lambda)(fitewgaussian(lambda,xx,yy)),cwnew
start,options);
    case 7
        cwnewstart(1)=newstart(1);
        for pc=2:NumPeaks,
            cwnewstart(pc)=newstart(2.*pc-1);
        end
        cwnewstart(NumPeaks+1)=(max(xx)-min(xx))/5;

TrialParameters=fminsearch(@(lambda)(fitewlorentzian(lambda,xx,yy)),cwn
ewstart,options);
    case 8
        cwnewstart(1)=newstart(1);
        for pc=2:NumPeaks,
            cwnewstart(pc)=newstart(2.*pc-1);
        end
        cwnewstart(NumPeaks+1)=(max(xx)-min(xx))/5;

TrialParameters=fminsearch(@(lambda)(fitexpewgaussian(lambda,xx,yy,-
extra)),cwnewstart,options);
      case 9

TrialParameters=fminsearch(@(lambda)(fitexppulse(lambda,xx,yy)),newstar
t,options);
      case 10

TrialParameters=fminsearch(@(lambda)(fitsigmoid(lambda,xx,yy)),newstart
,options);
      case 11
          fixedstart=[];
          for pc=1:NumPeaks,
              fixedstart(pc)=min(xx)+pc.*(max(xx)-
min(xx))./(NumPeaks+1);
          end

TrialParameters=fminsearch(@(lambda)(FitFWGaussian(lambda,xx,yy)),fixed
start,options);
      case 12
          fixedstart=[];
          for pc=1:NumPeaks,
              fixedstart(pc)=min(xx)+pc.*(max(xx)-
min(xx))./(NumPeaks+1);
          end

TrialParameters=fminsearch(@(lambda)(FitFWLorentzian(lambda,xx,yy)),fix
edstart,options);
      case 13

TrialParameters=fminsearch(@(lambda)(fitGL(lambda,xx,yy,extra)),newstar
t,options);
      case 14

TrialParameters=fminsearch(@(lambda)(fitBiGaussian(lambda,xx,yy,extra))
,newstart,options);
      case 15

TrialParameters=fminsearch(@(lambda)(fitBiLorentzian(lambda,xx,yy,extra
)),newstart,options);
      case 16
           fixedstart=[];
          for pc=1:NumPeaks,
              fixedstart(pc)=(max(xx)-min(xx))./(NumPeaks+1);
              fixedstart(pc)=fixedstart(pc)+.1*(rand-
.5).*fixedstart(pc);
          end

TrialParameters=fminsearch(@(lambda)(FitFPGaussian(lambda,xx,yy)),fixed
start,options);
      case 17
```

```
             fixedstart=[];
            for pc=1:NumPeaks,
                fixedstart(pc)=(max(xx)-min(xx))./(NumPeaks+1);
                fixedstart(pc)=fixedstart(pc)+.1*(rand-
.5).*fixedstart(pc);
            end

TrialParameters=fminsearch(@(lambda)(FitFPLorentzian(lambda,xx,yy)),fix
edstart,options);
        case 18
          zxx=[zeros(size(xx)) xx zeros(size(xx)) ];
          zyy=[ones(size(yy)).*yy(1) yy zeros(size(yy)).*yy(length(yy))
];
%           plot(zxx,zyy);pause

TrialParameters=fminsearch(@(lambda)(fitexplorentzian(lambda,zxx,zyy,-
extra)),newstart,options);
        case 19

TrialParameters=fminsearch(@(lambda)(fitalphafunction(lambda,xx,yy)),ne
wstart,options);
        case 20

TrialParameters=fminsearch(@(lambda)(fitvoigt(lambda,xx,yy,extra)),news
tart,options);
        case 21

TrialParameters=fminsearch(@(lambda)(fittriangular(lambda,xx,yy)),newst
art,options);
        case 22

TrialParameters=fminsearch(@(lambda)(fitmultiple(lambda,xx,yy,shapesvec
tor,extra)),newstart,options);
        otherwise
  end % switch peakshape

% Construct model from Trial parameters
A=zeros(NumPeaks,n);
for m=1:NumPeaks,
    switch peakshape(1)
        case 1
            A(m,:)=gaussian(xx,TrialParameters(2*m-
1),TrialParameters(2*m));
        case 2
            A(m,:)=lorentzian(xx,TrialParameters(2*m-
1),TrialParameters(2*m));
        case 3
            A(m,:)=logistic(xx,TrialParameters(2*m-
1),TrialParameters(2*m));
        case 4
            A(m,:)=pearson(xx,TrialParameters(2*m-
1),TrialParameters(2*m),extra);
        case 5
            A(m,:)=expgaussian(xx,TrialParameters(2*m-
1),TrialParameters(2*m),-extra)';
```

```
        case 6

A(m,:)=gaussian(xx,TrialParameters(m),TrialParameters(NumPeaks+1));
        case 7

A(m,:)=lorentzian(xx,TrialParameters(m),TrialParameters(NumPeaks+1));
        case 8

A(m,:)=expgaussian(xx,TrialParameters(m),TrialParameters(NumPeaks+1),-
extra)';
        case 9
            A(m,:)=exppulse(xx,TrialParameters(2*m-
1),TrialParameters(2*m));
        case 10
            A(m,:)=sigmoid(xx,TrialParameters(2*m-
1),TrialParameters(2*m));
        case 11
            A(m,:)=gaussian(xx,TrialParameters(m),FIXEDPARAMETERS);
        case 12
            A(m,:)=lorentzian(xx,TrialParameters(m),FIXEDPARAMETERS);
        case 13
            A(m,:)=GL(xx,TrialParameters(2*m-
1),TrialParameters(2*m),extra);
        case 14
            A(m,:)=BiGaussian(xx,TrialParameters(2*m-
1),TrialParameters(2*m),extra);
        case 15
            A(m,:)=BiLorentzian(xx,TrialParameters(2*m-
1),TrialParameters(2*m),extra);
        case 16
            A(m,:)=gaussian(xx,FIXEDPOSITIONS(m),TrialParameters(m));
        case 17
            A(m,:)=lorentzian(xx,FIXEDPOSITIONS(m),TrialParameters(m));
        case 18
            A(m,:)=explorentzian(xx,TrialParameters(2*m-
1),TrialParameters(2*m),-extra)';
        case 19
            A(m,:)=alphafunction(xx,TrialParameters(2*m-
1),TrialParameters(2*m));
        case 20
            A(m,:)=voigt(xx,TrialParameters(2*m-
1),TrialParameters(2*m),extra);
        case 21
            A(m,:)=triangular(xx,TrialParameters(2*m-
1),TrialParameters(2*m));
        case 22
            A(m,:)=peakfunction(shapesvector(m),xx,TrialParameters(2*m-
1),TrialParameters(2*m),extra(m));
        otherwise
    end % switch
    for parameter=1:2:2*NumPeaks,
        newstart(parameter)=newstart(parameter)*(1+delta*(rand-
.5)/500);
        newstart(parameter+1)=newstart(parameter+1)*(1+delta*(rand-
.5)/100);
```

```
    end
end % for NumPeaks

% Multiplies each row by the corresponding amplitude and adds them up
if AUTOZERO==3,
    baseline=PEAKHEIGHTS(1);
    Heights=PEAKHEIGHTS(2:1+NumPeaks);
    model=Heights'*A+baseline;
else
    model=PEAKHEIGHTS'*A;
    Heights=PEAKHEIGHTS;
    baseline=0;
end

% Compare trial model to data segment and compute the fit error
  MeanFitError=100*norm(yy-model)./(sqrt(n)*max(yy));
  % Take only the single fit that has the lowest MeanFitError
  if MeanFitError<LowestError,
      if min(Heights)>=-BIPOLAR*10^100,  % Consider only fits with
positive peak heights
        LowestError=MeanFitError;  % Assign LowestError to the lowest
MeanFitError
        FitParameters=TrialParameters;  % Assign FitParameters to the
fit with the lowest MeanFitError
        BestStart=newstart; % Assign BestStart to the start with the
lowest MeanFitError
        height=Heights; % Assign height to the PEAKHEIGHTS with the
lowest MeanFitError
        bestmodel=model; % Assign bestmodel to the model with the
lowest MeanFitError
      end % if min(PEAKHEIGHTS)>0
  end % if MeanFitError<LowestError
end % for k (NumTrials)
%
% Construct model from best-fit parameters
AA=zeros(NumPeaks,600);
xxx=linspace(min(xx),max(xx),600);
% xxx=linspace(min(xx)-length(xx),max(xx)+length(xx),200);
for m=1:NumPeaks,
   switch peakshape(1)
    case 1
        AA(m,:)=gaussian(xxx,FitParameters(2*m-1),FitParameters(2*m));
    case 2
        AA(m,:)=lorentzian(xxx,FitParameters(2*m-
1),FitParameters(2*m));
    case 3
        AA(m,:)=logistic(xxx,FitParameters(2*m-1),FitParameters(2*m));
    case 4
        AA(m,:)=pearson(xxx,FitParameters(2*m-
1),FitParameters(2*m),extra);
    case 5
        AA(m,:)=expgaussian(xxx,FitParameters(2*m-
1),FitParameters(2*m),-extra*length(xxx)./length(xx))';
    case 6
```

```
AA(m,:)=gaussian(xxx,FitParameters(m),FitParameters(NumPeaks+1));
    case 7

AA(m,:)=lorentzian(xxx,FitParameters(m),FitParameters(NumPeaks+1));
    case 8

AA(m,:)=expgaussian(xxx,FitParameters(m),FitParameters(NumPeaks+1),-
extra*length(xxx)./length(xx))';
    case 9
        AA(m,:)=exppulse(xxx,FitParameters(2*m-1),FitParameters(2*m));
    case 10
        AA(m,:)=sigmoid(xxx,FitParameters(2*m-1),FitParameters(2*m));
    case 11
        AA(m,:)=gaussian(xxx,FitParameters(m),FIXEDPARAMETERS);
    case 12
        AA(m,:)=lorentzian(xxx,FitParameters(m),FIXEDPARAMETERS);
    case 13
        AA(m,:)=GL(xxx,FitParameters(2*m-1),FitParameters(2*m),extra);
    case 14
        AA(m,:)=BiGaussian(xxx,FitParameters(2*m-
1),FitParameters(2*m),extra);
    case 15
        AA(m,:)=BiLorentzian(xxx,FitParameters(2*m-
1),FitParameters(2*m),extra);
    case 16
        AA(m,:)=gaussian(xxx,FIXEDPOSITIONS(m),FitParameters(m));
    case 17
        AA(m,:)=lorentzian(xxx,FIXEDPOSITIONS(m),FitParameters(m));
    case 18
        AA(m,:)=explorentzian(xxx,FitParameters(2*m-
1),FitParameters(2*m),-extra*length(xxx)./length(xx))';
    case 19
        AA(m,:)=alphafunction(xxx,FitParameters(2*m-
1),FitParameters(2*m));
    case 20
        AA(m,:)=voigt(xxx,FitParameters(2*m-
1),FitParameters(2*m),extra);
    case 21
        AA(m,:)=triangular(xxx,FitParameters(2*m-
1),FitParameters(2*m));
    case 22
        AA(m,:)=peakfunction(shapesvector(m),xxx,FitParameters(2*m-
1),FitParameters(2*m),extra(m));
       otherwise
  end % switch
end % for NumPeaks

% Multiplies each row by the corresponding amplitude and adds them up
heightsize=size(height');
AAsize=size(AA);
if heightsize(2)==AAsize(1),
   mmodel=height'*AA+baseline;
else
    mmodel=height*AA+baseline;
```

```
end
% Top half of the figure shows original signal and the fitted model.
if plots,
    subplot(2,1,1);plot(xx+xoffset,yy,'b.'); % Plot the original signal
in blue dots
    hold on
end
for m=1:NumPeaks,
    if plots, plot(xxx+xoffset,height(m)*AA(m,:)+baseline,'g'),end  %
Plot the individual component peaks in green lines
    area(m)=trapz(xxx+xoffset,height(m)*AA(m,:)); % Compute the area of
each component peak using trapezoidal method
    yi(m,:)=height(m)*AA(m,:); % (NEW) Place y values of individual
model peaks into matrix yi
end
xi=xxx+xoffset; % (NEW) Place the x-values of the individual model
peaks into xi

if plots,
    % Mark starting peak positions with vertical dashed lines
    if peakshape(1)==16||peakshape(1)==17
    else
        for marker=1:NumPeaks,
            markx=BestStart((2*marker)-1);
            subplot(2,1,1);plot([markx+xoffset markx+xoffset],[0
max(yy)],'m--')
        end % for
    end % if peakshape
    plot(xxx+xoffset,mmodel,'r');  % Plot the total model (sum of
component peaks) in red lines
    hold off;
    lyy=min(yy);
    uyy=max(yy)+(max(yy)-min(yy))/10;
    if BIPOLAR,
        axis([min(xx) max(xx) lyy uyy]);
        ylabel('+ - mode')
    else
        axis([min(xx) max(xx) 0 uyy]);
        ylabel('+ mode')
    end
    switch AUTOZERO,
        case 0
            title(['peakfit 5.1   No baseline correction'])
        case 1
            title(['peakfit 5.1   Linear baseline subtraction'])
        case 2
            title(['peakfit 5.1   Quadratic subtraction baseline'])
        case 3
            title(['peakfit 5.1   Flat baseline correction'])
    end

    switch peakshape(1)
    case {4,20}
```

```
        xlabel(['Peaks = ' num2str(NumPeaks) '     Shape = '
ShapeString '      Shape Constant = ' num2str(extra) '   Error = '
num2str(round(1000*LowestError)/1000) '%' ] )
    case {5,8,18}
        xlabel(['Peaks = ' num2str(NumPeaks) '     Shape = '
ShapeString '      Time Constant = ' num2str(extra) '   Error = '
num2str(round(1000*LowestError)/1000) '%' ] )
    case 13
        xlabel(['Peaks = ' num2str(NumPeaks) '     Shape = '
ShapeString '      % Gaussian = ' num2str(extra)  '     Error = '
num2str(round(1000*LowestError)/1000) '% ' ] )
    case {14,15,22}
        xlabel(['Peaks = ' num2str(NumPeaks) '     Shape = '
ShapeString '      extra = ' num2str(extra) '     Error = '
num2str(round(1000*LowestError)/1000)  '% ' ] )
    otherwise
        xlabel(['Peaks = ' num2str(NumPeaks) '     Shape = '
ShapeString '     Error = ' num2str(round(1000*LowestError)/1000) '% '
] )
    end

    % Bottom half of the figure shows the residuals and displays RMS
error
    % between original signal and model
    residual=yy-bestmodel;
    subplot(2,1,2);plot(xx+xoffset,residual,'b.')
    axis([min(xx)+xoffset max(xx)+xoffset min(residual)
max(residual)]);
    xlabel('Residual Plot')
end % if plots

% Put results into a matrix, one row for each peak, showing peak index
number,
% position, amplitude, and width.
for m=1:NumPeaks,
    if m==1,
        if peakshape(1)==6||peakshape(1)==7||peakshape(1)==8, % equal-
width peak models only
            FitResults=[[round(m) FitParameters(m)+xoffset height(m)
abs(FitParameters(NumPeaks+1)) area(m)]];
        else
            if peakshape(1)==11||peakshape(1)==12, % Fixed-width shapes
only
                FitResults=[[round(m) FitParameters(m)+xoffset
height(m) FIXEDPARAMETERS area(m)]];
            else
                if peakshape(1)==16||peakshape(1)==17, % Fixed-position
shapes only
                    FitResults=[round(m) FIXEDPOSITIONS(m) height(m)
FitParameters(m) area(m)];
                else
                    FitResults=[round(m) FitParameters(2*m-1)+xoffset
height(m) abs(FitParameters(2*m)) area(m)];
                end
            end
        end % if peakshape
    else
        if peakshape(1)==6||peakshape(1)==7||peakshape(1)==8, % equal-
width peak models only
            FitResults=[FitResults ; [round(m) FitParameters(m)+xoffset
height(m) abs(FitParameters(NumPeaks+1)) area(m)]];
        else
            if peakshape(1)==11||peakshape(1)==12, % Fixed-width shapes
only
                FitResults=[FitResults ; [round(m)
FitParameters(m)+xoffset height(m) FIXEDPARAMETERS area(m)]];
            else
                if peakshape(1)==16||peakshape(1)==17, % Fixed-position
shapes only
                    FitResults=[FitResults ; [round(m)
FIXEDPOSITIONS(m) height(m) FitParameters(m) area(m)]];
                else
                    FitResults=[FitResults ; [round(m)
FitParameters(2*m-1)+xoffset height(m) abs(FitParameters(2*m))
area(m)]];
                end
            end
        end % if peakshape
    end % m==1
end % for m=1:NumPeaks
% Display Fit Results on upper graph
if plots,
    subplot(2,1,1);
    startx=min(xx)+xoffset+(max(xx)-min(xx))./20;
    dxx=(max(xx)-min(xx))./10;
    dyy=(max(yy)-min(yy))./10;
    starty=max(yy)-dyy;
    FigureSize=get(gcf,'Position');
    if peakshape(1)==9||peakshape(1)==10||peakshape(1)==19,  % Pulse
and sigmoid shapes only
        text(startx,starty+dyy/2,['Peak #          tau1
Height           tau2             Area'] );
    else
        text(startx,starty+dyy/2,['Peak #          Position
Height         Width              Area'] );
    end
    % Display FitResults using sprintf
    for peaknumber=1:NumPeaks,
        for column=1:5,
            itemstring=sprintf('%0.4g',FitResults(peaknumber,column));
            xposition=startx+(1.7.*dxx.*(column-
1).*(600./FigureSize(3)));
            yposition=starty-peaknumber.*dyy.*(400./FigureSize(4));
            text(xposition,yposition,itemstring);
        end
    end
    xposition=startx;
    yposition=starty-(peaknumber+1).*dyy.*(400./FigureSize(4));
    if AUTOZERO==3,
       text(xposition,yposition,[ 'Baseline= ' num2str(baseline) ]);
    end
end % if plots

if NumArgOut==7,
    if plots,disp('Computing bootstrap sampling statistics.....'),end
    BootstrapResultsMatrix=zeros(5,100,NumPeaks);
    BootstrapErrorMatrix=zeros(1,100,NumPeaks);
    clear bx by
    tic;
    for trial=1:100,
        n=1;
        bx=xx;
        by=yy;
        while n<length(xx)-1,
            if rand>.5,
                bx(n)=xx(n+1);
                by(n)=yy(n+1);
            end
            n=n+1;
        end
        bx=bx+xoffset;

[FitResults,BootFitError]=fitpeaks(bx,by,NumPeaks,peakshape,extra,NumTr
ials,start,AUTOZERO,FIXEDPARAMETERS);
        for peak=1:NumPeaks,
            BootstrapResultsMatrix(:,trial,peak)=FitResults(peak,:);
            BootstrapErrorMatrix(:,trial,peak)=BootFitError;
        end
    end
    if plots,toc;end
    for peak=1:NumPeaks,
        if plots,
            disp(' ')
            disp(['Peak #',num2str(peak) '         Position    Height
Width       Area']);
        end % if plots
        BootstrapMean=mean(real(BootstrapResultsMatrix(:,:,peak)'));
        BootstrapSTD=std(BootstrapResultsMatrix(:,:,peak)');
        BootstrapIQR=iqr(BootstrapResultsMatrix(:,:,peak)');
        PercentRSD=100.*BootstrapSTD./BootstrapMean;
        PercentIQR=100.*BootstrapIQR./BootstrapMean;
        BootstrapMean=BootstrapMean(2:5);
        BootstrapSTD=BootstrapSTD(2:5);
        BootstrapIQR=BootstrapIQR(2:5);
        PercentRSD=PercentRSD(2:5);
        PercentIQR=PercentIQR(2:5);
        if plots,
            disp(['Bootstrap Mean: ', num2str(BootstrapMean)])
            disp(['Bootstrap STD:  ', num2str(BootstrapSTD)])
            disp(['Bootstrap IQR:  ', num2str(BootstrapIQR)])
            disp(['Percent RSD:    ', num2str(PercentRSD)])
            disp(['Percent IQR:    ', num2str(PercentIQR)])
        end % if plots
        BootResults(peak,:)=[BootstrapMean BootstrapSTD PercentRSD
BootstrapIQR PercentIQR];
```

```
    end % peak=1:NumPeaks,
end % if NumArgOut==6,
% ---------------------------------------------------------------------
-
function
[FitResults,LowestError]=fitpeaks(xx,yy,NumPeaks,peakshape,extra,NumTri
als,start,AUTOZERO,fixedparameters)
% Based on peakfit Version 3: June, 2012.
global PEAKHEIGHTS FIXEDPARAMETERSS AUTOZERO BIPOLAR
format short g
format compact
warning off all
FIXEDPARAMETERS=fixedparameters;
xoffset=0;
if start==0;start=calcstart(xx,NumPeaks,xoffset);end
PEAKHEIGHTS=zeros(1,NumPeaks);
n=length(xx);
newstart=start;

% Perform peak fitting for selected peak shape using fminsearch
function
options = optimset('TolX',.001,'Display','off','MaxFunEvals',1000 );
LowestError=1000; % or any big number greater than largest error
expected
FitParameters=zeros(1,NumPeaks.*2);
BestStart=zeros(1,NumPeaks.*2);
height=zeros(1,NumPeaks);
bestmodel=zeros(size(yy));
for k=1:NumTrials,
    % StartVector=newstart
    switch peakshape(1)
        case 1

TrialParameters=fminsearch(@(lambda)(fitgaussian(lambda,xx,yy)),newstar
t,options);
        case 2

TrialParameters=fminsearch(@(lambda)(fitlorentzian(lambda,xx,yy)),newst
art,options);
        case 3

TrialParameters=fminsearch(@(lambda)(fitlogistic(lambda,xx,yy)),newstar
t,options);
        case 4

TrialParameters=fminsearch(@(lambda)(fitpearson(lambda,xx,yy,extra)),ne
wstart,options);
        case 5
            zxx=[zeros(size(xx)) xx zeros(size(xx)) ];
            zyy=[zeros(size(yy)) yy zeros(size(yy)) ];

TrialParameters=fminsearch(@(lambda)(fitexpgaussian(lambda,zxx,zyy,-
extra)),newstart,options);
        case 6
            cwnewstart(1)=newstart(1);
            for pc=2:NumPeaks,
                cwnewstart(pc)=newstart(2.*pc-1);
            end
            cwnewstart(NumPeaks+1)=(max(xx)-min(xx))/5;

TrialParameters=fminsearch(@(lambda)(fitewgaussian(lambda,xx,yy)),cwnew
start,options);
        case 7
            cwnewstart(1)=newstart(1);
            for pc=2:NumPeaks,
                cwnewstart(pc)=newstart(2.*pc-1);
            end
            cwnewstart(NumPeaks+1)=(max(xx)-min(xx))/5;

TrialParameters=fminsearch(@(lambda)(fitewlorentzian(lambda,xx,yy)),cwn
ewstart,options);
        case 8
            cwnewstart(1)=newstart(1);
            for pc=2:NumPeaks,
                cwnewstart(pc)=newstart(2.*pc-1);
            end
            cwnewstart(NumPeaks+1)=(max(xx)-min(xx))/5;

TrialParameters=fminsearch(@(lambda)(fitexpewgaussian(lambda,xx,yy,-
extra)),cwnewstart,options);
        case 9

TrialParameters=fminsearch(@(lambda)(fitexppulse(lambda,xx,yy)),newstar
t,options);
        case 10

TrialParameters=fminsearch(@(lambda)(fitsigmoid(lambda,xx,yy)),newstar,
optionst);
        case 11
            fixedstart=[];
            for pc=1:NumPeaks,
                fixedstart(pc)=min(xx)+pc.*(max(xx)-
min(xx))./(NumPeaks+1);
            end

TrialParameters=fminsearch(@(lambda)(FitFWGaussian(lambda,xx,yy)),fixed
start,options);
        case 12
            fixedstart=[];
            for pc=1:NumPeaks,
                fixedstart(pc)=min(xx)+pc.*(max(xx)-
min(xx))./(NumPeaks+1);
            end

TrialParameters=fminsearch(@(lambda)(FitFWLorentzian(lambda,xx,yy)),fix
edstart,options);
        case 13

TrialParameters=fminsearch(@(lambda)(fitGL(lambda,xx,yy,extra)),newstar
t,options);
```

```
        case 14

TrialParameters=fminsearch(@(lambda)(fitBiGaussian(lambda,xx,yy,extra))
,newstart,options);
        case 15

TrialParameters=fminsearch(@(lambda)(fitBiLorentzian(lambda,xx,yy,extra
)),newstart,options);
        case 16
            fixedstart=[];
            for pc=1:NumPeaks,
                fixedstart(pc)=(max(xx)-min(xx))./(NumPeaks+1);
            end

TrialParameters=fminsearch(@(lambda)(FitFPGaussian(lambda,xx,yy)),fixed
start,options);
        case 17
            fixedstart=[];
            for pc=1:NumPeaks,
                fixedstart(pc)=(max(xx)-min(xx))./(NumPeaks+1);
            end

TrialParameters=fminsearch(@(lambda)(FitFPLorentzian(lambda,xx,yy)),fix
edstart,options);
        case 18
            zxx=[zeros(size(xx)) xx zeros(size(xx)) ];
            zyy=[zeros(size(yy)) yy zeros(size(yy)) ];

TrialParameters=fminsearch(@(lambda)(fitlorentzian(lambda,zxx,zyy,-
extra)),newstart,options);
        case 19

TrialParameters=fminsearch(@(lambda)(alphafunction(lambda,xx,yy)),newst
art,options);
        case 20

TrialParameters=fminsearch(@(lambda)(fitvoigt(lambda,xx,yy,extra)),news
tart,options);
        case 21

TrialParameters=fminsearch(@(lambda)(fittriangular(lambda,xx,yy)),newst
art,options);
        case 22

TrialParameters=fminsearch(@(lambda)(fitmultiple(lambda,xx,yy,shapesvec
tor,extra)),newstart,options);
        otherwise
    end % switch peakshape


for peaks=1:NumPeaks,
     peakindex=2*peaks-1;
     newstart(peakindex)=start(peakindex)-xoffset;
end
```

```
    % Construct model from Trial parameters
    A=zeros(NumPeaks,n);
    for m=1:NumPeaks,
        switch peakshape(1)
            case 1
                A(m,:)=gaussian(xx,TrialParameters(2*m-
1),TrialParameters(2*m));
            case 2
                A(m,:)=lorentzian(xx,TrialParameters(2*m-
1),TrialParameters(2*m));
            case 3
                A(m,:)=logistic(xx,TrialParameters(2*m-
1),TrialParameters(2*m));
            case 4
                A(m,:)=pearson(xx,TrialParameters(2*m-
1),TrialParameters(2*m),extra);
            case 5
                A(m,:)=expgaussian(xx,TrialParameters(2*m-
1),TrialParameters(2*m),-extra)';
            case 6

A(m,:)=gaussian(xx,TrialParameters(m),TrialParameters(NumPeaks+1));
            case 7

A(m,:)=lorentzian(xx,TrialParameters(m),TrialParameters(NumPeaks+1));
            case 8

A(m,:)=expgaussian(xx,TrialParameters(m),TrialParameters(NumPeaks+1),-
extra)';
            case 9
                A(m,:)=exppulse(xx,TrialParameters(2*m-
1),TrialParameters(2*m));
            case 10
                A(m,:)=sigmoid(xx,TrialParameters(2*m-
1),TrialParameters(2*m));
            case 11
                A(m,:)=gaussian(xx,TrialParameters(m),FIXEDPARAMETERS);
            case 12

A(m,:)=lorentzian(xx,TrialParameters(m),FIXEDPARAMETERS);
            case 13
                A(m,:)=GL(xx,TrialParameters(2*m-
1),TrialParameters(2*m),extra);
            case 14
                A(m,:)=BiGaussian(xx,TrialParameters(2*m-
1),TrialParameters(2*m),extra);
            case 15
                A(m,:)=BiLorentzian(xx,TrialParameters(2*m-
1),TrialParameters(2*m),extra);
            case 16

A(m,:)=gaussian(xx,FIXEDPOSITIONS(m),TrialParameters(m));
            case 17

A(m,:)=lorentzian(xx,FIXEDPOSITIONS(m),TrialParameters(m));
```

```
            case 18
                A(m,:)=explorentzian(xx,TrialParameters(2*m-
1),TrialParameters(2*m),-extra)';
            case 19
                A(m,:)=alphafunction(xx,TrialParameters(2*m-
1),TrialParameters(2*m));
            case 20
                A(m,:)=voigt(xx,TrialParameters(2*m-
1),TrialParameters(2*m),extra);
            case 21
                A(m,:)=triangular(xx,TrialParameters(2*m-
1),TrialParameters(2*m));
            case 22

A(m,:)=peakfunction(shapesvector(m),xx,TrialParameters(2*m-
1),TrialParameters(2*m),extra(m));
        end % switch
        %     for parameter=1:2:2*NumPeaks,
        %         newstart(parameter)=newstart(parameter)*(1+(rand-
.5)/50);
        %         newstart(parameter+1)=newstart(parameter+1)*(1+(rand-
.5)/10);
        %     end
    end % for

    % Multiplies each row by the corresponding amplitude and adds them
up
    if AUTOZERO==3,
        baseline=PEAKHEIGHTS(1);
        Heights=PEAKHEIGHTS(2:1+NumPeaks);
        model=Heights'*A+baseline;
    else
        model=PEAKHEIGHTS'*A;
        Heights=PEAKHEIGHTS;
        baseline=0;
    end

    % Compare trial model to data segment and compute the fit error
    MeanFitError=100*norm(yy-model)./(sqrt(n)*max(yy));
    % Take only the single fit that has the lowest MeanFitError
    if MeanFitError<LowestError,
        if min(Heights)>=-BIPOLAR*10^100,  % Consider only fits with
positive peak heights
            LowestError=MeanFitError;  % Assign LowestError to the
lowest MeanFitError
            FitParameters=TrialParameters;  % Assign FitParameters to
the fit with the lowest MeanFitError
            height=Heights; % Assign height to the PEAKHEIGHTS with the
lowest MeanFitError
        end % if min(PEAKHEIGHTS)>0
    end % if MeanFitError<LowestError
end % for k (NumTrials)

for m=1:NumPeaks,
    area(m)=trapz(xx+xoffset,height(m)*A(m,:)); % Compute the area of
each component peak using trapezoidal method
end

for m=1:NumPeaks,
    if m==1,
        if peakshape(1)==6||peakshape(1)==7||peakshape(1)==8, % equal-
width peak models
            FitResults=[[round(m) FitParameters(m)+xoffset height(m)
abs(FitParameters(NumPeaks+1)) area(m)]];
        else
            if peakshape(1)==11||peakshape(1)==12,  % Fixed-width
shapes only
                FitResults=[[round(m) FitParameters(m)+xoffset
height(m) FIXEDPARAMETERS area(m)]];
            else
                FitResults=[[round(m) FitParameters(2*m-1)+xoffset
height(m) abs(FitParameters(2*m)) area(m)]];
            end
        end % if peakshape
    else
        if peakshape(1)==6||peakshape(1)==7||peakshape(1)==8, % equal-
width peak models
            FitResults=[FitResults ; [round(m) FitParameters(m)+xoffset
height(m) abs(FitParameters(NumPeaks+1)) area(m)]];
        else
            if peakshape(1)==11||peakshape(1)==12, % Fixed-width shapes
only
                FitResults=[FitResults ; [round(m)
FitParameters(m)+xoffset height(m) FIXEDPARAMETERS area(m)]];
            else
                FitResults=[FitResults ; [round(m) FitParameters(2*m-
1)+xoffset height(m) abs(FitParameters(2*m)) area(m)]];
            end
        end % if peakshape
    end % m==1
end % for m=1:NumPeaks
% ---------------------------------------------------------------------
-
function start=calcstart(xx,NumPeaks,xoffset)
  n=max(xx)-min(xx);
  start=[];
  startpos=[n/(NumPeaks+1):n/(NumPeaks+1):n-(n/(NumPeaks+1))]+min(xx);
  for marker=1:NumPeaks,
      markx=startpos(marker)+ xoffset;
      start=[start markx n/ (3.*NumPeaks)];
  end % for marker
% ---------------------------------------------------------------------
-
function [index,closestval]=val2ind(x,val)
% Returns the index and the value of the element of vector x that is
closest to val
% If more than one element is equally close, returns vectors of
indicies and values
% Tom O'Haver (toh@umd.edu) October 2006
% Examples: If x=[1 2 4 3 5 9 6 4 5 3 1], then val2ind(x,6)=7 and
val2ind(x,5.1)=[5 9]
% [indices values]=val2ind(x,3.3) returns indices = [4 10] and values =
[3 3]
dif=abs(x-val);
index=find((dif-min(dif))==0);
closestval=x(index);
% ---------------------------------------------------------------------
-
function err = fitgaussian(lambda,t,y)
% Fitting function for a Gaussian band signal.
global PEAKHEIGHTS AUTOZERO BIPOLAR
numpeaks=round(length(lambda)/2);
A = zeros(length(t),numpeaks);
for j = 1:numpeaks,
    A(:,j) = gaussian(t,lambda(2*j-1),lambda(2*j))';
end
if AUTOZERO==3,A=[ones(size(y))' A];end
if BIPOLAR,PEAKHEIGHTS=A\y';else PEAKHEIGHTS=abs(A\y');end
z = A*PEAKHEIGHTS;
err = norm(z-y');
% ---------------------------------------------------------------------
-
function err = fitewgaussian(lambda,t,y)
% Fitting function for a Gaussian band signal with equal peak widths.
global PEAKHEIGHTS AUTOZERO BIPOLAR
numpeaks=round(length(lambda)-1);
A = zeros(length(t),numpeaks);
for j = 1:numpeaks,
    A(:,j) = gaussian(t,lambda(j),lambda(numpeaks+1))';
end
if AUTOZERO==3,A=[ones(size(y))' A];end
if BIPOLAR,PEAKHEIGHTS=A\y';else PEAKHEIGHTS=abs(A\y');end
z = A*PEAKHEIGHTS;
err = norm(z-y');
% ---------------------------------------------------------------------
-
function err = FitFWGaussian(lambda,t,y)
%   Fitting function for a fixed width Gaussian
global PEAKHEIGHTS AUTOZERO FIXEDPARAMETERS BIPOLAR
numpeaks=round(length(lambda));
A = zeros(length(t),numpeaks);
for j = 1:numpeaks,
    A(:,j) = gaussian(t,lambda(j),FIXEDPARAMETERS)';
end
if AUTOZERO==3,A=[ones(size(y))' A];end
if BIPOLAR,PEAKHEIGHTS=A\y';else PEAKHEIGHTS=abs(A\y');end
z = A*PEAKHEIGHTS;
err = norm(z-y');
% ---------------------------------------------------------------------
-
function err = FitFPGaussian(lambda,t,y)
%   Fitting function for fixed-position Gaussians
global PEAKHEIGHTS AUTOZERO FIXEDPARAMETERS BIPOLAR
numpeaks=round(length(lambda));
```

```
A = zeros(length(t),numpeaks);
for j = 1:numpeaks,
    A(:,j) = gaussian(t,FIXEDPARAMETERS(j), lambda(j))';
end
if AUTOZERO==3,A=[ones(size(y))' A];end
if BIPOLAR,PEAKHEIGHTS=A\y';else PEAKHEIGHTS=abs(A\y');end
z = A*PEAKHEIGHTS;
err = norm(z-y');
% ----------------------------------------------------------------------
-
function err = FitFPLorentzian(lambda,t,y)
%   Fitting function for fixed-position Lorentzians
global PEAKHEIGHTS AUTOZERO FIXEDPARAMETERS BIPOLAR
numpeaks=round(length(lambda));
A = zeros(length(t),numpeaks);
for j = 1:numpeaks,
    A(:,j) = lorentzian(t,FIXEDPARAMETERS(j), lambda(j))';
end
if AUTOZERO==3,A=[ones(size(y))' A];end
if BIPOLAR,PEAKHEIGHTS=A\y';else PEAKHEIGHTS=abs(A\y');end
z = A*PEAKHEIGHTS;
err = norm(z-y');
% ----------------------------------------------------------------------
-
function err = FitFWLorentzian(lambda,t,y)
%   Fitting function for fixed width Lorentzian
global PEAKHEIGHTS AUTOZERO FIXEDPARAMETERS BIPOLAR
numpeaks=round(length(lambda));
A = zeros(length(t),numpeaks);
for j = 1:numpeaks,
    A(:,j) = lorentzian(t,lambda(j),FIXEDPARAMETERS)';
end
if AUTOZERO==3,A=[ones(size(y))' A];end
if BIPOLAR,PEAKHEIGHTS=A\y';else PEAKHEIGHTS=abs(A\y');end
z = A*PEAKHEIGHTS;
err = norm(z-y');
% ----------------------------------------------------------------------
-
function err = fitewlorentzian(lambda,t,y)
% Fitting function for a Lorentzian band signal with equal peak widths.
global PEAKHEIGHTS AUTOZERO BIPOLAR
numpeaks=round(length(lambda)-1);
A = zeros(length(t),numpeaks);
for j = 1:numpeaks,
    A(:,j) = lorentzian(t,lambda(j),lambda(numpeaks+1))';
end
if AUTOZERO==3,A=[ones(size(y))' A];end
if BIPOLAR,PEAKHEIGHTS=A\y';else PEAKHEIGHTS=abs(A\y');end
z = A*PEAKHEIGHTS;
err = norm(z-y');
% ----------------------------------------------------------------------
-
function g = gaussian(x,pos,wid)
%  gaussian(X,pos,wid) = gaussian peak centered on pos, half-width=wid
%  X may be scalar, vector, or matrix, pos and wid both scalar
% Examples: gaussian([0 1 2],1,2) gives result [0.5000    1.0000
0.5000]
% plot(gaussian([1:100],50,20)) displays gaussian band centered at 50
with width 20.
g = exp(-((x-pos)./(0.6005615.*wid)).^2);
% -----------------------------------------------------------------------
-
function err = fitlorentzian(lambda,t,y)
%   Fitting function for single lorentzian, lambda(1)=position,
lambda(2)=width
%   Fitgauss assumes a lorentzian function
global PEAKHEIGHTS AUTOZERO BIPOLAR
A = zeros(length(t),round(length(lambda)/2));
for j = 1:length(lambda)/2,
    A(:,j) = lorentzian(t,lambda(2*j-1),lambda(2*j))';
end
if AUTOZERO==3,A=[ones(size(y))' A];end
if BIPOLAR,PEAKHEIGHTS=A\y';else PEAKHEIGHTS=abs(A\y');end
z = A*PEAKHEIGHTS;
err = norm(z-y');
% -----------------------------------------------------------------------
-
function g = lorentzian(x,position,width)
% lorentzian(x,position,width) Lorentzian function.
% where x may be scalar, vector, or matrix
% position and width scalar
% T. C. O'Haver, 1988
% Example: lorentzian([1 2 3],2,2) gives result [0.5 1 0.5]
g=ones(size(x))./(1+((x-position)./(0.5.*width)).^2);
% -----------------------------------------------------------------------
-
function err = fitlogistic(lambda,t,y)
%   Fitting function for logistic, lambda(1)=position, lambda(2)=width
%   between the data and the values computed by the current
%   function of lambda.  Fitlogistic assumes a logistic function
%  T. C. O'Haver, May 2006
global PEAKHEIGHTS AUTOZERO BIPOLAR
A = zeros(length(t),round(length(lambda)/2));
for j = 1:length(lambda)/2,
    A(:,j) = logistic(t,lambda(2*j-1),lambda(2*j))';
end
if AUTOZERO==3,A=[ones(size(y))' A];end
if BIPOLAR,PEAKHEIGHTS=A\y';else PEAKHEIGHTS=abs(A\y');end
z = A*PEAKHEIGHTS;
err = norm(z-y');
% -----------------------------------------------------------------------
-
function g = logistic(x,pos,wid)
% logistic function.  pos=position; wid=half-width (both scalar)
% logistic(x,pos,wid), where x may be scalar, vector, or matrix
% pos=position; wid=half-width (both scalar)
% T. C. O'Haver, 1991
n = exp(-((x-pos)/(.477.*wid)) .^2);
g = (2.*n)./(1+n);
```

```
% ----------------------------------------------------------------------
-
function err = fittriangular(lambda,t,y)
%   Fitting function for triangular, lambda(1)=position,
lambda(2)=width
%   between the data and the values computed by the current
%   function of lambda.  Fittriangular assumes a triangular function
%  T. C. O'Haver, May 2006
global PEAKHEIGHTS AUTOZERO BIPOLAR
A = zeros(length(t),round(length(lambda)/2));
for j = 1:length(lambda)/2,
    A(:,j) = triangular(t,lambda(2*j-1),lambda(2*j))';
end
if AUTOZERO==3,A=[ones(size(y))' A];end
if BIPOLAR,PEAKHEIGHTS=A\y';else PEAKHEIGHTS=abs(A\y');end
z = A*PEAKHEIGHTS;
err = norm(z-y');
% ----------------------------------------------------------------------
-
function g = triangular(x,pos,wid)
%triangle function.  pos=position; wid=half-width (both scalar)
%triangle(x,pos,wid), where x may be scalar or vector,
%pos=position; wid=half-width (both scalar)
% T. C. O'Haver, 1991
% Example
% x=[0:.1:10];plot(x,triangle(x,5.5,2.3),'.')
g=1-(1./wid) .*abs(x-pos);
for i=1:length(x),
if g(i)<0,g(i)=0;end
end
% ----------------------------------------------------------------------
-
function err = fitpearson(lambda,t,y,shapeconstant)
%   Fitting functions for a Pearson 7 band signal.
% T. C. O'Haver (toh@umd.edu),   Version 1.3, October 23, 2006.
global PEAKHEIGHTS AUTOZERO BIPOLAR
A = zeros(length(t),round(length(lambda)/2));
for j = 1:length(lambda)/2,
    A(:,j) = pearson(t,lambda(2*j-1),lambda(2*j),shapeconstant)';
end
if AUTOZERO==3,A=[ones(size(y))' A];end
if BIPOLAR,PEAKHEIGHTS=A\y';else PEAKHEIGHTS=abs(A\y');end
z = A*PEAKHEIGHTS;
err = norm(z-y');
% ----------------------------------------------------------------------
-
function g = pearson(x,pos,wid,m)
% Pearson VII function.
% g = pearson7(x,pos,wid,m) where x may be scalar, vector, or matrix
% pos=position; wid=half-width (both scalar)
% m=some number
%  T. C. O'Haver, 1990
g=ones(size(x))./(1+((x-pos)./((0.5.^(2/m)).*wid)).^2).^m;
% ----------------------------------------------------------------------
-
```

```
function err = fitexpgaussian(lambda,t,y,timeconstant)
%   Fitting functions for a exponentially-broadened Gaussian band
signal.
%  T. C. O'Haver, October 23, 2006.
global PEAKHEIGHTS AUTOZERO BIPOLAR
A = zeros(length(t),round(length(lambda)/2));
for j = 1:length(lambda)/2,
    A(:,j) = expgaussian(t,lambda(2*j-1),lambda(2*j),timeconstant);
end
if AUTOZERO==3,A=[ones(size(y))' A];end
if BIPOLAR,PEAKHEIGHTS=A\y';else PEAKHEIGHTS=abs(A\y');end
z = A*PEAKHEIGHTS;
err = norm(z-y');
% ---------------------------------------------------------------------
-
function err = fitexplorentzian(lambda,t,y,timeconstant)
%   Fitting functions for a exponentially-broadened lorentzian band
signal.
%  T. C. O'Haver, 2013.
global PEAKHEIGHTS AUTOZERO BIPOLAR
A = zeros(length(t),round(length(lambda)/2));
for j = 1:length(lambda)/2,
    A(:,j) = explorentzian(t,lambda(2*j-1),lambda(2*j),timeconstant);
end
if AUTOZERO==3,A=[ones(size(y))' A];end
if BIPOLAR,PEAKHEIGHTS=A\y';else PEAKHEIGHTS=abs(A\y');end
z = A*PEAKHEIGHTS;
err = norm(z-y');
% ---------------------------------------------------------------------
-
function err = fitexpewgaussian(lambda,t,y,timeconstant)
% Fitting function for exponentially-broadened Gaussian bands with
equal peak widths.
global PEAKHEIGHTS AUTOZERO BIPOLAR
numpeaks=round(length(lambda)-1);
A = zeros(length(t),numpeaks);
for j = 1:numpeaks,
    A(:,j) = expgaussian(t,lambda(j),lambda(numpeaks+1),timeconstant);
end
if AUTOZERO==3,A=[ones(size(y))' A];end
if BIPOLAR,PEAKHEIGHTS=A\y';else PEAKHEIGHTS=abs(A\y');end
z = A*PEAKHEIGHTS;
err = norm(z-y');
% ---------------------------------------------------------------------
-
function g = expgaussian(x,pos,wid,timeconstant)
%  Exponentially-broadened gaussian(x,pos,wid) = gaussian peak centered
on pos, half-width=wid
%  x may be scalar, vector, or matrix, pos and wid both scalar
%  T. C. O'Haver, 2006
g = exp(-((x-pos)./(0.6005615.*wid)) .^2);
g = ExpBroaden(g',timeconstant);
% ---------------------------------------------------------------------
-
function g = explorentzian(x,pos,wid,timeconstant)
```

```
%  Exponentially-broadened lorentzian(x,pos,wid) = lorentzian peak
centered on pos, half-width=wid
%  x may be scalar, vector, or matrix, pos and wid both scalar
%  T. C. O'Haver, 2013
g = ones(size(x))./(1+((x-pos)./(0.5.*wid)).^2);
g = ExpBroaden(g',timeconstant);
% ---------------------------------------------------------------------
-
function yb = ExpBroaden(y,t)
% ExpBroaden(y,t) zero pads y and convolutes result by an exponential
decay
% of time constant t by multiplying Fourier transforms and inverse
% transforming the result.
hly=round(length(y)./2);
ey=[y(1).*ones(1,hly)';y;y(length(y)).*ones(1,hly)'];
% figure(2);plot(ey);figure(1);
fy=fft(ey);
a=exp(-(1:length(fy))./t);
fa=fft(a);
fy1=fy.*fa';
ybz=real(ifft(fy1))./sum(a);
yb=ybz(hly+2:length(ybz)-hly+1);
% ---------------------------------------------------------------------
-
function err = fitexppulse(tau,x,y)
% Iterative fit of the sum of exponential pulses
% of the form Height.*exp(-tau1.*x).*(1-exp(-tau2.*x)))
global PEAKHEIGHTS AUTOZERO BIPOLAR
A = zeros(length(x),round(length(tau)/2));
for j = 1:length(tau)/2,
    A(:,j) = exppulse(x,tau(2*j-1),tau(2*j));
end
if AUTOZERO==3,A=[ones(size(y))' A];end
if BIPOLAR,PEAKHEIGHTS=A\y';else PEAKHEIGHTS=abs(A\y');end
z = A*PEAKHEIGHTS;
err = norm(z-y');
% ---------------------------------------------------------------------
-
function g = exppulse(x,t1,t2)
% Exponential pulse of the form
% g = (x-spoint)./pos.*exp(1-(x-spoint)./pos);
e=(x-t1)./t2;
p = 4*exp(-e).*(1-exp(-e));
p=p .* (p>0);
g = p';
% ---------------------------------------------------------------------
-
function err = fitalphafunction(tau,x,y)
% Iterative fit of the sum of alpha funciton
% of the form Height.*exp(-tau1.*x).*(1-exp(-tau2.*x)))
global PEAKHEIGHTS AUTOZERO BIPOLAR
A = zeros(length(x),round(length(tau)/2));
for j = 1:length(tau)/2,
    A(:,j) = alphafunction(x,tau(2*j-1),tau(2*j));
end
```

```
if AUTOZERO==3,A=[ones(size(y))' A];end
if BIPOLAR,PEAKHEIGHTS=A\y';else PEAKHEIGHTS=abs(A\y');end
z = A*PEAKHEIGHTS;
err = norm(z-y');
% ---------------------------------------------------------------------
-
function g = alphafunction(x,pos,spoint)
% alpha function.  pos=position; wid=half-width (both scalar)
% alphafunction(x,pos,wid), where x may be scalar, vector, or matrix
% pos=position; wid=half-width (both scalar)
% Taekyung Kwon, July 2013
g = (x-spoint)./pos.*exp(1-(x-spoint)./pos);
for m=1:length(x);if g(m)<0;g(m)=0;end;end
% ---------------------------------------------------------------------
-
function err = fitsigmoid(tau,x,y)
% Fitting function for iterative fit to the sum of
% sigmiods of the form Height./(1 + exp((t1 - t)/t2))
global PEAKHEIGHTS AUTOZERO BIPOLAR
A = zeros(length(x),round(length(tau)/2));
for j = 1:length(tau)/2,
    A(:,j) = sigmoid(x,tau(2*j-1),tau(2*j));
end
if AUTOZERO==3,A=[ones(size(y))' A];end
if BIPOLAR,PEAKHEIGHTS=A\y';else PEAKHEIGHTS=abs(A\y');end
z = A*PEAKHEIGHTS;
err = norm(z-y');
% ---------------------------------------------------------------------
-
function g=sigmoid(x,t1,t2)
% g=1./(1 + exp((t1 - x)./t2))'; % old version of sigmoid
g=1/2 + 1/2* erf(real((x-t1)/sqrt(2*t2))); % Modified sigmoid
% Bifurcated sigmoid
% lx=length(x);
% hx=val2ind(x,t1);
% g(1:hx)=1./(1 + exp((t1 - x(1:hx))./t2));
% g(hx+1:lx)=1./(1 + exp((t1 - x(hx+1:lx))./(1.3*t2)));
% ---------------------------------------------------------------------
-
function err = fitGL(lambda,t,y,shapeconstant)
%   Fitting functions for Gaussian/Lorentzian blend.
% T. C. O'Haver (toh@umd.edu), 2012.
global PEAKHEIGHTS AUTOZERO BIPOLAR
A = zeros(length(t),round(length(lambda)/2));
for j = 1:length(lambda)/2,
    A(:,j) = GL(t,lambda(2*j-1),lambda(2*j),shapeconstant)';
end
if AUTOZERO==3,A=[ones(size(y))' A];end
if BIPOLAR,PEAKHEIGHTS=A\y';else PEAKHEIGHTS=abs(A\y');end
z = A*PEAKHEIGHTS;
err = norm(z-y');
% ---------------------------------------------------------------------
-
function g = GL(x,pos,wid,m)
% Gaussian/Lorentzian blend. m = percent Gaussian character
% pos=position; wid=half-width
% m = percent Gaussian character.
%  T. C. O'Haver, 2012
% sizex=size(x)
% sizepos=size(pos)
% sizewid=size(wid)
% sizem=size(m)
g=2.*((m/100).*gaussian(x,pos,wid)+(1-
(m(1)/100)).*lorentzian(x,pos,wid))/2;
% ---------------------------------------------------------------------
-
function err = fitvoigt(lambda,t,y,shapeconstant)
% Fitting functions for Voigt profile function
% T. C. O'Haver (toh@umd.edu), 2013.
global PEAKHEIGHTS AUTOZERO BIPOLAR
A = zeros(length(t),round(length(lambda)/2));
for j = 1:length(lambda)/2,
    A(:,j) = voigt(t,lambda(2*j-1),lambda(2*j),shapeconstant)';
end
if AUTOZERO==3,A=[ones(size(y))' A];end
if BIPOLAR,PEAKHEIGHTS=A\y';else PEAKHEIGHTS=abs(A\y');end
z = A*PEAKHEIGHTS;
err = norm(z-y');
% ---------------------------------------------------------------------
-
function g=voigt(xx,pos,gD,alpha)
% Voigt profile function. xx is the independent variable (energy,
% wavelength, etc), gD is the Doppler (Gaussian) width, and alpha is
the
% shape constant (ratio of the Lorentzian width gL to the Doppler width
gD.
% Based on Chong Tao's "Voigt lineshape spectrum simulation",
% File ID: #26707
% alpha=alpha
gL=alpha.*gD;
gV = 0.5346*gL + sqrt(0.2166*gL.^2 + gD.^2);
x = gL/gV;
y = abs(xx-pos)/gV;
g = 1/(2*gV*(1.065 + 0.447*x + 0.058*x^2))*((1-x)*exp(-0.693.*y.^2) +
(x./(1+y.^2)) + 0.016*(1-x)*x*(exp(-0.0841.*y.^2.25)-1./(1 +
0.021.*y.^2.25)));
g=g./max(g);
% ---------------------------------------------------------------------
-
function err = fitBiGaussian(lambda,t,y,shapeconstant)
%   Fitting functions for BiGaussian.
% T. C. O'Haver (toh@umd.edu),  2012.
global PEAKHEIGHTS AUTOZERO BIPOLAR
A = zeros(length(t),round(length(lambda)/2));
for j = 1:length(lambda)/2,
    A(:,j) = BiGaussian(t,lambda(2*j-1),lambda(2*j),shapeconstant)';
end
if AUTOZERO==3,A=[ones(size(y))' A];end
if BIPOLAR,PEAKHEIGHTS=A\y';else PEAKHEIGHTS=abs(A\y');end
z = A*PEAKHEIGHTS;
```

```
err = norm(z-y');
% ---------------------------------------------------------------------
-
function g = BiGaussian(x,pos,wid,m)
% BiGaussian (different widths on leading edge and trailing edge).
% pos=position; wid=width
% m determines shape; symmetrical if m=50.
%  T. C. O'Haver, 2012
lx=length(x);
hx=val2ind(x,pos);
g(1:hx)=gaussian(x(1:hx),pos,wid*(m/100));
g(hx+1:lx)=gaussian(x(hx+1:lx),pos,wid*(1-m/100));
% ---------------------------------------------------------------------
-
function err = fitBiLorentzian(lambda,t,y,shapeconstant)
%   Fitting functions for BiGaussian.
% T. C. O'Haver (toh@umd.edu),  2012.
global PEAKHEIGHTS AUTOZERO BIPOLAR
A = zeros(length(t),round(length(lambda)/2));
for j = 1:length(lambda)/2,
    A(:,j) = BiLorentzian(t,lambda(2*j-1),lambda(2*j),shapeconstant)';
end
if AUTOZERO==3,A=[ones(size(y))' A];end
if BIPOLAR,PEAKHEIGHTS=A\y';else PEAKHEIGHTS=abs(A\y');end
z = A*PEAKHEIGHTS;
err = norm(z-y');
% ---------------------------------------------------------------------
-
function g = BiLorentzian(x,pos,wid,m)
% BiLorentzian (different widths on leading edge and trailing edge).
% pos=position; wid=width
% m determines shape; symmetrical if m=50.
%  T. C. O'Haver, 2012
lx=length(x);
hx=val2ind(x,pos);
g(1:hx)=lorentzian(x(1:hx),pos,wid*(m/100));
g(hx+1:lx)=lorentzian(x(hx+1:lx),pos,wid*(1-m/100));
% ---------------------------------------------------------------------
-
function b=iqr(a)
% b = IQR(a)  returns the interquartile range of the values in a.  For
%  vector input, b is the difference between the 75th and 25th
percentiles
%  of a.  For matrix input, b is a row vector containing the
interquartile
%  range of each column of a.
%  T. C. O'Haver, 2012
mina=min(a);
sizea=size(a);
NumCols=sizea(2);
for n=1:NumCols,b(:,n)=a(:,n)-mina(n);end
Sorteda=sort(b);
lx=length(Sorteda);
SecondQuartile=round(lx/4);
FourthQuartile=3*round(lx/4);
```

```
b=abs(Sorteda(FourthQuartile,:)-Sorteda(SecondQuartile,:));
% ----------------------------------------------------------------------
-
function err = fitmultiple(lambda,t,y,shapesvector,m)
% Fitting function for a multiple-shape band signal.
% The sequence of peak shapes are defined by the vector "shape".
% The vector "m" determines the shape of variable-shape peaks.
global PEAKHEIGHTS AUTOZERO BIPOLAR
numpeaks=round(length(lambda)/2);
A = zeros(length(t),numpeaks);
for j = 1:numpeaks,
    A(:,j) = peakfunction(shapesvector(j),t,lambda(2*j-
1),lambda(2*j),m(j))';
end
if AUTOZERO==3,A=[ones(size(y))' A];end
if BIPOLAR,PEAKHEIGHTS=A\y';else PEAKHEIGHTS=abs(A\y');end
z = A*PEAKHEIGHTS;
err = norm(z-y');
% ----------------------------------------------------------------------
-
function p=peakfunction(shape,x,pos,wid,m)
switch shape,
    case 1
        p=gaussian(x,pos,wid);
    case 2
        p=lorentzian(x,pos,wid);
    case 3
        p=logistic(x,pos,wid);
    case 4
        p=pearson(x,pos,wid,m);
    case 5
        p=expgaussian(x,pos,wid,m)';
    case 6
        p=gaussian(x,pos,wid);
    case 7
        p=lorentzian(x,pos,wid);
    case 8
        p=expgaussian(x,pos,wid,m)';
    case 9
        p=exppulse(x,pos,wid);
    case 10
        p=sigmoid(x,pos,wid);
    case 11
        p=gaussian(x,pos,wid);
    case 12
        p=lorentzian(x,pos,wid);
    case 13
        p=GL(x,pos,wid,m);
    case 14
        p=BiGaussian(x,pos,wid,m);
    case 15
        p=BiLorentzian(x,pos,wid,m);
    case 16
        p=gaussian(x,pos,wid);
    case 17
```

```
        p=lorentzian(x,pos,wid);
    case 18
        p=explorentzian(x,pos,wid,m)';
    case 19
        p=alphafunction(x,pos,wid);
    case 20
        p=voigt(x,pos,wid,m);
    case 21
        p=triangular(x,pos,wid);
    otherwise
end % switch
```

Appendix B - Data

B.1 Voigt Fitting Results

Data Run	Peak Shape	Position	Height	FWHM	Area	Error	Acquisition Time	Corrected Counting Rate	Baseline Counting Rate
		Channel	[counts]	#of Channels	[counts]	%	Hours	counts/s	counts/s
19	Voigt	503	432.45	7.1464	9876.6	1.2282	23.98	0.1144	64.3528
20	Voigt	505	49.104	7.1397	1120	3.9207	1.92	0.1625	65.6858
21	Voigt	505	463.74	7.0052	10380	1.2141	24.23	0.1196	69.7729
23	Voigt	505	431.37	6.621	9167.1	1.2274	24.00	0.1075	62.7447
24	Voigt	503	458.48	6.7393	9884.1	1.214	24.45	0.1140	64.3948
25A	Voigt	506	292.15	8.8164	8242.8	1.5978	15.13	0.1540	66.0402
25B	Voigt	506	306.26	8.5416	8373.8	1.5876	17.97	0.1318	57.4869
25C	Voigt	505	823.62	8.0428	13445	1.2268	28.20	0.1349	60.8434
25D	Voigt	504	794.81	7.3456	18680	1.0028	40.63	0.1301	63.3667
25E	Voigt	505	916.42	7.4891	21935	0.90651	48.00	0.1294	64.7769
26A	Voigt	503	462.88	6.96	10297	1.2039	24.00	0.1219	67.5719
26B	Voigt	503	561.56	7.0275	12608	1.0921	28.20	0.1271	67.6066
26C	Voigt	503	650.75	7.105	14788	0.99285	40.63	0.1035	54.1916
27A	Voigt	504	519.88	7.873	13116	1.2598	27.00	0.1388	57.8341
27B	Voigt	504	914.47	7.963	23316	0.97692	48.00	0.1389	57.7644
28A	Voigt	502	415.88	7.8286	10450	1.369	24.00	0.1250	60.1788
28B	Voigt	503	846.46	7.603	20552	0.93126	48.00	0.1231	60.2617
29A	Voigt	504	517.25	6.6798	11120	1.2346	26.35	0.1218	61.6498
29B	Voigt	504	1797	7.0597	40791	0.64934	96.32	0.1227	61.1697
30A	Voigt	504	420.11	9.5035	12751	1.3038	26.35	0.1411	60.2988
30B	Voigt	504	1672.5	7.7995	41739	0.69631	96.00	0.1273	59.9423

31A	Voigt	503	810.14	7.7978	20184	1.0284	48.08	0.1238	55.2106
31B	Voigt	504	2297.4	7.4786	54957	0.59453	136.08	0.1197	54.7913
32	Voigt	523	2742.7	6.7363	59296	0.5636	182.47	0.0980	49.6278
33	Voigt	523	2828.5	6.9767	63336	0.53576	182.53	0.1068	52.5943
34	Voigt	523	3239.5	6.6635	69480	0.49264	217.42	0.1014	52.7001
35	Voigt	523	2243.7	6.9366	49768	0.64051	167.53	0.0962	45.2429
36	Voigt	522	2036.8	6.7615	44010	0.69932	165.52	0.0876	42.3495
37	Voigt	522	2246.5	6.9039	49551	0.60025	167.17	0.0994	51.2964
38	Voigt	523	1168.4	6.3551	23844	0.92096	91.08	0.0890	42.9836
39	Voigt	508	1550.1	3.6104	17922	0.81536	164.17	0.0377	31.4784
40A	Voigt	508	647.48	3.8257	7937.9	1.0675	122.17	0.0242	20.4819
40B	Voigt	509	1307.6	3.7372	15776	0.796	239.58	0.0247	19.8717
40C	Voigt	509	1571.5	3.816	19440	0.73465	293.33	0.0249	19.6138
40D	Voigt	509	2163.6	3.8406	26920	0.64376	410.83	0.0248	18.7794
40E	Voigt	509	2241.8	3.8398	27934	0.63683	433.58	0.0244	18.5651
40F	Voigt	509	2638.3	3.8187	32711	0.59823	510.92	0.0243	18.3068
41A	Voigt	509	580.76	3.5276	6642	1.3307	116.58	0.0224	14.7692
41B	Voigt	509	819.32	3.586	9477.4	1.1052	167.50	0.0223	15.1097
41C	Voigt	509	1223	3.3698	13361	0.92571	237.50	0.0222	15.5701
41D	Voigt	509	1432.6	3.3941	15730	0.85239	283.17	0.0220	15.5920
41E	Voigt	509	1660.4	3.5329	18955	0.78441	332.75	0.0226	15.7153
41F	Voigt	509	2280.4	3.6287	26746	0.67888	497.75	0.0215	14.5894
42A	Voigt	509	302.08	3.6969	3590	1.8754	73.93	0.0201	12.4693
42C	Voigt	509	727.04	3.7607	8949	1.4607	172.95	0.0215	13.4099
42D	Voigt	509	959.01	3.874	12173	1.2268	240.38	0.0211	12.6064
42E	Voigt	509	1074.6	3.8151	13393	1.1604	266.75	0.0210	12.3562
42F	Voigt	509	1374.9	3.6986	16611	1.0151	335.80	0.0207	12.3067
42G	Voigt	509	1608.8	3.8125	20037	0.91382	1331.05	0.0067	3.9655
43A	Voigt	509	314.13	3.519	3628.3	1.7108	168.33	0.0103	8.1159
44A	Voigt	508	1016.8	3.3359	10873	0.95713	218.08	0.0243	20.4399
44B	Voigt	508	1629.6	3.6707	19156	0.75078	383.42	0.0245	19.6792

44C	Voigt	508	1899.5	3.7191	22666	0.67164	459.92	0.0243	19.6987
44D	Voigt	508	2318.4	3.679	27375	0.61831	552.92	0.0245	19.6415
44E	Voigt	508	2874.4	3.6188	33489	0.56005	675.75	0.0247	19.5978
44F	Voigt	508	3770.1	3.5969	43662	0.48875	893.25	0.0247	19.5755
44G	Voigt	508	4726.7	3.6643	55892	0.4447	1151.25	0.0248	19.1552
44H	Voigt	508	5338.7	3.6651	63205	0.41616	1319.58	0.0247	18.9945
44I	Voigt	508	7029	3.6574	82884	0.38194	1803.58	0.0243	17.9034
45A	Voigt	508	655.07	3.9297	8241.1	1.176	188.08	0.0258	18.3417
45B	Voigt	508	953.11	3.7329	11436	1.0069	384.92	0.0177	12.7004
45C	Voigt	508	1602.6	3.781	19503	0.78065	547.33	0.0214	15.4783

B.2 Bootstrap Sampling Method Data

Note: Mean – Bootstrap Mean, STD – Standard Deviation

Run	Parameters	Peak Position	FWHM	Area	Counting Rate	Run	Parameters	Peak Position	FWHM	Area	Counting Rate
19	Mean	503.22	7.07	9839	0.1140	40A	Mean	508.44	3.81	7931.32	0.0242
	STD	0.475	0.582	528	0.006121		STD	0.335	0.216	465.130	0.001418
	Variance, s	0.225	0.339	279273	3.75E-05		Variance, s	0.112	0.047	216345.983	2.01E-06
20	Mean	504.763	7.109	1117	0.1620	40B	Mean	508.71	3.71	15679.19	0.0245
	STD	0.925	0.816	87	0.012557		STD	0.210	0.162	629.423	0.000985
	Variance, s	0.855	0.665	7487	1.58E-04		Variance, s	0.044	0.026	396173.726	9.70E-07
21	Mean	504.60	7.01	10412	0.1200	40C	Mean	508.87	3.79	19144.96	0.0245
	STD	0.407	0.404	476	0.086256		STD	0.167	0.121	691.079	0.000886
	Variance, s	0.166	0.163	226225	7.44E-03		Variance, s	0.028	0.015	477589.926	7.84E-07
23	Mean	505.43	6.61	9143	0.1072	40D	Mean	508.83	3.83	26580.49	0.0245

🟩	STD	0.326	0.348	406	0.004764
	Variance, s	0.106	0.121	165171	2.27E-05
🟥 24	Mean	503.43	6.77	9886	0.1140
	STD	0.331	0.370	422	0.004872
	Variance, s	0.110	0.137	178371	2.37E-05
🟩 25A	Mean	505.95	8.79	8178	0.1527
	STD	0.623	0.962	608	0.011350
	Variance, s	0.388	0.925	369310	1.29E-04
🟩 25B	Mean	505.86	8.57	8370	0.1317
	STD	0.644	0.872	603	0.009481
	Variance, s	0.415	0.761	363056	8.99E-05
🟩 25C	Mean	504.77	8.01	13431	0.1347
	STD	0.402	0.497	604	0.006057
	Variance, s	0.162	0.247	364660	3.67E-05
🟩 25D	Mean	504.41	7.36	18677	0.1301
	STD	0.328	0.317	606	0.004223
	Variance, s	0.107	0.100	367523	1.78E-05
🟩 25E	Mean	504.52	7.42	21802	0.1286
	STD	0.286	0.279	625	0.003686
	Variance, s	0.082	0.078	390555	1.36E-05
🟥 26A	Mean	502.85	6.98	10202	0.1208
	STD	0.416	0.364	464	0.005491
	Variance, s	0.173	0.133	214969	3.01E-05
🟥 26B	Mean	503.12	7.04	12576	0.1268
	STD	0.381	0.411	576	0.005809
	Variance, s	0.145	0.169	332025	0.000034
🟥	STD	0.105	0.083	459.547	0.000423
	Variance, s	0.011	0.007	211183.030	1.79E-07
🟥 40E	Mean	508.87	3.83	27618.23	0.0241
	STD	0.104	0.073	518.715	0.000453
	Variance, s	0.011	0.005	269065.001	2.05E-07
🟥 40F	Mean	508.88	3.81	32205.54	0.0240
	STD	0.117	0.073	569.073	0.000424
	Variance, s	0.014	0.005	323844.391	1.79E-07
🟩 41A	Mean	508.81	3.53	6579.41	0.0222
	STD	0.176	0.157	257.709	0.000868
	Variance, s	0.031	0.025	66414.075	7.54E-07
🟩 41B	Mean	508.67	3.61	9521.49	0.0224
	STD	0.140	0.135	337.935	0.000795
	Variance, s	0.020	0.018	114200.293	6.32E-07
🟩 41C	Mean	508.77	3.37	13265.91	0.0221
	STD	0.111	0.103	341.532	0.000569
	Variance, s	0.012	0.011	116643.971	3.23E-07
🟩 41D	Mean	508.74	3.37	15553.14	0.0218
	STD	0.113	0.084	337.704	0.000473
	Variance, s	0.013	0.007	114044.088	2.23E-07
🟩 41E	Mean	508.70	3.54	18892.65	0.0226
	STD	0.110	0.073	416.812	0.000498
	Variance, s	0.012	0.005	173732.444	2.48E-07
🟩 41F	Mean	508.75	3.63	26628.30	0.0214
	STD	0.085	0.092	486.976	0.000392
	Variance, s	0.007	0.008	237145.944	1.54E-07

26C	Mean	503.46	7.11	14804	0.1036	**42A**	Mean	508.57	3.67	3578.51	0.0200
	STD	0.338	0.423	650	0.004552		STD	0.277	0.177	205.298	0.001148
	Variance, s	0.114	0.179	422810	2.07E-05		Variance, s	0.077	0.031	42147.299	1.32E-06
27A	Mean	503.76	7.84	13046	0.1381	**42C**	Mean	509.02	3.76	8754.28	0.0210
	STD	0.283	0.293	391	0.004133		STD	0.169	0.107	260.983	0.000627
	Variance, s	0.080	0.086	152529	1.71E-05		Variance, s	0.028	0.011	68112.236	3.94E-07
27B	Mean	504.19	7.95	23268	0.1387	**42D**	Mean	509.09	3.88	11886.69	0.0206
	STD	0.230	0.269	616	0.003669		STD	0.173	0.133	430.358	0.000747
	Variance, s	0.053	0.072	379052	1.35E-05		Variance, s	0.030	0.018	185208.429	5.58E-07
28A	Mean	502.30	7.82	10391	0.1243	**42E**	Mean	509.01	3.81	13162.84	0.0206
	STD	0.369	0.268	356	0.004263		STD	0.131	0.133	423.351	0.000663
	Variance, s	0.136	0.072	126973	1.82E-05		Variance, s	0.017	0.018	179226.204	4.40E-07
28B	Mean	503.06	7.61	20515	0.1229	**42F**	Mean	508.99	3.69	16335	0.0204
	STD	0.234	0.194	522	0.003126		STD	0.121	0.123	461	0.000576
	Variance, s	0.055	0.037	272380	9.77E-06		Variance, s	0.015	0.015	212632	3.32E-07
29A	Mean	503.95	6.67	11016	0.1207	**42G**	Mean	509.02	3.81	19694	0.0065
	STD	0.328	0.234	365	0.003998		STD	0.122	0.136	523	0.000174
	Variance, s	0.108	0.055	133194	1.60E-05		Variance, s	0.015	0.019	273770	3.02E-08
29B	Mean	504.00	7.10	40692	0.1224	**43A**	Mean	509.06	3.54	3556	0.0101
	STD	0.127	0.150	624	0.001875		STD	0.188	0.251	167	0.000472
	Variance, s	0.016	0.023	388753	3.52E-06		Variance, s	0.035	0.063	27734	2.23E-07
30A	Mean	503.65	9.45	12774	0.1414	**44A**	Mean	508.07	3.32	10864	0.0243
	STD	0.465	0.566	449	0.004966		STD	0.216	0.166	537	0.001199
	Variance, s	0.216	0.320	201389	2.47E-05		Variance, s	0.046	0.028	288273	1.44E-06
30B	Mean	503.62	7.78	41707	0.1272	**44B**	Mean	508.14	3.66	19117	0.0245
	STD	0.214	0.275	990	0.003018		STD	0.129	0.088	421	0.000539

🟥	Variance, s	0.046	0.076	979729	9.11E-06	🟩	Variance, s	0.017	0.008	176986	2.90E-07
🟥 **31A**	Mean	503.39	7.80	20226	0.1241	🟩 **44C**	Mean	507.98	3.73	22710	0.0244
	STD	0.223	0.203	406	0.002491		STD	0.103	0.082	430	0.000462
	Variance, s	0.050	0.041	164881	6.20E-06		Variance, s	0.011	0.007	185312	2.13E-07
🟥 **31B**	Mean	503.53	7.48	55036	0.1198	🟩 **44D**	Mean	507.97	3.67	27327	0.0245
	STD	0.098	0.124	614	0.001338		STD	0.091	0.071	477	0.000428
	Variance, s	0.010	0.015	377302	1.79E-06		Variance, s	0.008	0.005	227705	1.83E-07
🟩 **32**	Mean	522.98	6.73	59106	0.0977	🟩 **44E**	Mean	507.83	3.62	33389	0.0246
	STD	0.132	0.105	843	0.001394		STD	0.075	0.058	481	0.000355
	Variance, s	0.017	0.011	711161	1.94E-06		Variance, s	0.006	0.003	231229	1.26E-07
🟥 **33**	Mean	522.92	7.00	63155	0.1065	🟩 **44F**	Mean	507.85	3.59	43426	0.0245
	STD	0.111	0.131	865	0.001458		STD	0.060	0.044	474	0.000268
	Variance, s	0.012	0.017	747715	2.13E-06		Variance, s	0.004	0.002	224212	7.16E-08
🟥 **34**	Mean	522.79	6.67	69059	0.1008	🟩 **44G**	Mean	507.76	3.66	55584	0.0247
	STD	0.083	0.093	890	0.001299		STD	0.058	0.054	576	0.000256
	Variance, s	0.007	0.009	792436	1.69E-06		Variance, s	0.003	0.003	331636	6.55E-08
🟩 **35**	Mean	523.28	6.94	49763	0.0961	🟩 **44H**	Mean	507.73	3.67	62890	0.0246
	STD	0.121	0.167	830	0.001603		STD	0.049	0.054	623	0.000244
	Variance, s	0.015	0.028	688640	2.57E-06		Variance, s	0.002	0.003	387565	5.93E-08
36	Mean	521.79	6.76	44006	0.0876	🟩 **44I**	Mean	507.79	3.65	82261	0.0242
	STD	0.154	0.165	826	0.001644		STD	0.052	0.051	889	0.000261
	Variance, s	0.024	0.027	682357	2.70E-06		Variance, s	0.003	0.003	789771	6.81E-08
37	Mean	521.89	6.91	49551	0.0994	🟥 **45A**	Mean	508.21	3.92	8260	0.0258
	STD	0.128	0.133	725	0.001455		STD	0.199	0.221	367	0.001147
	Variance, s	0.016	0.018	525605	2.12E-06		Variance, s	0.040	0.049	134406	1.32E-06
38	Mean	522.53	6.35	23839	0.0890	🟥 **45B**	Mean	507.91	3.76	11418	0.0176

	STD	0.182	0.180	436	0.001629			STD	0.129	0.165	377	0.000582
	Variance, s	0.033	0.032	190358	2.65E-06			Variance, s	0.017	0.027	142014	3.39E-07
39	Mean	508.18	3.61	17927	0.0377		**45C**	Mean	507.84	3.78	19384	0.0212
	STD	0.091	0.087	360	0.000756			STD	0.085	0.139	413	0.000453
	Variance, s	0.008	0.008	129387	5.71E-07			Variance, s	0.007	0.019	170532	2.05E-07

B.3 Peak Asymmetry Fitting Results

Data Run	Peak Shape	Center	Acq. Time	Left Side						Right Side					
		Ch #	hours	FWHM #of Chs	Area counts	Error %	Corrected Counting Rate counts/s	Baseline counts	Baseline Counting Rate	FWHM #of Chs	Area counts	Error %	Corrected Counting Rate counts/s	Baseline counts	Baseline Counting Rate
19	Voigt	503	23.98	7.7051	10473	1.2205	0.1213	5415	64.2224	6.8146	9638	1.2176	0.1116	5435	64.4596
20	Voigt	505	1.92	6.5184	1173	4.0149	0.1702	442	65.6858	8.3816	1146	3.9738	0.1663	442	65.6858
21	Voigt	505	24.23	7.016	10559	1.1917	0.1217	5919	69.8319	7.0569	10459	1.2322	0.1205	5907	69.6903
23	Voigt	505	24.00	6.8276	8939	1.227	0.1048	5225	62.7207	6.4991	9509	1.2232	0.1115	5229	62.7687
24	Voigt	503	24.45	5.8801	9290	1.1595	0.1072	5452	64.4066	7.5266	10553	1.2475	0.1217	5452	64.4066
25A	Voigt	506	15.13	7.879	7796	1.594	0.1456	3457	66.1167	10.8780	9307	1.5901	0.1738	3448	65.9446
25B	Voigt	506	17.97	7.8091	7975	1.5956	0.1255	3571	57.5353	10.6060	9525	1.5668	0.1499	3563	57.4064
25C	Voigt	505	28.20	8.2209	13503	1.2642	0.1354	5929	60.8948	7.8551	13530	1.1939	0.1357	5920	60.8024
25D	Voigt	504	40.63	7.0675	17767	1.0354	0.1238	8890	63.4095	7.6124	19772	0.9722	0.1377	8879	63.3310
25E	Voigt	505	48.00	7.7236	23063	0.9230	0.1360	10727	64.7950	7.2763	21164	0.8897	0.1248	10720	64.7528
26A	Voigt	503	24.00	6.9833	10712	1.1956	0.1269	5569	67.5355	6.9255	9996	1.2144	0.1184	5576	67.6204
26B	Voigt	503	28.20	6.982	12842	1.0746	0.1295	6544	67.5550	7.0680	12529	1.1185	0.1263	6553	67.6479
26C	Voigt	503	40.63	6.8624	14400	0.9821	0.1008	7556	54.1701	7.3452	15362	1.0136	0.1076	7562	54.2131
27A	Voigt	504	27.00	7.6703	13697	1.2557	0.1449	5332	57.7799	8.0790	12581	1.2806	0.1331	5341	57.8774
27B	Voigt	504	48.00	7.6812	23047	1.0027	0.1373	9462	57.7400	8.2198	23681	0.9461	0.1411	9470	57.7888
28A	Voigt	502	24.00	7.716	10251	1.3484	0.1226	4910	60.1543	7.9045	10591	1.3968	0.1267	4915	60.2156
28B	Voigt	503	48.00	7.7115	20680	0.9288	0.1239	9826	60.2679	7.4848	20596	0.9499	0.1234	9826	60.2679
29A	Voigt	504	26.35	6.4009	11332	1.1829	0.1241	5492	61.6050	7.0470	11002	1.2734	0.1205	5500	61.6947
29B	Voigt	504	96.32	6.8558	40216	0.6695	0.1210	19863	61.1820	7.3156	41617	0.6270	0.1252	19851	61.1450
30A	Voigt	504	26.35	9.4424	13207	1.2592	0.1462	5323	60.3215	9.5124	12285	1.3686	0.1360	5321	60.2988
30B	Voigt	504	96.00	7.0289	42615	0.6801	0.1299	19202	59.9485	9.0144	42212	0.7070	0.1287	19194	59.9236

31A	Voigt	503	48.08	7.2214	19252	0.9845	0.1181	8794	55.2357	8.3330	21309	1.0666	0.1307	8787	55.1917
31B	Voigt	504	136.08	7.5511	57747	0.5930	0.1257	24570	54.7846	7.4659	53063	0.5963	0.1155	24573	54.7913
32	Voigt	523	182.47	6.8311	60009	0.5657	0.0992	29313	49.6193	6.6495	59014	0.6548	0.0976	29321	49.6329
33	Voigt	523	182.53	6.6956	63799	0.5324	0.1076	30441	52.5718	7.3747	63740	0.5414	0.1075	30464	52.6116
34	Voigt	523	217.42	6.6126	71190	0.4868	0.1039	35265	52.6837	6.7452	67952	0.4994	0.0991	35287	52.7165
35	Voigt	523	167.53	7.243	50066	0.6243	0.0967	22857	45.2231	6.7813	50721	0.6471	0.0980	22874	45.2567
36	Voigt	522	165.52	7.1609	45078	0.6451	0.0897	20786	42.3719	6.3394	43520	0.7473	0.0866	20764	42.3270
37	Voigt	522	167.17	6.8121	50488	0.5940	0.1013	24961	51.2923	7.0286	49515	0.6030	0.0994	24962	51.2943
38	Voigt	523	91.08	6.5012	25027	0.9455	0.0935	11242	42.9875	6.2743	23045	0.8992	0.0861	11241	42.9836
39	Voigt	508	164.17	3.5287	17573	0.8484	0.0369	14636	31.4914	3.6958	19231	0.7858	0.0404	14625	31.4677
40A	Voigt	508	122.17	3.5033	7524	1.0764	0.0229	6562	20.4882	4.1130	8768	1.0730	0.0267	6558	20.4757
40B	Voigt	509	239.58	3.9037	16732	0.8176	0.0262	12406	19.8749	3.5711	15412	0.7784	0.0241	12401	19.8669
40C	Voigt	509	293.33	3.919	20120	0.7607	0.0258	14947	19.6138	3.7130	19226	0.7117	0.0246	14947	19.6138
40D	Voigt	509	410.83	3.9592	28001	0.6456	0.0258	19918	18.7785	3.7252	26533	0.6370	0.0244	19917	18.7776
40E	Voigt	509	433.58	3.9219	28760	0.6345	0.0251	20756	18.5642	3.7625	27718	0.6352	0.0242	20754	18.5624
40F	Voigt	509	510.92	3.9119	33739	0.5953	0.0251	24022	18.3084	3.7332	32395	0.5983	0.0241	24015	18.3030
41A	Voigt	509	116.58	3.6042	6947	1.3186	0.0234	4280	14.7692	3.4659	6568	1.3287	0.0221	4280	14.7692
41B	Voigt	509	167.50	3.7684	10293	1.0862	0.0242	6273	15.1073	3.4129	9117	1.1218	0.0214	6273	15.1073
41C	Voigt	509	237.50	3.5388	14217	0.9220	0.0237	9135	15.5735	3.1949	13025	0.9288	0.0217	9131	15.5666
41D	Voigt	509	283.17	3.5633	16901	0.8418	0.0237	10879	15.5934	3.2255	15274	0.8629	0.0214	10873	15.5848
41E	Voigt	509	332.75	3.6781	20317	0.7773	0.0243	12852	15.7178	3.3994	18430	0.7941	0.0220	12847	15.7117
41F	Voigt	509	497.75	3.7208	28483	0.6722	0.0229	17688	14.5886	3.5516	26029	0.6885	0.0210	17690	14.5902
42A	Voigt	509	73.93	4.0944	3962	1.791	0.0222	2178	12.4751	3.2158	3375	1.9352	0.0189	2177	12.4693
42C	Voigt	509	172.95	3.7745	8765	1.1952	0.0211	5444	13.4001	3.7432	9153	1.6902	0.0220	5437	13.3829
42D	Voigt	509	240.38	3.7238	11757	1.031	0.0204	7097	12.6135	4.0458	12606	1.3946	0.0219	7089	12.5993
42E	Voigt	509	266.75	3.7087	13212	0.979	0.0207	7707	12.3611	3.9423	13684	1.3146	0.0214	7700	12.3498
42F	Voigt	509	335.80	3.6408	16574	0.8980	0.0207	9627	12.3106	3.7749	16849	1.1233	0.0210	9621	12.3029
42G	Voigt	509	1331.05	3.7131	19864	0.8368	0.0066	11663	3.9669	3.9328	20395	0.9837	0.0068	11654	3.9638
43A	Voigt	509	168.33	2.9351	3569	1.6707	0.0101	2797	8.1159	4.2225	3767	1.7894	0.0107	2796	8.1130
44A	Voigt	508	218.08	3.3525	10925	0.9748	0.0244	8942	20.4421	3.3302	11517	0.9388	0.0257	8939	20.4353

44B	Voigt	508	383.42	3.7266	19081	0.7386	0.0244	15005	19.6831	3.6457	20329	0.7640	0.0260	14997	19.6726
44C	Voigt	508	459.92	3.8108	23258	0.6514	0.0249	17944	19.7031	3.6446	23192	0.6861	0.0249	17934	19.6921
44D	Voigt	508	552.92	3.8107	28338	0.6026	0.0254	21398	19.6406	3.5709	27820	0.6277	0.0249	21394	19.6369
44E	Voigt	508	675.75	3.8121	35513	0.5443	0.0262	25923	19.5963	3.4449	33095	0.5635	0.0244	25922	19.5955
44F	Voigt	508	893.25	3.7764	46213	0.4953	0.0261	33829	19.5708	3.4209	43149	0.4727	0.0244	33838	19.5761
44G	Voigt	508	1151.25	3.8415	59859	0.4441	0.0266	42080	19.1493	3.4987	54352	0.4353	0.0242	42096	19.1566
44H	Voigt	508	1319.58	3.8607	68220	0.4172	0.0267	47398	18.9869	3.4795	60853	0.4045	0.0238	47426	18.9981
44I	Voigt	508	1803.58	3.823	88693	0.3793	0.0260	59512	17.8965	3.5045	80745	0.3724	0.0237	59546	17.9067
45A	Voigt	508	188.08	3.7678	7987	1.2046	0.0250	5728	18.3545	4.0797	8870	1.1574	0.0278	5721	18.3321
45B	Voigt	508	384.92	3.7245	11823	1.0303	0.0183	8032	12.7084	3.7502	11542	0.9873	0.0178	8023	12.6941
45C	Voigt	508	547.33	3.9735	2500	0.7974	0.0027	13791	15.4783	3.5743	19269	0.7756	0.0211	13788	15.4750

Bibliography

1. Chen, YL, Yang, DP. *Mössbauer Effect in Lattice Dynamics*. Wiley-VCH: KGaA, Weinham, 2007.

2. Cranshaw, TE, Dale BW, Longworth GO and Johnson CE. *Mössbauer Spectroscopy and its Applications*. Cambridge Univ. Press: Cambridge, 1985.

3. Cranshaw, T.E., Schiffer, J. P., *Measurement of the gravitational red shift with the Mössbauer effect.* Proc. Physic. Soc. 84 245pp, 1964.

4. DeGrave E, Vandenberghe RE, Dauwe C. ILEEMS: *Methodology and applications to iron oxides. Hyperfine Interactions*, 161 (1-4): 147-160, 2005.

5. Dickson DPE and Berry FJ. *Mössbauer Spectroscopy*. Cambridge Univ. Press: Cambridge, 1986.

6. Dyar, MD, Agresti, DG, Schaefer, M, Grant, CA, and Sklute, EC. "Mössbauer spectroscopy of earth and planetary materials." *Annual Reviews of Earth and Planetary Science*, 34, 83-125, 2006.

7. Frauenfelder, H. *The Mössbauer Effect*. Benjamin: New York, 1962.

8. Fultz, B. "*Mössbauer Spectroscopy*," in Characterization of Materials. Kaufmann, Editor. John Wiley: New York, 2011.

9. Jones, W., Thomas, J.M., Thorpe, R.K., Tricker, M.J. "*Conversion Electron Mössbauer Spectroscopy and the Study of Surface Properties and Reactions*", Applications of Surface Science pg. 388-407., North-Holland Publishing Company (1978)

10. Kankeleit, E. Feedback in electromechanical drive systems. *In Mössbauer Effect Methodology*, vol. 1. Plenum Press, New York. (1965)

11. Knoll, G. E., Radiation Detection and Measurement, John Wiley & Sons, New York, NY, USA, 3rd edition, 2000

12. Krane, K. S. *Introductory Nuclear Physics*. Oregon State University: John Wiley & Sons, 1988.

13. Lang, G., (1970) "Mössbauer Spectroscopy of Haem Proteins", Quart. Rev. Biophysics 3, I 1-60.

14. Lang, G. and Marshall, W. (1966) "Mössbauer Effect in Some Hemoglobin Compounds", Proc. Phys. Soc. 87, 3-34.

15. Long, GJ and Grandjean, F, eds. *Mössbauer Spectroscopy Applied to Magnetism and Materials Science* Vol. 1. Plenum: New York, 1993.

16. Long, G. J. and Stevens, J. G., eds. (1986) "Industrial applications of the Mössbauer Effect", Plenum Press, New York.

17. May L, ed. *An Introduction toMössbauer Spectroscopy*. New York: Plenum. 203pp, 1971.

18. McKelvey, J., *Solid State Physics for Engineering and Material Science*, Krieger Publishing Co. 1st ed. (2003)

19. Mössbauer, R. L. *Kernresonanzfluoreszenz von Gamma-strahlung in* Ir^{191}. Z. Phys. 151:124, 1958.

20. O'Haver, T., *Pragmatic Introduction to Signal Processing with applications in chemical analysis*. University of Maryland, 16 Mar 2014.

21. Seberini, M. and Sitek, J. Surface Analysis of Iron – Containing Samples by CEMS an Overview of the Method. *Journal of Electrical Engineering*, Vol 59, No 5: pg 234-240 (2008)

22. Seitz, F. and Koehler, J. S., in Solid State Physics, edited by H. Ehrenreich, F. Seitz, and D. Turnbull (Academic, New York, 1956), Vol. 2, p. 351

23. Spikerman, J.J. Conversion Electron Mössbauer Spectroscopy. *In Mössbauer Effect Methodology*, vol. 7. Plenum Press, New York. (1971)

24. Spikerman, J.J. *Mossbauer Spectroscopy Instruction Manual for the MS-1200*. Ranger Scientific, Inc., Burleson, TX.

25. Stewart, I., Tricker, M. J., Cairns, J. A. "*Mössbauer Spectroscopic Studies of Chromium Depletion in a 310 Stainless Steel During Air Oxidation*", Corrosion Science Vol 26., Pergamon Journals Ltd, Great Britain (1986)

26. Tanis, E.A., *Partial phonon densitiy of states of 57-iron and 161-dysprosium in DyFe3 by nuclear resonant inelastic X-ray scattering under high pressure*. MS Thesis. University of Nevada, Las Vegas. (2006)

27. Thompson, B., *Exploring the Replicability of a Study's results: Bootstrap Statistics for the Multivariate Case*. Texas A&M University Sage Journals. (2012)

28. Vandenberghe R.E., DeGrave E., Dauwe C. ILEEMS: *On the methodology of Mossbauer spectra. Hyperfine Interactions 83*: pg 29-49, 1994.

29. Wegener H. 1965. *Der M¨ossbauer-Effekt und Seine Anwendung in Physik und Chemie*. Mannheim: Bibliogr. Institut. 214pp.

30. Wit, H.P., Hoeksema, G., Niesen, L. and de Waard, H. A multi-purpose velocity transducer for Mössbauer spectrometers. *Nuclear Instrument Methods,* vol 141 (1977)

REPORT DOCUMENTATION PAGE	*Form Approved* *OMB No. 074-0188*

1. REPORT DATE *(DD-MM-YYYY)* **04-03-2015**	2. REPORT TYPE **Master's Thesis**	3. DATES COVERED *(From – To)* **20 Aug 2010 – 22 Jan 2015**

4. TITLE AND SUBTITLE Coupling Nuclear Induced Phonon Propagation with Conversion Electron Mössbauer Spectroscopy	5a. CONTRACT NUMBER 5b. GRANT NUMBER 5c. PROGRAM ELEMENT NUMBER
6. AUTHOR(S) **Parker, Michael J., Captain, USAF**	5d. PROJECT NUMBER **N/A** 5e. TASK NUMBER 5f. WORK UNIT NUMBER
7. PERFORMING ORGANIZATION NAMES(S) AND ADDRESS(S) **Air Force Institute of Technology** **Graduate School of Engineering and Management (AFIT/EN)** **2950 Hobson Way, Building 640** **WPAFB OH 45433-8865**	8. PERFORMING ORGANIZATION REPORT NUMBER AFIT-ENP-MS-15-J-054
9. SPONSORING/MONITORING AGENCY NAME(S) AND ADDRESS(ES) **Department of Homeland Security – Domestic Nuclear Detection Office** **245 Murray Dr, Building 410 Washington, DC 20528** **Attn: DNDO Email: William.Ulicny@HQ.DHS.GOV**	10. SPONSOR/MONITOR'S ACRONYM(S) **DHS/DNDO** 11. SPONSOR/MONITOR'S REPORT NUMBER(S)

12. DISTRIBUTION/AVAILABILITY STATEMENT

DISTIBUTION STATEMENT A. APPROVED FOR PUBLIC RELEASE; DISTRIBUTION UNLIMITED.

13. SUPPLEMENTARY NOTES

This material is declared a work of the U.S. Government and is not subject to copyright protection in the United States.

14. ABSTRACT

Mössbauer spectroscopy is a very sensitive measurement technique (~10-8 eV) which prompted motivation for the experiment described in this thesis. Namely, can a sensitive detection system be developed to detect nuclear recoils on the order of 10 to 100 of eVs? The hypothesis that this thesis tests is: Nuclear induced phonon bursts caused by Rutherford scattered alphas, decayed from 241Am, in a type-310 stainless steel material can couple with 7.3keV conversion electron Mössbauer events at the other end of the material which will have a statistically significant effect on a Mössbauer spectrum. The phonon bursts produced by the alpha collisions are expected to be very low energy at the other end of length of material. Since Mössbauer spectroscopy is sensitive and can detect the very low energy phonons, the spectrum is expected to change in at least one of the five areas after coupling occurs: broadening in the spectrum peaks, increased/decreased background counting rate, Mössbauer peak asymmetry, increased/decreased counting rate under the peak, and/or a peak centroid shift. This research aims to determine the significance of changes between spectra with phonon bursts and with no phonon bursts through hypothesis testing, where the null hypothesis is where phonons do not affect Mössbauer spectra in one of the five areas mentioned previously. After the spectra and results were analyze using an f-test and t-test comparisons, this experiment failed to reject the null result. Leading to the conclusion that additional research must be conducted.

15. SUBJECT TERMS

Mössbauer Spectroscopy, Detection, Phonons

16. SECURITY CLASSIFICATION OF:			17. LIMITATION OF ABSTRACT	18. NUMBER OF PAGES	19a. NAME OF RESPONSIBLE PERSON **Dr. Larry Burggraf**
a. REPORT	b. ABSTRACT	c. THIS PAGE			19b. TELEPHONE NUMBER *(Include area code)*
U	**U**	**U**	**U**	**154**	**(937) 255-3636, x 4507** **(Larry.Burggraf@afit.edu)**